Model Predictive Control for Spacecraft Rendezvous and Docking with Uncooperative Targets

Iskender Omer Burak

School of Electrical & Electronic Engineering

A thesis submitted to the Nanyang Technological University
in partial fulfillment of the requirements for the degree of
Doctor of Philosophy

2020

Statement of Originality

I hereby certify that the work embodied in this thesis is the result of original research, is free of plagiarised materials, and has not been submitted for a higher degree to any other University or Institution.

07 Oct. 2020

....

Date Iskender Omer Burak

Supervisor Declaration Statement

I have reviewed the content and presentation style of this thesis and declare it is free of plagiarism and of sufficient grammatical clarity to be examined. To the best of my knowledge, the research and writing are those of the candidate except as acknowledged in the Author Attribution Statement. I confirm that the investigations were conducted in accord with the ethics policies and integrity standards of Nanyang Technological University and that the research data are presented honestly and without prejudice.

31 Aug. 2020

.....

Date

.....

Assoc. Prof. Ling Keck Voon

Authorship Attribution Statement

This thesis contains material from 4 papers that are published in the following conferences where I was the first author and founder of the idea who prepared the draft and completed the papers based on the contributions of the co-authors.

Chapter 4 is published as **Iskender, O. B.,** Ling, K. V., Dubanchet, V., "Constraints Tightening Approach Towards Model Predictive Control Based Rendezvous and Docking with Uncooperative Targets." 2018 European Control Conference (ECC). IEEE, 2018, pp. 380-385.
The contributions of the co-authors are as follows:

- Prof. Ling has guided the MPC theory part and edited the manuscript draft.
- Dr. Vincent Dubanchet supported the work in the problem definition and running simulations on high fidelity model.

Iskender, O. B., Ling, K. V., Dubanchet, V., Simonini, L., "Inscribed Polygon Method for Spacecraft Maneuvering Problem Arising in Single Axis Thruster Configuration." 2019 12th Asian Control Conference (ASCC). IEEE, 2019, 1466–1471.
The contributions of the co-authors are as follows:

- Prof. Ling has guided the MPC formulation and simulations and, guided the entire paper.
- Dr. Dubanchet supported the work in the problem definition and running simulations on high fidelity model.
- Mr. Simonini has provided system level support that includes challenges arising in the single axis thruster configuration as well as the constraints to be defined during the proximity operations.

Chapter 5 is based on the following two papers that are published and accepted for publication respectively: **Iskender, O. B.,** Ling, K. V., Dubanchet, V., Simonini, L., Schlotterer, M., Seelbinder, D., Theil, S., Maciejowski, J.M., "Dual Quaternion Based Autonomous Rendezvous and Docking Via Model Predictive Control." In 70th International Astronautical Congress (IAC). International Astronautical Federation, 2019.
The contributions of the co-authors are as follows:

- Prof. Ling guided the MPC formulation and simulations and, guided the entire paper.
- Dr. Dubanchet has casted his expertise on kinematics and dynamics.
- Mr. Simonini contributed in the introduction section where he shared his expertise on the future space systems.
- Dr. Schlotterer supported the experimental work.

- Dr. Seelbinder shared his expertise on the optimization theory.
- Dr. Theil shared his expertise on the space systems.
- Prof. Maciejowski showed his expertise on MPC and its applications on Mars Sample Return Mission.

Chapter 6 is based on the following two papers that are accepted for publication and under review respectively:

Iskender, O. B., Ling, K. V., Dubanchet, V., Simonini, L., Schlotterer, M., Seelbinder, D., Theil, S., "Attitude Control of Spacecrafts with Thrusters and Embedded Optimization." In 70th International Astronautical Congress (IAC). International Astronautical Federation, 2019.
The contributions of the co-authors are as follows:

- Prof. Ling guided the MPC formulation and addressed the challenges of MPC for real-time implementation.
- Dr. Dubanchet has casted his expertise on real-time implementation related issues including editing on the code and running experiments.
- Mr. Simonini provided the system level support that includes revising the paper and writing the introduction section.
- Dr. Schlotterer shared his experience on the attitude control of satellites and real-time tests.
- Dr. Seelbinder showed his support on the optimization aspects of the paper.
- Dr. Theil supported his expertise in the embedded systems.

07 Oct 2020

....

Date Iskender Omer Burak

Acknowledgements

Firstly, I would like to sincerely thank my supervisor for his continuous support. Secondly, I would like to thank Mr. Luca Simonini and Dr. Vincent Dubanchet from Thales Alenia Space for being inspirer leaders who have always shown their faith in me and who continuously supported my dreams to come true. Next, the core part of my thesis is achieved in DLR/German facilities. Hence, I would like to thank the head of GNC/Bremen department Dr. Stephan Theil, head of G&C department Dr. David Seelbinder for providing me the opportunity to conduct my experiments. In DLR, Dr. Markus Schlotterer had always been supportive in the test, and verification phase of the embedded systems. That was remarkable and I appreciate to receive his support. Last but not the least, I am grateful to have Prof. Jan Maciejowski in my thesis advisory committee. I would like to thank Prof Jan. for his support and enthusiasm for my work.

"If I had one hour to save the world, I would spend 55 minutes defining the problem and only five minutes finding the solution."

—Einstein, Albert

To my dear family

Abstract

This thesis develops guidance & control strategies for rendezvous and docking with uncooperative targets in space. The past and current state of art for rendezvous missions are capable of docking with stable and cooperative targets. However, future applications will require full autonomy on-board, robustness to the changing environments and explicit handling of constraints due to the absence of communication with potential targets. In our approach, we employ Model Predictive Control (MPC) paradigm that generates a set of control inputs and the resulting predicted states to optimize performance objectives while respecting the dynamic and physical constraints. Only the first set of inputs are implemented and based on the new states, the optimization is repeated as the spacecraft moves. Moreover, Guidance and Control (G&C) blocks are unified via the MPC paradigm and the coupling between translational motion and rotational motion is addressed via dual quaternion based kinematic description. The design of the G&C controller is formulated as a convex optimization problem where constraints such as thruster limits are explicitly handled. The proposed strategy allows safe and fuel-efficient trajectories for space servicing missions including tasks such as approaching, inspecting and capturing. The proposed controllers are evaluated in a High Fidelity Engineering Model (HFEM) in simulation, and are validated with Hardware-In-The-Loop (HIL) experimental results. Because MPC implementation relies on finding in real-time the solution to constrained optimization problems, computational aspects are also examined and the gap is addressed via experiments in a "zero-G" (air cushion) environment with real sensors, actuators, and on-board processor. This thesis concludes that the proposed dual quaternion based MPC paradigm is a promising framework for the crossroads of future space applications.

Contents

List of Figures

List of Tables

Symbols and Acronyms

Symbols

$\{\cdot, \ldots, \cdot\}$	a set or sequence
$\emptyset$	the empty set
$\mathcal{N}(S)$	neighborhood of the set S
$\mathbb{R}$	set of real numbers
$\mathbb{R}^n$	set of n-dimensional Euclidean space
$\mathbb{R}^{n\times m}$	set of n by m matrices with real entries
$\mathbb{N}$	set of natural numbers (non-negative integers)
$\mathbb{N}_r$	set of natural numbers from 0 to r, $\mathbb{N}_r = (0..., r)$ for $r \in \mathbb{N}$
Let $A \in \mathbb{R}^{m\times n}$	be a matrix, $x \in \mathbb{R}^n$ be a vector and $\mathcal{E} \subseteq \mathbb{N}_m, \mathcal{F} \subseteq \mathbb{N}_n$ be sets.
null(A)	null-space of A, null(A) $\triangleq \{x \in \mathbb{R}^n \vert Ax = 0\}$
$A \succcurlyeq 0$	positive semi-definite matrix
$A > 0$	positive definite matrix
I_n	n-dimentional identity matrix
$I_{n\times m}$	$n \times m$-dimentional zero matrix
1	vector of ones of appropriate dimension, $1 \triangleq [1, \ldots, 1]^T$
diag(s)	diagonal matrix whose diagonal entries are given by the vector s
SO(3)	special orthogonal group in dimension three
SE(3)	special Euclidean group in dimension three
det($\cdot$)	determinant of a given matrix
$[\mathbf{x}]_\times$	cross product operator associated with a vector $\mathbf{x}$
$\mathbf{x} \cdot \mathbf{y}$	dot product between vectors $\mathbf{x}$ and $\mathbf{y}$
$\vert\cdot\vert$	absolute value
$\mathcal{N}$	inertial frame
$\mathcal{C}$	chaser spacecraft body frame
$\mathcal{T}$	target spacecraft body frame

$\mathbf{q}$	unit quaternion
q	vector part of the unit quaternion $\mathbf{q}$
q_0	scalar part of the unit quaternion $\mathbf{q}$
$\mathbf{q_I}$	identity unit quaternion
$\mathbf{q}^*$	conjugate of unit quaternion $\mathbf{q}$
$\mathbf{q_e}$	quaternion error
$\otimes$	quaternion product
$[\mathbf{q}]_\otimes$	quaternion product operator
$\times$	cross product between two quaternions
$[\mathbf{q}]_\times$	quaternion cross product operator
ϵ	dual unit for dual quaternions
$\tilde{\mathbf{q}}$	unit dual quaternion
$\tilde{\mathbf{q}}^*$	conjugate dual quaternion
$\tilde{\otimes}$	dual quaternion product
$[\tilde{\mathbf{q}}]_{\tilde{\otimes}}$	dual quaternion product operator
$\tilde{\times}$	dual quaternion cross product
$[\tilde{\mathbf{q}}]_{\tilde{\times}}$	dual quaternion cross product operator
ω	angular velocity vector in unit quaternion
v	velocity vector in unit quaternion
$\tilde{\omega}$	angular velocity vector in dual quaternion
$\tilde{v}$	velocity vector in dual quaternion
$\mathbf{r}_\mathcal{C}$	position vector in $\mathcal{C}$ frame components
$\mathbf{r}_\mathcal{N}$	position vector in $\mathcal{N}$ frame components
N_p	prediction horizon
N_c	control horizon
T_s	sampling time
T_{comp}	computation time
k	time step
Φ	roll angle of Euler angles
θ	pitch angle of Euler angles
Ψ	yaw angle of Euler angles
h	altitude of a satellite/spacecraft
e	eccentricity of an orbit
a	semimajor axis of an orbit
i	inclination of an orbit

ω	argument of periapsis
Ω	longitude of the ascending node
v	true anomaly
M	mean anomaly
$\|\cdot\|$	the 2-norm of a vector or matrix in Euclidean space
$\|\cdot\|_G$	the induced norm of a vector in G-space
$\|\cdot\|_E$	the induced norm of a vector or matrix in probabilistic space
$\langle\cdot,\cdot\rangle$	the inner product of two vectors
∇f	the gradient vector
$\mathcal{C}^k$	the function with continuous partial derivatives up to k orders
$x_{i,k}$	the i-th component of a vector x at time k

Acronyms

ATV	Automated Transfer Vehicle
COM	Center-Of-Mass
DART	Demonstration for Autonomous Rendezvous Technology
DOF	Degree of Freedom
ECI	Earth Centered Inertial Frame
ESA	European Space Agency
ETS	Engineering Test Satellite
FDIR	Fault-Detection-Isolation and Recovery
FLOPs	Floating Point Operations
FOV	Field-of-View
GN&C	Guidance, Navigation and Control
GPS	Global Positioning System
HCW	Clohessy Wiltshere
HFEM	High Fidelity Engineering Model
HIL	Hardware-In-The-Loop
IMU	Inertial Measurement Unit
ISS	International Space Station
LOS	Line-Of-Sight
LP	Linear Programming
LPV	Linear Parameter Varying
LQR	Linear Quadratic Regulator

LTV	Linear-Time-Varying
LVLH	Local-Vertical-Local-Horizontal
MIMO	Multi-Input and Multi-Output
MoI	Moment of Inertia
MPC	Model Predictive Control
NASA	National Aeronautics and Space Administration
NHFEM	Nonlinear High Fidelity Engineering Model
NP	Nonlinear Programming
PAM	Pulse Amplitude Modulated
PD	Proportional-Derivative
PWA	Piece-Wise Affine
PWM	Pulse-Width Modulated
QCQP	Quadratically Constrained Quadratic Programming
QP	Quadratic Programming
RVD	Rendezvous and Docking
SDP	Semi-Definite Programming
SIL	Software-In-The-Loop
SISO	Single-Input and Single-Output
SOCP	Second Order Cone Programming
SPHERES	Synchronized Position Hold Engage and Reorient Experimental Satellite
SRP	Solar Radiation Pressure
STM	State Transition Matrix
TEAMS	Test Environment for Applications of Multiple Spacecrafts
UAV	Unmanned Aerial Vehicle

Chapter 1

Introduction & Motivation

Model Predictive Control (MPC) is commonly criticized by its real-time implementation requirements and therefore initially used for applications with slow dynamics where the sampling rate is measured in seconds or minutes [30–32]. However today, with efficient online Quadratic Programming (QP) solver algorithms, the control frequency can be as high as megahertz and with even relatively conservative processors in kilohertz depending on the size of the problem [33–35]. Hence, the great advantages of MPC can now be beneficial for fast applications where input use, constraint handling and robustness to the system uncertainties are crucial. The common current implementation examples are race cars, helicopters and Unmanned Aerial Vehicles (UAVs) where the control loop should be closed as fast as 100Hz in real-time [36–38]. This paved the way for researching the MPC in more critical and demanding applications namely Space Missions.

The objective of this thesis is to bridge the gap between the matured Linear Model Predictive Control theory with the final phase of an automated Rendezvous and Docking (RVD) scenario, with a consideration for 6-Degrees-of-Freedom (DOF) translational and rotational motion couplings, constraints, real-time implementation issues and validation with experimental work. The use case for the developed MPC design is rendezvous and docking with uncooperative targets in space which are potentially uncontrolled and/or dead.

1.1 Spacecraft Rendezvous and Docking

Given two space vehicles orbiting a central body, the purpose of RVD is for two spacecrafts to reach a predefined relative configuration in each other's proximity [39]. To this extent, NASA initiated the Gemini mission which occurred from 1962 to 1966 to develop and test RVD scenarios [40, 41]. The ultimate purpose was landing on the Moon, hence, the whole Gemini mission can be considered as an experiment of RVD technology towards the "...giant leap for mankind". Despite the fact that there was a level of autonomy in the sensing and maneuvering towards RVD with the target, Neil Armstrong manually performed the rendezvous in a Gemini spacecraft and docked with an unmanned Agena target. Due to safety reasons, Americans preferred manual RVD missions whilst it did not take too long for Russians to accomplish the first fully autonomous RVD between Cosmos 186 and 188 back in 1967 [8]. After that, autonomous rendezvous has been employed for numerous missions and the most critical and popular ones are US Apollo Mission (1968-1972), US Skylab (1973-1974) mission, Russian Salyut & Mir Space Station Programs (1971-1999); docking of manned Soyuz and unmanned spaceships, US & Russian Apollo-Soyuz docking mission (1975) and US & Russian preparation of International Space Station (ISS) program (1990s). In addition, the US Space Shuttle servicing missions, started in 1984, transport of crew & goods, resupply and assembly of ISS. In 1998 these services were carried out by European Automated Transfer Vehicle (ATV), US Cygnus Spacecraft, US Dragon Cargo Spacecraft, Japanese H-II Transfer Vehicle and Russian Progress Spacecraft [8].

1.1.1 Definitions

Before going any further, basic definitions are given as

Cooperative: The target is actively controlled to assist the rendezvous phase by either maintaining an attitude/position, or by remaining passive whatever the force/torque applied by the chaser.

Collaborative: The target is designed to be captured (and serviced, if needed), by including dedicated markers for relative navigation, handles or specific interfaces compliant with the mechanical interfaces from the chaser side.

Uncooperative: The target is not taking any control action to assist the chaser satellite and might be potentially tumbling. In addition, there is no certain knowledge of the target, i.e., its final shape and the attitude motion. Finally, there is no communication link between the target and the chaser. (The chaser satellite must rely on its own sensors and the trajectory generated on-board in real-time that shows robustness to the sensor and actuator errors while minimizing the fuel consumption and respecting the constraints). Fig. 1.5 refers to mission characteristics & examples of spacecraft proximity operations in-orbit.

FIGURE 1.1: Manual - Cooperative: The Capture of Dragon [1]

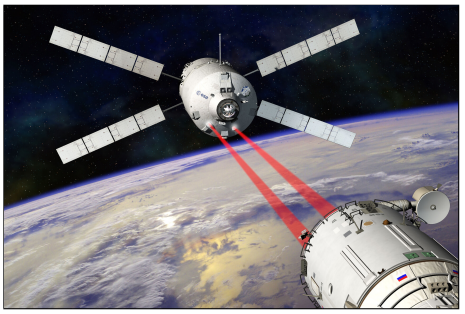

FIGURE 1.2: Autonomous - Cooperative: The ATV-5 docking [2]

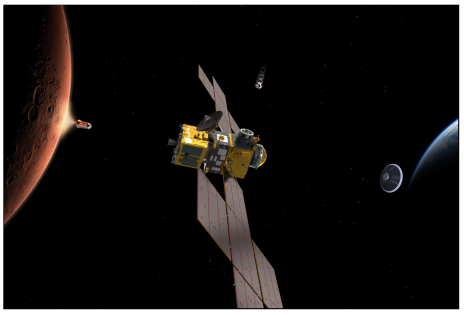

FIGURE 1.3: Autonomous - Collaborative Target: Mars Sample Return [3]

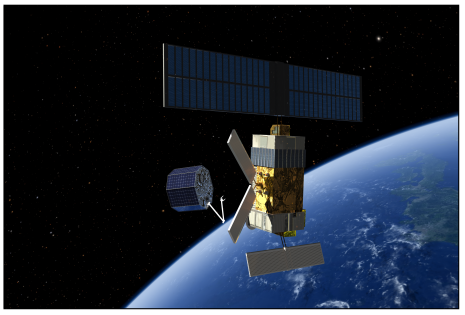

FIGURE 1.4: Autonomous - Uncooperative Target: Space Debris Capture [4]

FIGURE 1.5: Mission Characteristics & Examples of Spacecraft Proximity Operations In-orbit

1.1.2 Recent Missions

The historic rendezvous and docking missions are summarized in Table 1.1 in the chronological order. It is evident that all of the past RVD missions are with cooperative targets except a unique one; the DEOS mission. Furthermore, the target orbital geometry is circular or with low eccentricity, near-circular; therefore, well-known Linear-Time-Invariant (LTI) Hill-Clohessy-Wilthshere (HCW) Eqns. were employed. On the other hand, for the upcoming missions such as Elsa-D, e-Deorbit, CleanSpace-1, etc., the target is uncooperative while the target orbit remains circular. Lastly, due to mainly the uncertainties, latency, and constraints, it is now clear that the demand for autonomous rendezvous and docking operations are in the rise and the RVD with uncooperative targets both in circular and elliptic orbits are still yet to be addressed.

Table 1.1: Past & Planned Missions [8, 15–28]

Mission	Target Orbit	Target Characteristics	Autonomy Level	Guidance Algorithm / targeting principle
Gemini	Circular	Cooperative and mostly active target	Man-in-loop, extensive support from ground	Based on HCW Eqns. for near-range; far range with Hohmann-like transfers
Apollo	Circular	Cooperative and active target	Man-in-loop, extensive support from ground	Based on Lambert targetting
Soyuz/Progress Missions	Circular	Cooperative and mostly active target	Automated, ground and crew support when required	Based on HCW Eqns. for near-range; far range with Hohmann-like transfers
Space Shuttle Program	Circular	Mostly cooperative targets; occasionally passive targets	Far-range rendezvous is automated, near-range required man-in-loop, (extensive support from the ground)	Based on Lambert targetting
ETS-VII	Near Circular	Cooperative and active target	Autonomous	Based on HCW Eqns. for near-range; far range with Hohmann-like transfers
ATV	Near Circular	Cooperative and active target	Highly automated with occasional ground support	Based on HCW Eqns. for near-range; far range with Hohmann-like transfers
XSS	Near Circular	Cooperative and passive target	Semi-autonomous	Partly based on HCW Eqns.; further information unavailable
DART	Near Circular	Cooperative and passive target	Autonomous	Information unavailable
Orbital Express	Circular	Cooperative and passive target	Autonomous	Information unavailable
DEOS	Circular	Uncooperative target	Autonomous	Based on HCW Eqns. for near-range; far range with Hohmann-like transfers
Orion Program	Near Circular	Cooperative and active target	Semi-autonomous	Information unavailable
ELSA-D	Near Circular	Semi-uncooperative and semi-active target	Autonomous	Information unavailable
e-Deorbit	Near Circular	Uncooperative and passive target	Autonomous	Information unavailable
ClearSpace-1	Near Circular	Uncooperative and passive target	Autonomous	Information unavailable

1.1.3 Challenges

The ultimate guidance and control objective of autonomous rendezvous and docking with uncooperative targets is to compute a set of inputs and corresponding state trajectory that safely brings the chaser spacecraft as close as possible to its target objective while optimizing fuel consumption. These missions pose problems to be tackled. The major ones are the constraints on both state and control variable, robustness to the dynamic uncertainties and environmental disturbances, and real-time implementation capability. In this section, a list of examples are given to clarify the challenges from the optimization and real-time implementation points of view.

1. **Thruster Limitation Constraint:** Simply, it's the limits of an actuator with the force/torque lower and upper bounds. Moreover, *minimum impulse bit* problem occurs between the thruster being fully off and generating its minimum thrust which is slightly above zero. This is known as the dead-zone problem [42] and is illustrated in Fig. 1.6-a). The resulting optimization problem is non-convex.

   Remark 1. Throughout this thesis, the dead-zone is neglected and the convex quadratic constraint is formulated. The limits on the torque and force values are selected either from realistic satellite data provided by the industrial partner, Thales Alenia Space[1], or the experimental setup at German Aerospace Center (DLR)[2]. As an example, consider the DLR spacecraft simulator robot (see also Chapter 6 where details of the robot, as well as the constraint formulation and the multiple thruster allocation problem are described). The robot has 16 thrusters and each of them is able to deliver 65mN of thrust. After taking into account the geometry, 210mN of net thrust can be delivered along both x-axis and y-axis. Hence, input constraints exist. However, because each thruster is fired to generate the commanded force and torque values, there exists a conflict when the individual constraints are fully utilized. This problem results in global suboptimal solutions and loss in the control authority, and in Chapter 7, it is explained that future work will

[1]Thales Alenia Space is Europe's largest satellite manufacturer, and was responsible for the manufacturing of the ESA built modules of the International Space Station [43].

[2]The German Aerospace Center (Deutsches Zentrum für Luft- und Raumfahrt; DLR) is the national aeronautics and space research centre of the Federal Republic of Germany [44, 45].

take the thruster configuration into account as a constraint to ensure feasible input commands at all times.

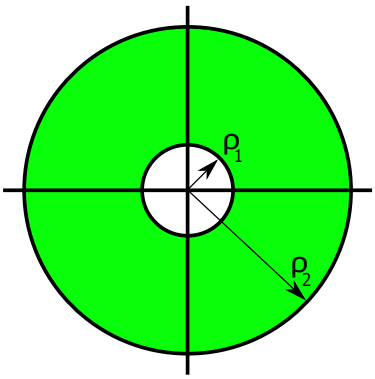

a) Thruster Limitation [46]

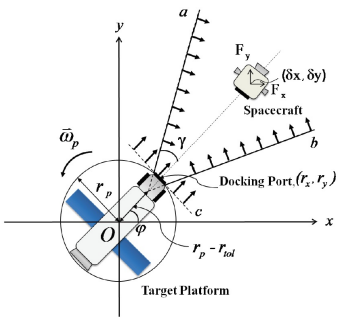

b) Line-Of-Sight [47]

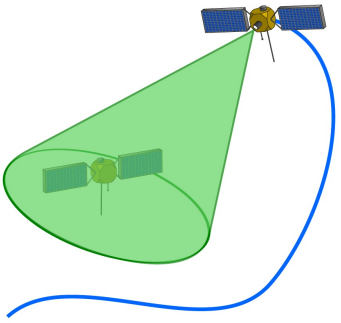

c) Field-Of-View [48]

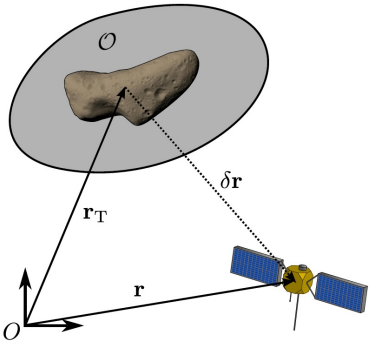

d) Obstacle/Collision Avoidance [48]

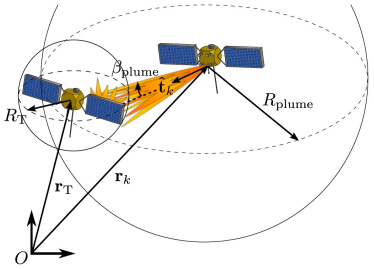

e) Plume Impingement [48]

FIGURE 1.6: Artistic Illustrations of Various Spacecraft Proximity Operations Guidance & Control Constraints

2. **Line-of-Sight (LOS) Constraint:** It is crucial to ensure that the spacecraft is always within a safe approach corridor and could finally dock with the target.

   Remark 2. In this thesis, we formulated the related LOS constraints as a set of linear time-varying inequalities, so that the resulting MPC problem remains convex, and be able to solve efficiently in real-time for practical implementations. The angle of the cone is set to be 45 degrees in order not to excessively tighten the constraints. In addition, the size of the bottom of the cone is set according to the RVD requirements which is to allow a ± 5 cm margins from the center of the docking port.

3. **Sensor Field-of-View (FOV) Constraint:** Sensors constraints to maintain the target pointing during the entire proximity operation. This constraint couples the translational motion with rotational motion and the resulting optimization problem is non-convex.

   Remark 3. Throughout this thesis, non-convex problems are either convexified or neglected and FOV is one of them. For the sake of real-time implementation capability and the reliability of the solutions, FOV constraint is not formulated. A recent work [49] shows that a problem formulation with a FOV constraint formulation can take up to 4.5 seconds for each time step even with a strong processor (A desktop with i7 Processor). Such computational load would violate the real-time requirement which is to close the loop every 0.5s.

4. **Plume Impingement Constraint:** These are guidance constraints to avoid undesirable effects of plumes exhausted from thrusters that could push the target away or blind the on-board navigation sensors of the chaser satellite. The resulting optimization problem is non-convex. This problem can be formulated using mixed-integer programming or convexification techniques.

   Remark 4. Throughout this thesis, non-convex problems are either convexified or neglected. The plume impingement constraint is one of them. For the sake of real-time implementation capability, plume impingement constraint is not considered.

5. **Collision Avoidance Constraint:** Violating this constraint would result in the worst scenario - loss of satellites. Hence, guidance strategy must ensure that chaser satellite must not collide with the target. In other words, the chaser satellite must not overshoot the docking port. This constraint can be formulated as a linear inequality constraint starting from the docking port; therefore, convex.

   Remark 5. Throughout this thesis, collision avoidance is guaranteed with explicit handling of the docking port constraint. This constraint is illustrated in Fig. 1.6-b) and the formulation is given in Subsection 4.3.1. The ultimate objective is not to overshoot, crash with the target satellite and with constrained optimization, this constraint is addressed.

6. **Obstacle Avoidance Constraint:** Another version of collision avoidance is with external objects such as space junk. Similarly, the resulting optimization problem is non-convex.

   Remark 6. Throughout this thesis, non-convex problems are either convexified or neglected and obstacle avoidance constraint is one of them. It is assumed that the chaser satellite starts its final proximity maneuver from the vicinity of the target, i.e. less than 200m away from the target, and hence, the potential space obstacles are neglected.

7. **Real-time Implementation:** The algorithms must meet the real-time requirement when implemented on a spacecraft which often has limited computational power.

   Remark 7. An important contribution of this thesis is the validation that the proposed controller can be implemented in real-time on a start-of-the-art experimental test bench. Hence, the ideal problem formulation is accordingly adjusted. The two major considerations are the convexity of the problem and the on-board solution time of the formulated problem.

   (a) In this thesis, non-convex problems are either convexified or neglected because as of today, there is no guarantee of finding the solution of the optimization problem while meeting the real-time limit.

   (b) For reducing the computational complexity of the resulting convex problem, the following considerations are taken into account:

   - The integral action is only applied to the position and attitude states; therefore, reducing the dimensions of the matrices in the problem formulation.
   - Quadratic constraints are transformed into linear constraints in order to cast the problem as a Quadratic Program.
   - The RVD problem in long range can be formulated with a sampling time of as long as 120s whereas, in the close proximity, it is desired to close the loop 0.1s to 1s time interval.

8. **Fuel limit:** Each mission is constrained by a finite supply of fuel. The access to space is costly and hence, each satellite must optimize the use of their fuel during the mission while giving the priority to the safety of the mission.

Remark 8. Throughout this thesis, inputs and rate of change of inputs are included in the cost function to address the fuel optimization. It is demonstrated that the fuel can be obtained by minimizing the cost function especially when the constraints are included in the problem formulation.

9. **Uncertainty & Disturbance Handling:** Imperfect initial condition knowledge, unmodeled dynamics, orbital disturbances, sensor drift, thruster mismatch, and signal time delays could all introduce uncertainties into relative state knowledge and control implementation accuracy. Feedback control has inherent robustness property to handle uncertainties, such as gain or phase margins. In this thesis, we particularly focus on systematically incorporate integral actions in the MPC formulation.

   Remark 9. Offset free docking in the presence of an unknown but constant disturbance is obviously necessary. Surprisingly, this is seldom done or emphasized in the existing literature for such applications. Within the MPC framework, integral actions can be included by augmenting the state vector. The details are given in Section 4.2.1: "*Handling Disturbances and Modeling Uncertainties*".

1.1.4 Space Servicing

The RVD capability enabled new space concepts. Specifically, robotics systems have merged with proximity operations, which is termed as *space-servicing*. The summary of past & upcoming space servicing missions are listed in Fig. 1.7.The red colored part shows the historic "sampled" missions that have successfully flown in space whereas the blue colored "unsampled" ones are yet to be achieved due to increased complexity. Although Fig. 1.7 dates back to 2010, only docking with another satellite in GEO orbit for life extension has been achieved on the historic 25th of 2020 when Northrop Grumman's MEV-1 docked with Intelsat 901. This mission is noted as "...beginning of a new era that will see robotic spacecraft giving new life to older satellites that are low on fuel or require repairs." [50]. Ever since the first space mission, space servicing has been a continuously attractive concept. Especially, in the last two decades, use-cases of RVD missions increased dramatically. Main application areas of RVD missions include, but not limited to,

- Assembly of large structures in orbit

- Servicing of spacecraft; supply experiments and other goods
- Inspection, payload and satellite deployment, manipulation, retrieval and maintenance
- Transport of crew & goods to/from a manned space station and landing on celestial bodies
- Re-orbiting & de-orbiting
- Asteroid explorations
- Sample and return

In view of the increasing number of space missions and advances in technology, it is anticipated that the RVD technology will play an even more important role in the future especially when asteroid mining operations, unmanned space missions and the number of space stations increase [51–53]. Explicit constraint handling capability of MPC is a game-changer opportunity to address both safety and fuel efficiency of the future space missions. Table 1.2 summarizes the constraints, the problem types, their existence in the thesis and the motivation of formulating them.

Table 1.2: The Summary of the Constraints

Constraint	Problem Type	Thesis Content	Motivation
Line-Of-Sight	Convex	Included	Safety
Collision Avoidance	Convex	Included	Safety
Thruster Limitation	Non-convex	Included	Safety - Fuel Efficiency
Obstacle Avoidance	Non-convex	Not included	Safety
Field-of-View	Non-convex	Not included	Safety
Plume Impingement	Non-convex	Not Included	Safety

With this in mind, this thesis develops and validates guidance and control strategies for motion planning for rendezvous and docking with uncooperative targets. In this scenario, a controlled vehicle will be also termed as *chaser spacecraft* and an uncontrolled vehicle to be captured is termed as *target spacecraft*. One of the main challenges is that such a scenario has never been successfully demonstrated in space and our optimization-based novel formulation will be the first strategy is tested in a 5-DOF rendezvous and docking experimental setup for dynamics and will be tested in a 13-DOF setup for kinematics validations experimentally, with a possibility of in-orbit demonstration in future.

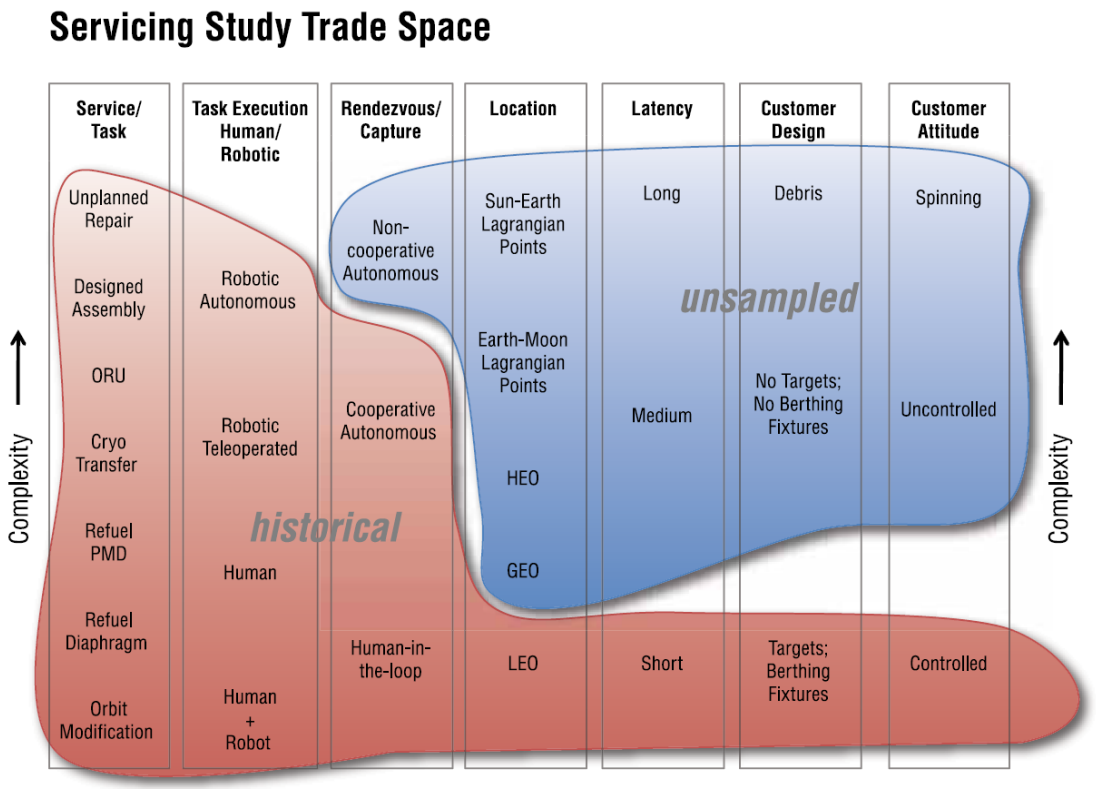

FIGURE 1.7: Servicing Study Trade Space Regions Covered by Historical Missions – This graphic summarizes the regions of the trade space diagram that have been sampled already (historical) or are yet to be sampled (unsampled) [5]

1.2 Motivational Examples

Spacecraft rendezvous and docking (RVD) missions are crucial phases for a number of astronautical missions. The capability of two or more spacecrafts to mechanically dock with each other enabled key maneuvers in spaceflights to come true such as manned lunar missions, in-orbit assembly of International Space Station , etc. Still, these missions were manually assisted by the crew of the space vehicles and the target vehicle was cooperative where further help was provided, e.i., sharing state information, control for attitude alignment and relative distance keeping. Use-cases of RVD missions are given previously, and now, its time to address the need of the current state of art, future applications, challenges, unresolved issues and research gaps in RVD missions and therefore emphasize the research direction in detail.

As motivating examples, one can consider the **RVD scenario depicted in Fig. 1.8** . It is seen that Space-X Dragon Cargo Ship is about to be captured by a robotic arm to be docked with International Space Station. Although RVD technology is

FIGURE 1.8: ISS Cargo Supply [1]

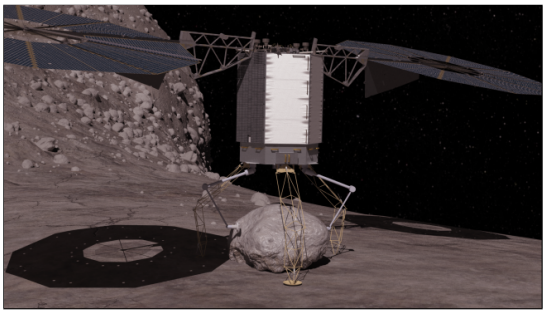

FIGURE 1.9: Asteroid Lander [6]

proven and widely studied, the cargo supply is not always fully autonomous but sometimes manual capture by a robotic arm controlled aboard ISS as depicted in Fig. 1.1 is required. In this scenario, enforcing **safety constraints** into the controller formulation would help to maintain the safety of the mission. **In another even more challenging example**, given in Fig. 1.9, where the target is not cooperative and the purpose of the chaser is to capture the target in orbit. Here, the chaser seeks a way to obtain information on the target's states because the target would not provide it. The uncertainties of the target, especially the angular rate, are challenges to be solved. Assuming on-board measurements and estimations are done, there is still a need to deal with the dynamic constraints of the system. These constraints can be collision avoidance, line-of-sight (LOS) or exhaust plume impingement avoidance. Therefore, such a guidance scheme requires relative state sensing and in-orbit trajectory generation which respects constraints.

In another example, consider the scenario demonstrated in Fig. 1.10 where a capture concept, which can be potentially used to mitigate space debris, is seen. Here, there is a negligible communication delay; however, the uncertainties of the target, mostly target states, is still high and target might be spinning or tumbling with a random rate. Moreover, time variant dynamic constraints such as feasible and safe approach corridor; line of sight constraint need to be respected. More details are given in Chapter 2 where challenges are further explained. Once again, such guidance scheme requires relative state sensing and in-orbit trajectory generation which complies with (respects) the constraints.

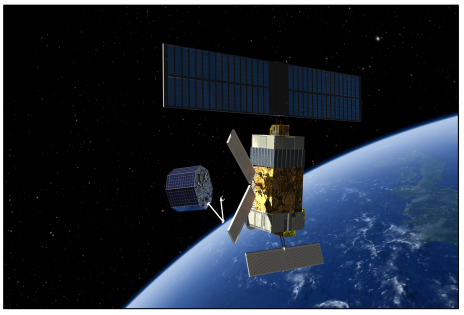

FIGURE 1.10: Robotic Capture Concept [7]

With this perspective; Guidance, Navigation and Control (GN&C) has vital importance [54–56] and despite given examples and capabilities envisioned to be in the near future, the logic behind rendezvous and docking with uncooperative targets to perform safe automated docking still needs to be developed. Particularly, recent technology demonstration attempts towards automated rendezvous and docking even with cooperative targets suggest that violating dynamic constraints as well as the uncertainties could result in catastrophic incidents. The first and only attempt of the in-orbit capture concept ended up with a failure to capture non-cooperative Spartan spacecraft with 2 $^\circ/s$ rotation rate during the STS-87 mission in 1997 [57]. Recently, the Demonstration of Autonomous Rendezvous Technology (DART) mission failed due to unexpected events, i.e., guidance navigation error and excessive fuel expenditure [9]. Eventually, these failures make it clear that autonomous rendezvous and docking missions must be established so that it can ensure that no-collision is guaranteed in the event of any failures, errors or uncertainties.

Today, there are solutions to concentrate on the full design process and conduct rapid design iterations that allows Software-In-The-Loop (SIL) and Hardware-In-The-Loop (HIL) simulations in real-time. However, there is still a need to conduct experiments where the actuators, sensors and processors are in the loop. Testing the RVD algorithms in zero-G environment is indeed expensive.

Throughout this thesis, we developed a convex optimization based Guidance and Control strategy that can respect the constraints, minimize the fuel expenditure, and is robust to uncertainties. The control strategy will be validated using state of the art experimental setups implementing real-time embedded optimization that addresses the gap between MPC theory and real missions. More details are provided in the literature review, Chapter 2, where challenges, current work across the globe with theory and implementation are explained in detail.

Before continuing, rendezvous and docking related terminology should be explained. The **chaser** or deputy satellite refers to the artificial spacecraft that will intentionally follow the required maneuvers to perform the proximity operation and finally mechanically dock with the target or chief spacecraft. In addition, there are a number of scenarios in RVD missions. The research gap and the most challenging case is where the target is a non-cooperative and possibly tumbling object. *Tumbling* refers to a satellite that has lost its control capability at least in one axis and rotates with a random rate; however, it has capability to communicate its states, i.e.,

attitude. Furthermore, *non-cooperative target* is a spacecraft that takes no control action to synchronize its attitude with the chaser or share information about its orientation in space. Hence, on-board perception or vision algorithms are also essential to complete in orbit capture missions. As an example of non-cooperative target, dead satellites or military satellites which attempt to get rid of the chaser will have no intention to share information. *Guidance* is the process of planning the translational and rotational motion of spacecraft trajectories in orbit. Hence, desired sets of states and associated control inputs, i.e., thruster force and reaction wheel torque, as a function of time. However, *control* is to keep spacecraft close to these trajectories using the real-time obtained state updates delivered by *navigation* sensors. Commonly, these three requirements/processes are called GN&C. In pure path planning, guidance can be separated and individually developed. Yet, in our approach, control and guidance will be coupled to obtain the optimum path while assuming that navigation state updates are provided. The orientation and rotational motion of target satellite has a critical impact on the guidance strategy. Orientation refers to the current attitude and attitude rates of the target where facing front meaning that the target spacecraft's docking port is facing towards the chaser. When its facing back, the chaser is no longer able to see the docking port [58]. In addition, for more complex scenarios such as a tumbling target, these definitions are no longer significant as the attitude of the target keeps changing with time.

1.3 Stages of Rendezvous & Docking Mission

The goal of this section is to introduce the different stages of rendezvous missions and to address challenges of these stages. A rendezvous and docking mission can be summarized in 5 main steps: *launch, phasing, far & close range rendezvous, and finally docking or capture* [8]. These stages have particular challenges and purposes regarding to guidance, navigation and control system of the follower spacecraft to achieve.

Phasing Stage After the launch stage, the launcher has brought the chaser to a 'virtual' target plane since the target's orbital plane will drift with time [8]. Fig. 1.11 illustrates that there are 2 main phasing stages followed by a far range

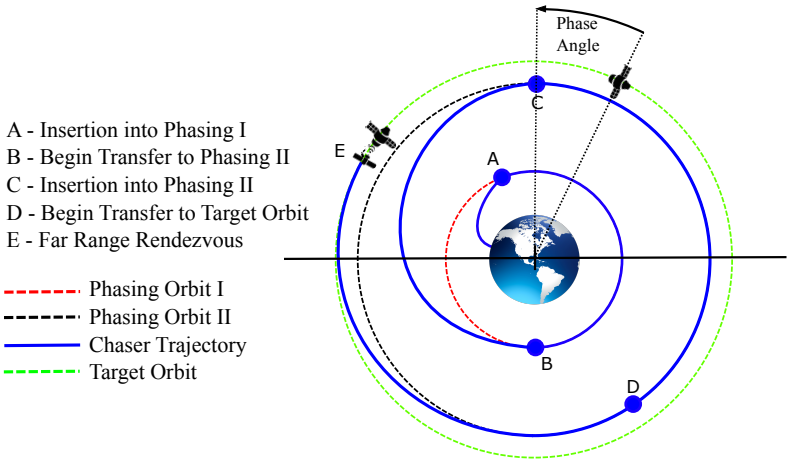

FIGURE 1.11: RVD Stages [8]

rendezvous. It is seen that chaser spacecraft is on a lower orbit (shown with "C") with an initial *phase angle*, behind the target. Absolute navigation sensors, such as GPS or ground-based navigation, are employed in the first phase and commands are directly sent from the ground station; therefore, autonomy is not needed or essential for this stage. The objective of the initial phasing stages is to reduce the phase angle by benefiting from the orbital mechanics laws that lower orbit has a shorter orbital period. In the second phasing stage, the chaser is transferred to the target orbit to proceed with the far range relative rendezvous stage.

Far Range Rendezvous This stage is also known as 'homing' that has an ultimate purpose of bringing the chaser in the vicinity of the target and achieve the relative position, velocity and if the possible angular rate conditions to be able to commence the close range rendezvous stage. The main responsibilities of this stage is to synchronize with the mission time-line, reach the target orbit and lessen the approach velocity. Unlike *phasing stage*, during the rest of the operations, relative measurements (radar, relative GPS, etc.) of distance, direction and orientation between chaser and target satellite will be taken into account. Furthermore, in the presence of a cooperative target, *far range rendezvous* is the stage where communication between chaser and target satellite is established.

Close Range Rendezvous Often called '*Closing*' and as stated in [8], close range proximity operation is generally investigated in two categories: a preparation phase from a few kilometers away from the target to final approach range and from

a few hundreds of metres to docking conditions. The ultimate goal of the closing stage is to prepare the chaser satellite to reach the final approach corridor or line of sight of the docking port while reducing the distance to the target. In other words, after the closing phase, chaser must be able to begin for the final proximity operation up to mating with adequate states: relative position & velocity, attitude and rates.

Final Approach The last proximity operation in RVD missions aims to bring the chaser from a few hundred meters to a position a few (1-3m) metres from the target in the presence of a robotic arm capture phase. This approach is also addressed as the final terminal translational guidance in [59]. It is stated that control accuracy is critical because of the extremely challenging capture tolerances [11]. For instance, in ESA *Advanced Guidance, Navigation and Control for Assembly of Large and Flexible Structures and Vehicles Project*, control requirements are specified as; For Docking/ Berthing modules: the lateral position error must be less than 5cm, the lateral relative velocity error must be less than 5mm/s and alignment error must be less than 2 degree. Moreover, unlike the previous stages where the distance between chaser and target is relatively high, in the final approach, guidance strategies have to guarantee that in the presence of fault in the actuators or any subsystem, the chaser does not follow a trajectory that ends up with a collision. Hence, rather than fuel optimality, **safety criticality** has the highest concern in this phase.

Furthermore, space systems operate in changing, dynamic and uncertain environments; therefore, contingent on undesirable factors such as atmospheric drag, solar pressure, third body perturbation, oblateness of Earth, space debris, etc. Moreover, the modeling uncertainty can arise during the emergency cases where system dynamics might go through crucial changes. Therefore, it is one of the main considerations in the controller designs to guarantee robust and satisfactory control while not only in the presence of modeling uncertainties of controlled spacecraft but also during lack of knowledge about the target vehicle. In addition, mismatch on the actuators, i.e., thrusters, or failure of any subsystem, i.e., wheels, must be included in our control strategy. In this case, as a part of the worst case scenario, fault tolerance must include detection, identification and solution strategy. Therefore, robustness analysis must be studied to ensure that the guidance strategy is robust enough to address imperfections in the system, such as unmodeled disturbances or measurement errors. In the work [60], details of rendezvous mission errors and

uncertainties are categorized in 4 main groups (initial condition error, unmodeled disturbances, sensor error and actuator error) with examples.

In addition to overall rendezvous final approach challenges, this thesis focused on proximity operations and docking with a non-cooperative target. To this extent, on top of all of the mentioned considerations, changing orientation of target, therefore, the docking port; the absence of communication and finally flexible modes of the target brings additional challenges to RVD mission.

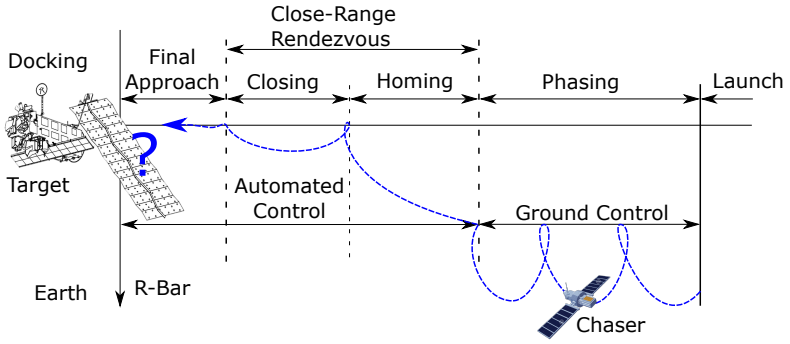

FIGURE 1.12: RVD Process [8, 9]

Capture & Manipulation This phase is also known as mating where the chaser is able to sense the target with its on-board sensors. Relative distance, velocity, attitude & attitude rates are critical in this phase. For instance, lateral relative velocity must be less than 0.001m/s for segments in the docking missions. Finally, this is the phase where a structural connection is achieved between chaser and target by either robotic arm or simply with the mating of docking ports.

1.4 Contribution of the Thesis

The objective of this thesis is to bridge the gap between the matured Linear Model Predictive Control theory and the final phase of an automated Rendezvous and Docking scenario, with a consideration for 6-DOF translational and rotational motion couplings, thruster configuration, constraints, real-time implementation issues and validation with experimental work. Hence the contributions of this thesis consist of development of methodologies and approaches to the problems arising from 6-DOF coupled control in real-time MPC implementations. The main contributions can be summarized as:

1. The thesis addressed the real-time implementation problems of spacecraft design and the corresponding problem formulation for embedded optimization. To this end, the *Inscribed Polygon Approach* (IPA) is developed and proposed to address the Quadratically Constrained Quadratic Programming (QCQP) problem arising in single-axis thruster configuration. It has been validated via simulations in Nonlinear High Fidelity Engineering Model (NHFEM). The algorithm can address the rendezvous and docking problem in both circular and elliptic orbits by employing Linear-Time Varying models. The proposed controller can well approximate the quadratic input constraint to full utilization of the thruster. In addition, requirements of advanced optimization methods and tools are relaxed. The QCQP can be approximated by QP and be solved using matured & reliable QP solvers for fast, real-time implementations.

2. This thesis also addresses the couplings of translational and rotational motion in close proximity operations, incorporating operational constraints which could arise in the real environmental problems such as safe Line-of-Sight and thruster's physical constraints, and external disturbances as well as the dynamic uncertainties. To this end, a constrained MPC with integral action using the dual quaternion to represent the spacecraft dynamics is formulated. As opposed to the traditional point mass approach, the proposed approach relaxes the Centre-Of-Mass assumption on the relative position of interest. It also addresses the practical real-time implementation of such control schemes. Using dual quaternion facilitates more general representation of docking port or grasping region of interest for potentially robotic operations. Lastly, integral action allows offset free docking capability in the presence of external disturbance and dynamic uncertainty within the tolerance level, an issue surprisingly not usually addressed in the current literature.

3. The strong cross-couplings of translational motion and rotational motion is addressed by the Model Predictive Control framework that has the capability to take into account Multi-Input and Multi-Output (MIMO) systems. In addition, thanks to the optimization theory behind, MPC can save fuel and respect the physical and geometric constraints in the application. Algorithms are developed accordingly. Also, in our formulation, the integral term is included in the design so that offset free docking operations can be achieved.

4. An important contribution of this thesis is the validation that the proposed controller can be implemented real-time on an experimental test bench in German Aerospace Center (DLR) [44, 45]. Therefore, this thesis bridges the gap between theory and real practice with hardware-in-the-loop tests. Specifically, the pioneering work which addresses the practical implementation of MPC using models that handles the coupling between translational and rotational dynamics via dual quaternions, multiple thruster allocation problem and constraints. The technical challenges of solving two separate optimization problem online & on-board and actuating the spacecraft with only thrusters are explained in Chapter 5. The work paves the way for future satellite servicing missions as it can save fuel & address safety concerns due to constrained optimization-based formulation. In addition, this work can enable agile maneuvers due to the thruster allocation strategy and full utilization capability thanks to the optimization theory behind.

1.5 Thesis Organization

1.5.1 Chapter 2: Literature Review

This chapter discusses the recent advances and future prospects of spacecraft position and attitude control for rendezvous and docking with MPC and other competitive paradigms. First, the challenges of the space missions are summarized, in particular, taking into account the errors, uncertainties and constraints imposed by the mission, i.e., spacecraft and on-board processing capabilities. The constraints are classified into two categories: physical and geometric constraints. Then, real-time implementation capability is discussed regarding the required computation time and the impact of sensor & actuator errors based on the Hardware-In-The-Loop (HIL) experiments. The rationales behind the scenarios definition are also presented in the scope of space applications as formation flying, attitude control, rendezvous & docking, rover steering and precision landing. The objectives of these missions are explained, and the generic constrained MPC problem formulation are summarized. Three key design elements used in MPC design: the prediction model, the constraints formulation and the objective cost function are discussed. The prediction models can be linear time invariant or time varying

depending on the geometry of the orbit, whether it is circular or elliptic. The constraints are presented as linear inequalities or in the conic form for input or output constraints. Moreover, the recent convexification techniques for the non-convex geometrical constraints (plume impingement, Field-of-View (FOV)) are presented in detail. Next, different objectives are provided in a mathematical framework and explained accordingly. Then, since MPC implementation relies on finding in real-time the solution to constrained optimization problems, computational aspects are also examined. In particular, high-speed implementation capabilities and HIL challenges are presented towards representative space avionics. This covers an analysis of future space processors as well as the requirements of sensors and actuators on the HIL experiments' outputs. The HIL tests are investigated for kinematic and dynamic tests where robotic arms and floating robots are used respectively.

1.5.2 Chapter 3: Relative Motion Dynamics & Dual Quaternions

In this chapter, there are two main parts. First, the relative motion dynamics between chaser and target spacecraft on an elliptic & circular orbit is provided. The literature concerning simplified State Transition Matrices (STM) for the propagation of the relative trajectories of two orbiting objects is presented with their particular solutions. Subsequently, the general nonlinear dynamics and kinematics models for attitude motion is derived. This includes the nonlinear models for orbiting satellites and experimental setups. After that, the couplings between translational and rotational motion are introduced. Next, definitions of the coordinate frames adopted in this thesis for the description of the orbital motion, for absolute and relative trajectory and attitude motions are accordingly explained. Secondly, a comprehensive introduction to unit and dual quaternion algebra is given. The mathematical preliminaries that includes all algebraic operations, frame transformations and properties of dual quaternions employed throughout the thesis are explained. One must note that the materials provided are from the field of mathematics and the background is not novel. Then, those background is employed to couple the translational motion with rotational motion. To this end, *dual inertia matrix*, an $8 - by - 8$ symmetric positive definite matrix is constructed from the mass and moment of inertia of the chaser spacecraft. The corresponding 6-DOF coupled nonlinear equations of motion is provided for actual orbiting simulations

and simplified zero-G experiments. Finally, the dual quaternion framework is developed and used to address the couplings of the model.

1.5.3 Chapter 4: Model Predictive Control for Spacecraft Rendezvous and Docking

This chapter covers the formulation of MPC for spacecraft assuming a full state feedback condition is available. Also, the benefits of MPC paradigm is provided as well as its disadvantages. This includes definitions and use of the three main components: prediction model, objective function and the constraints. The dynamic model is discussed in Chapter 3; the constraints are discussed in Chapter 2 where the challenges are presented. Because MPC paradigm is an optimal control technique, the desired closed loop is reflected in the choice of the objective function. One of the most common critics that MPC faces is the computational demands; thus, in this chapter, MPC using different classes of constrained quadratic optimization algorithms are investigated. This includes the condensing algorithms that are used to transform the original optimal control problem into QP problem in the MPC form and the state of the art QP solvers.

1.5.4 Chapter 5: Rendezvous and Docking Problem with Multiple Thruster Configuration

This chapter presents a Guidance and Control (G&C) strategy to address 6-DOF spacecraft attitude and position control for future Rendezvous and Docking (RVD) missions. Future RVD missions, specifically when the target is uncooperative, are challenging as geometric constraints and parameter uncertainties are both present. In addition, due to close proximity and potential angular motion of the target satellite, the point mass approach is no longer sufficient to represent the relative motion dynamics. Hence, throughout this chapter, the coupling between translational and rotational motion of spacecraft relative motion is addressed via Dual Quaternions and Piece-wise Model Predictive Control framework. The algorithm is developed such that the relative position of interest is no longer Centre-Of-Mass (COM) position of the target satellite but can be docking port or a predefined

grasping feature. Secondly, physical and geometric constraints are explicitly formulated and respected by formulating a constrained optimization problem. The proposed framework is real-time implementable because the control problem is formulated as a convex optimization problem. Simulation results show that the proposed algorithm is promising because it can respect the physical and geometric constraints and minimize the propellant consumption while coupling translational and rotational motion and still being real-time implementable.

1.5.5 Chapter 6: Dynamic Experiment Results

This chapter presents pioneer and novel dynamics experiments to test the Guidance and Control (G&C) strategy to address spacecraft maneuvering problems for future Rendezvous and Docking (RVD) missions. We formulated an offset free 6-DOF RVD problem and thruster allocation problem as two separate convex optimization problem and, solved them with active set and standard primal-dual interior-point methods. The proposed strategy allows safe and propellant efficient trajectories for space servicing missions including tasks such as approaching, inspecting and capturing. This work provides the validation test results of the G&C laws using a hardware-in-the-loop (HIL) setup with two robotic mock-ups representing the chaser and the target spacecraft. Through this chapter, the laboratory and the robots are introduced. Besides the challenges presented in Chapter 2, the thruster characteristics and sensor errors are presented in detail. The distinctive challenge is the allocation of the thrusters. The experimental setup has 16 unilateral thrusters that generate both force and torque values. Due to the multiplicative nonlinear coupling, the convex programming approach is posed to achieve the commanded force and torque values as a result of a 6-DOF motion planning algorithm. The results also cover a comparison between the proposed algorithms with the PD controller highlight the clear advantages of the MPC formulation.

1.5.6 Chapter 7: Conclusions and the Future Work

This chapter summarizes the work presented and emphasizes potential future research directions.

Finally, several appendices are given to provide completeness to the thesis besides the main scopes. These appendices include the relative motion dynamic models for a circular orbit, Clohessy-Wiltshere Equations, and an elliptic orbit, Yamanaka-Ankersen Equations.

Chapter 2

Literature Review

Summary: *This chapter discusses the recent advances and future prospects of spacecraft position and attitude control for rendezvous and docking with MPC and other competitive paradigms. First, the challenges of the space missions are summarized, in particular, taking into account the errors, uncertainties, and constraints imposed by the mission, spacecraft and, on-board processing capabilities. The constraints are classified into two categories: physical and geometric constraints. Lastly, real-time implementation capability is discussed regarding the required computation time and the impact of sensor & actuator errors based on the Hardware-In-The-Loop (HIL) experiments.*

From the beginning of spaceflight history, guidance and control for spacecraft maneuvers, such as docking and rendezvous, has been a crucial topic. Upon the launch of the construction of the ISS, joint maneuvers had also become an issue to be addressed for maintenance. Scientists approached these problems with a collection of different techniques.

In a control problem, the aim is to minimize the fuel consumption or mission time or to optimize the combination of them. Scientists have studied real-time online computations and offline presumed trajectory plans along with formal proofs for further academic applications. All of the methods, explained through an extensive literature survey that covers theory, simulation and experimental results.

2.1 Glideslope, R-bar and V-bar

A glideslope is a trajectory that employs an exponential decrease in velocity as the chaser spacecraft approaches the target body. A radial trajectory is labeled as an R-bar approach, and a trajectory in the forward velocity direction is called a V-bar approach. Conventionally, a trajectory does not consist of a direct glideslope. A spacecraft travels through way-points on a trajectory to make use of the natural dynamics and to minimize fuel consumption. There are multiple tracking and control methods tested on orbit and offered in the literature [61–69].

2.2 Sliding Mode and Phase-Plane

In both 3-DOF and 6-DOF space docking problems, Sliding Mode Controllers have proven to be reliable [70–75]. These controllers have an n-DOF state feedback form and they mostly ensure a linear convergence to a virtual sliding surface of order n-1. Sliding mode controllers also guarantee an exponential convergence after reaching the sliding surface. In the literature, phase-plane controllers are employed to address the rendezvous problem with a stat-feedback form by altering the gains with respect to the evaluation of the state [76, 77]. These methods do not explicitly accept path constraints, and they require probabilistic analysis to confirm constraint adherence. Despite the effective computation speed and guaranteed convergence, these techniques are not optimal for either fuel or time consumption. In [78], a novel Artificial Potential Function (APF) and Sliding Mode Control (SMC) paradigms are combined and a time-varying sliding mode strategy is used to address the time-varying motion constraints. Furthermore, adaptive SMC is employed to enable the achievement of RVD with uncooperative targets in the presence of constraints, disturbances and uncertainties. Even more recently, [79] shows that SMC can meet with the RVD requirements and a comparison study with MPC is conducted. In the comparison, it was demonstrated that previously proposed MPC approach in

[49] can not address RVD problems because the MPC formulation is to address regulation type of problem which does not allow to do reference tracking. However, when MPC is compared to SMC in [79] for a similar problem, precision landing on an asteroid, MPC shows superior performance with roughly 50% cut in the fuel use. This study demonstrates how MPC can be effective for space systems where the saving fuel plays a critical role but there is still developments required in the MPC formulations to address RVD problem.

2.3 Artificial Potential Functions

Similar to the sliding mode and phase-plane controllers, artificial potential functions are not optimal for either fuel or time; however, they allow path constraints in rendezvous and docking problems [80–85]. Artificial potential functions create high potential in areas where constraints would be violated and low potential in the rendezvous locations, which leads to augmented dynamics. A state feedback controller guarantees the convergence to the target location, but constraint adherence is still not absolute.

2.4 Genetic Algorithms

Genetic algorithms are used to optimize trajectories for fuel and time usage in rendezvous of spacecrafts. These trajectories mostly include a small number of ΔV burns, and they are for spacecraft in orbits of great difference [86–90]. They are specifically capable of finding global optima in non-convex problems with discrete variables. Disregarding the computational cost, they can also be used for a priory trajectories. However, genetic algorithms are not appropriate for real-time docking systems since the computation times are rather long due to the poor scaling of the solution times with the number and discretization level of variables used in those operations.

2.5 Search Methods

For the rendezvous and docking problem, general path planning methods that include exploring of diverse areas to find globally optimum solutions have also been developed. These methods have been developed for scenarios with and without obstacles. A^* search method has been used in planning of both 3-DOF [91, 92] and 6-DOF trajectories [93]. Rapidly exploring Random Trees (RRT^*) and other randomized search methods have been researched too [94–96]. Moreover, connectivity graph methods, dynamic programming [97], generalized Voronoi graphs [98], etc., have been employed.

2.6 Convex Optimization

An alternative to avoid the problems associated with non-convex optimization, is to convexify the constraints and cost function. A recent and interesting work presented in [99] proposes an algorithm and experimental results to guide the capture of a tumbling space object. A sequential convex programming is used to overcome non-convex constraints and nonlinear dynamics. As convex programming offers deterministic convergence properties, this algorithm is suitable for onboard implementation and real-time use. They divided the problem into 2 stages, system wide translational maneuver and internal reconfiguration. In other words, the translational motion is decoupled from the rotational motion and they are solved in two consecutive steps. What is more, the attitude motion is restricted to 1-DOF; therefore, the efficacy of the approach is arguable. Having said that, addressing the couplings between translational and rotational motion is still yet to be addressed.

2.6.1 Model Predictive Control

Constraint satisfaction and performance optimality are vital for the control problem. The control methods explained above are generally used in ground tests prior to a mission. For the missions employing these techniques, a trajectory or a set of way-points is assigned to the target spacecraft to follow. This trajectory does not respond to the changes such as the chaser diverging from its path or improper

modeling of dynamics. On the other hand, model predictive control (MPC) updates and optimizes the trajectory using the current state data of the chaser and target.

MPC has been studied thoroughly in the literature because of the compatibility with the rendezvous and docking problem while allowing constraint satisfaction [11, 47, 59, 100–114]. MPC typically implements a plan in a step by step manner. At each step, MPC implements the first phase of the generated plan, then re-optimizes the plan and employs the first step of the newly generated plan until a minimum objective function is achieved. Initially, the main objective was to control the power plants and refineries. Hence, MPC has been broadly used in the process industry, followed by automotive, aeronautics and now can be applicable to even more complex and critical space missions. The number of publications provides theoretical and practical approaches associated with MPC applications in the past. The remarkable ones can be Rawling's work [115] where an introductory tutorial is given and Allgower's effort is based on nonlinear MPC and moving horizon estimation [116]. In addition, [31] provides a comprehensive survey based on industrial MPC technology, including theoretical developments and solution strategies. The most recent publication that gives an overall view to MPC applications in space is by Hartley [39] which is a tutorial on MPC for spacecraft rendezvous. As can be grasped from the mentioned inspiring research, there is no particular study that encompasses MPC applications in space although it is known that space applications of MPC have resulted in outstanding successes [31].

The focus of this thesis is the application of MPC to G&C problems. In this chapter, an abbreviated history of MPC space studies, the evolution of the paradigm with most significant algorithms and implementations, initial MPC proposals in space for different use-cases and pioneer real applications are summarized stressing the contributions and novelties compared to former ones [31, 117] whilst keeping the focus applications in space and particularly, rendezvous and docking missions.

2.6.2 The Evolution of MPC for Space Systems

The advantages of MPC have drawn attention to applications in vehicle maneuvering problems in which the target regions do not need to contain equilibrium

points [118]. Today, formation flying, rover steering in Mars, powered descent for Mars landing, subsystem control such as reaction wheel and torquer, etc. employ MPC. In presenting the literature, our intention is to stress the significant features of different techniques & algorithms and detect the possible gap. With this understanding in mind, we first discuss the pioneer approaches to maneuvering space vehicles in space for control design while emphasizing their contributions.

Initially, Manikonda proposed control laws for formation keeping and attitude control with a combination of feedback linearization and MPC. The study overcomes singularities associated with local feedback linearization by incorporating the switching between coordinate frames [119]. Still, an assumption of "no coupling between each spacecraft" was made for the N-spacecraft formation flying case; therefore, the dynamics of the overall mission are represented with a collection of N sets of equations. It was realized that despite the constraints in the actuators, a future work must include a robust fault tolerant algorithm design in the presence of communication or sensor failures while benefiting from optimization of set points feature of MPC.

In this regard, vehicle maneuvers with guaranteed completion time and robust feasibility is studied by Richard and How [118]. Unlike the previous MPC approaches, this study proposes a formulation for MPC in which a maneuvering spacecraft and an aircraft are demonstrated. In order to solve trajectory optimizations, Mixed-Integer Linear Programming is used, allowing inclusion of non-convex avoidance constraints. The first contribution of the study is the formulation of MPC with general terminal constraints to ensure stability while MPC is used for steady state control. As a second contribution, a new strategy to achieve robustness is proposed. It is stated in [31] that better dynamic control allows the controlled variable set point to be moved closer to a constraint without violating it. While this is beneficial for performance, it also means that a small disturbance could push the state beyond the feasible region. In the presence of that, the trajectory optimization becomes infeasible and no control can be defined. Here the second innovation of the work comes, to avoid such situations modifications are derived; therefore, the optimization is always feasible as the disturbance stays within the known bounds. Previously, min-max problems or invariant set methods were used to achieve robustness [120, 121]. From this angle, one can realize the importance of the safety

concerns in space applications. Space systems operate in changing, dynamic and uncertain environment; therefore, contingent on undesirable factors such as atmospheric drag, solar pressure, third body perturbation, oblateness of Earth, space debris, etc. Moreover, the modeling uncertainty can arise during the emergency cases where system dynamics might go through crucial changes. Therefore, it is one of the main considerations in the controller designs to guarantee robust and satisfactory control while not only in the presence of modeling uncertainties of controlled spacecraft but also lack of knowledge about the target vehicle. In addition, mismatch on the actuators, thrusters, or failure of any subsystem, e.g., wheels, must be included in the control strategy. In the following, robustness to uncertainties, fault tolerance and lack of knowledge (i.e., dynamics of target) can be addressed regarding to the MPC capabilities and advantages over other methodologies. The current scope of the work is the formulation of the MPC to address for RVD problems. Hence, no more detail about robustness is required.

Regarding to the limited size of the space vehicles and extremely high operation costs, after handling the hard constraints, i.e., soft docking, obstacle avoidance, efficient fuel cost was one of the fundamental aim of using MPC in space applications [103, 122]. A pioneer study conducted by Breger and How [123] ensures safe trajectories for autonomous rendezvous of spacecrafts while keeping the fuel consumption optimized. They criticise the cost of imposing safety as an additional constraint that guarantees infinite horizon passive collision avoidance while enabling future docking retries. A formulation of convex collision avoidance was proposed to provide faster solutions but with an increasing fuel consumption. In another study, the European Mars Sample Return, it is demonstrated that MPC application is more fuel efficient with better trajectory compared to the current state of art control system High integrated multi-range rendezvous control system & Autonomous RendezVous and Docking (HARVD) [11]. Another European Project RobMPC (Robust Model Predictive Control for Space Constraint Systems), it was concluded that MPC is a reliable paradigm and applicable for space systems that have high dynamics such as wheeled autonomous unmanned rovers for planetary surface exploration. In [124], MPC was employed for guidance, trajectory control, and wheel traction and steering control. Moreover MPC paradigm is not only employed for ascending missiles or rockets, but also for the last phase of the launch missions; descending phase [125]. To this extend, in Carlo at al. [126], MPC real-time embedded technology is proposed to address powered descent. It

is suggested that adaptive & online model based controller is a key technology to handle mentioned problem. Another use-case of MPC is subsystem control, that is, reaction wheel. It has been pioneered by NTU and space application proven that MPC is an enabling technology for attitude control of nano-satellites [127]. Today, number of studies addressing attitude control of spacecraft problem is available and the number is increasing every day [128–130].

It is now clear that various studies have been conducted to assess the feasibility of model predictive control with a remarkable number of real-time space applications. In addition, NASA future GN&C Technology Assessment report for Planetary science missions suggests that using MPC for future applications would be beneficial as it can compensate modelling uncertainties, enables superior precision with feedback control and explicitly takes system behavior, i.e., constraints present in the system, into account for planning and control [131]. Similarly, ESA strongly suggest to European Space Industry to employ robust techniques for future space missions and MPC is the most favoured one due to the aforementioned advantages [132]. Though, in our specific problem; *"RVD with non-cooperative & possibly rotating space object"* is known and studied problem, there is not any successful space applications yet. Consequently, the strength of MPC to handle such diverse and complex constraints while providing robustness to the system in real-time applications appears promising for autonomous spacecraft control and guidance. As a result, we focus exclusively on model predictive control in this study.

The Rendezvous and Docking (RVD) technology dates back to the 1960s, when the Gemini program was initiated to test the RVD capability from 1962 to 1966. The ultimate purpose was landing on the Moon, hence, the whole Gemini mission can be considered as an experiment of RVD technology towards the "...giant leap for mankind". Despite the fact that there was a level of autonomy in the sensing and maneuvering towards RVD with the target, Neil Armstrong manually performed the rendezvous in a Gemini spacecraft and docked with an unmanned Agena target. Due to safety reasons, Americans preferred manual RVD missions whilst it did not take too long for Russians to accomplish the first fully autonomous RVD between Cosmos 186 and 188 back in 1967 [8].

Since then, the RVD technology has advanced and a number of automated missions accomplished [8]. However, the recent failure of the Demonstration for Autonomous

Rendezvous Technology (DART) spacecraft has revealed that, despite the great advances in RVD technology, several technical issues remain to be resolved even for RVD with cooperative targets. Thus, the high fidelity simulations, sensitivity analyses, and experiments have become prominent for space missions. Today, there are solutions to concentrate on the full design process and conduct rapid design iterations that allow Software-In-The-Loop (SIL) and Hardware-In-The-Loop (HIL) simulations in real-time. These studies bring a level of reliability to the algorithms but limited to the accuracy of the mathematical models. Hence, there is still a need in the final phase to conduct experiments where the actuators, sensors and processors are in the loop.

Testing the RVD algorithms in a zero-G environment is indeed expensive. To address this need, the Massachusetts Institute of Technology has developed miniaturized satellites, also known as Synchronized Position Hold Engage and Reorient Experimental Satellite (SPHERES), in collaboration with National Aeronautics and Space Administration (NASA). They consist of 12 thrusters, on-board sensors, and therefore able to conduct autonomous experiments without the necessity of humans in the loop as well as external sensors for localization. SPHERES can test distributed spacecraft missions such as formation flying, rendezvous & docking, and spacecraft autonomy aboard ISS. In [133], the H_∞ controller was implemented to take into account the uncertainties of the real system in a 6-DOF environment aboard the International Space Station (ISS). However, the controller fails in the criteria of zero overshoot. In [134], the algorithm on-board SPHERES has been advanced with the MPC paradigm to evaluate the performance in the presence of thruster failures which makes the system under-actuated. It has been demonstrated that MPC is robust to thruster failures and provided improved performance when compared to a simple path planning algorithms while addressing 6-DOF fuel optimal motion planning problem. Still, the couplings between translational and rotational motion and, constraints are not explicitly handled. Overall, despite the miniature size of SPHERES, experimenting RVD technology in Zero-G is an expensive, demanding and time-consuming test strategy.

Recently, the test setups on-ground (1-g) for multiple spacecraft dynamics and kinematics experiments have become mature and reliable test methods that can save a remarkable amount of time and experiment cost when compared to Zero-G experiments. However, despite the fact that running tests in 1-g environment

brings a certain level of conceptual proofs, it is not an easy endeavour as it brings additional constraints and challenges. Briefly, majority of the spacecraft simulators in 1-g are free-floating robots on a flat surface that could be potentially made of granite, glass, epoxy, etc. Thus, depending on the design, those robots can have 3, 5 or 6-DOF consisting of an upper attitude stage, lower translational platform and an air-bearing in between. For translational and rotational motion, double integrator dynamics model is employed. One could argue that the double integrator neither represents the 3-body relative motion problem in-orbit nor landing on an asteroid. However, the robots are capable to test the dynamic couplings, actuator misalignment & imperfections, sensor errors, delays and on-board processing capabilities.

Past experiments conducted in the Test Environment for Applications of Multiple Spacecrafts (TEAMS) laboratory, robots with 3-DOF (TEAMS_3D) have been used to demonstrate rendezvous and docking with uncooperative targets with unconstrained MPC design with double integrator based, decoupled translational and rotational motion model [135]. Using a double integrator as a prediction model, an unconstrained MPC was formulated and solved online. The results demonstrated that MPC is a potential paradigm for approaching uncooperative & tumbling targets. To address the Line-Of-Sight constraints for safe approach, soft docking constraint for overshoot-free docking, input constraints for thruster limitations: a constrained MPC framework was formulated in [136]. In addition in [136], a rotating hyper-plane method is employed to convexify obstacle avoidance constraints and Nonlinear MPC is formulated to solve the original non-convex problem via nonlinear solver. However, the nonlinear optimal control problems and solutions in [136] do not guarantee to be solved in polynomial time because they may be stuck with local optimum points that can eventually result in a failure of missions. Moreover, due to high computation time, real-time implementation requirements may not be met. Next, the enforced LOS constraints are formulated for the 2D case and can not be extrapolated into 3D with the proposed geometric approach of [136]. In [99], robotic capture of uncontrolled & tumbling satellite is tested with a real-time implementable convex programming algorithm.

In short, the proximity operation tests conducted with 3-DOF robots have been useful to evaluate the performance with double integrator dynamics and constrained real-time optimization formulation [99, 135, 136]. Speaking of the dynamics point

of view, there are a number of setups that have upper attitude stage which are similar to real satellite nonlinear attitude dynamics. Those vehicles consist of 3-DOF upper attitude stage and 2 or 3-DOF translational stage that shows a better representation of an actual orbiting satellite. Hence, the previous work [137] and the current work reported in this thesis used the robots with 5-DOF namely $TEAMS5D$. These robots have an upper attitude stage with 3-DOF and lower translational platform with 2-DOF. LQR based tuning for PD type of controllers are employed for coordinated attitude and orbit control in the formation flying in elliptic orbit applications [137].

There exist a number of spacecraft simulators with 5-DOF; however, the progress is still on-going and [138–141] are the main examples of the existing setups around the world yet to be tested for RVD applications. More details of planar air bearings experimental setups can be found at [142]. In [143], an additional degrees of freedom is included for translational motion along the z-axes (along gravitational acceleration direction) and real-time sub-optimal control algorithm for controlling 6-DOF spacecraft simulator is introduced. The employed algorithm is Linear-Quadratic-Regulator (LQR) in which the gains are recomputed and updated at each time step. However, the controller is used for reference tracking problem instead of trajectory generation and were not able to address the constraints of the system because of the limitations of LQR theory. Lastly, the 6-DOF dynamics have been separately considered where the cross-couplings of attitude dynamics and translational dynamics are neglected [143].

In [49, 144], MPC and Dual quaternions were employed for landing 2-body problems namely, landing on a Mars and an Asteroid. The proposed Piece-Wise Affine (PWA) modelling strategy in [49, 144] is also used in this thesis. However, the problem formulations in [49, 144] are unable to address the RVD problem because of the cost function, the dynamic model and the special case of single-axis thruster configuration differs from our 16 thrusters configured spacecraft. The experimental setup used in this thesis, $TEAMS5D$, consists of 2 robots representing a controlled chaser satellite and uncontrolled target satellite with 16 thrusters. More details will be given in the following section but the main difficulty is the allocation of thrusters as the same thrusters can be used for both translational and rotational motion in which the commands may conflict if the couplings between thrusters are not explicitly considered.

Still, 3-D Experimental demonstration of constrained Guidance strategy for given scenario has never been tested on Earth in 3-D environment because of the immature guidance technology. However, the following space agencies have experimental setups similar to Thales Alenia Space rendezvous & docking facility. Probably, they are already working on robust capture techniques to be tested; nevertheless, there is not any published yet.

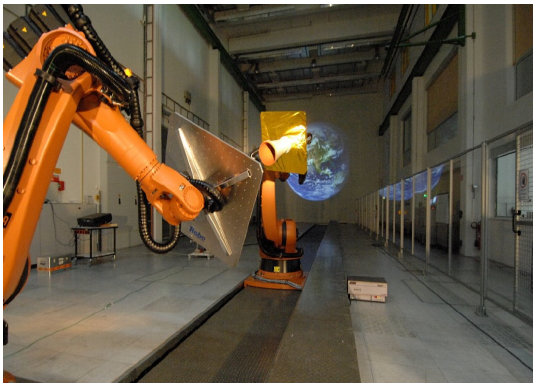

FIGURE 2.1: Robotic Based German Space Agency Rendezvous Simulator [10]

FIGURE 2.2: GMV, Spain Robotic Based Rendezvous & Docking Simulator [11]

Rendezvous and docking simulators have become popular in the world. For instance, apart from Thales Alenia Space, in Fig. 2.2 and 2.1, two other European Space Industry owned robotic simulators can be seen. The idea behind these three facilities is similar; two robotic arms have six degrees of freedom and one of them has additional translational motion capability up to 25m where a robot can simulate proximity operations in space. Generally, these robotic manipulators are used for the most critical phases of RVD missions. For instance, on the one hand, European Proximity Operations robotic based simulator hosted by German Space Agency (DLR) has been developed to test in orbit RVD sensors such as cameras whereas GMV RVD simulator facility was employed to run simulations for European *Mars Sample Return Mission* [11]. In this facility, both classical High-Integrity Autonomous RVD Control System and MPC were tested to compare the performances. It was concluded that MPC is an attractive tool for such applications where autonomy, optimal path and safety is crucial. Especially regarding the fuel consumption, MPC shows superior results after verification and validation with Monte Carlo simulations where uncertainties in the relative motion dynamic models, measurement and actuator errors together with a number of different scenarios are tested.

Similar facilities exist also in Hong Kong, USA and Canada and the studies [145–147] give details about their experiments. Again, none of them employed advanced guidance & control strategy to address RVD with uncooperative objects. The one in Hong Kong does not have a translational motion capability; still, they have demonstrated that these robotic arms can successfully capture an object neglecting orbital mechanics effect and in 1D motion.

In addition, Although DLR, collaborates with TU Delft and TU Munich or GMV with the University of Cambridge and the University of Bristol, not every university has access to such advanced robotics test facilities. To address this problem, Stanford University has started developing it's own 6-DOF experimental setup. Yet, the design does not cover the combination of chaser & target combination of relative motion to be further followed by in-orbit capture or docking but it is on-ground 3D zero-G experimental setup to demonstrate kinematics of the system [148].

Eventually, having all the experimental setups capabilities and their previous experiences, it can be stated that space industry and academia have been putting enormous effort on grounds simulations and tests for RVD problem. Still, as mentioned the applications were limited to cooperative target scenarios such as Mars Sample Return Mission. In addition, having the motivation of NASA and ESA, there is still a need for Model Predictive Control formulation and tests for space servicing missions, especially for docking or capture of non-cooperative, tumbling space objects. One can note that in 2D experimental facilities, orbital mechanics is ignored and the motion capability of robots is limited. Although a number of experimental studies have been conducted in 2D, current requirements are not satisfied with those setups.

The rationales behind the definition of the scenarios are also presented in the scope of space applications as formation flying, attitude control, rendezvous & docking, rover steering, and precision landing. The objectives of these missions are explained, and the generic constrained MPC problem formulation are summarized. Three key design elements used in MPC design: the prediction model, the constraints formulation and the objective cost function are discussed. The prediction models can be linear time-invariant or time-varying depending on the geometry of the orbit, whether it is circular or elliptic. The constraints are presented as linear inequalities or in the conic form for input or output constraints. Moreover, the

recent convexification techniques for the non-convex geometrical constraints (i.e., plume impingement, Field-of-View (FOV)) are presented in detail. Next, different objectives are provided in a mathematical framework and explained accordingly. Third, because MPC implementation relies on finding in real-time the solution to constrained optimization problems, computational aspects are also examined. In particular, high-speed implementation capabilities and HIL challenges are presented towards representative space avionics. This covers an analysis of future space processors as well as the requirements of sensors and actuators on the HIL experiment outputs. The HIL tests are investigated for kinematic and dynamic tests where robotic arms and floating robots are used respectively.

Chapter 3

Relative Motion Dynamics & Dual Quaternions

In this chapter, there are two main parts. First, the relative motion dynamics between chaser and target spacecraft on an elliptic & circular orbit is provided. The literature concerning simplified State Transition Matrices (STM) for the propagation of the relative trajectories of two orbiting objects is presented with their particular solutions. Subsequently, the general nonlinear dynamics and kinematics models for attitude motion is derived. This includes the nonlinear models for orbiting satellites and experimental setups. After that, the couplings between translational and rotational motion are introduced. Next, definitions of the coordinate frames adopted in this thesis for the description of the orbital motion, for absolute and relative trajectory and attitude motions are accordingly explained. Secondly, a comprehensive introduction to unit and dual quaternion algebra is given. The mathematical preliminaries that includes all algebraic operations, frame transformations and properties of dual quaternions employed throughout the thesis are explained. One must note that the materials provided are from the field of mathematics and the background is not novel. Then, those background is employed to couple the translational motion with rotational motion. To this end, dual inertia matrix, an $8-by-8$ *symmetric positive definite matrix is constructed from the mass and moment of inertia of the chaser spacecraft. The corresponding 6-DOF coupled nonlinear equations of motion is provided for actual orbiting simulations and simplified zero-G experiments. Finally, the dual quaternion framework is developed and used to address the couplings of the model.*

3.1 Translational Dynamics

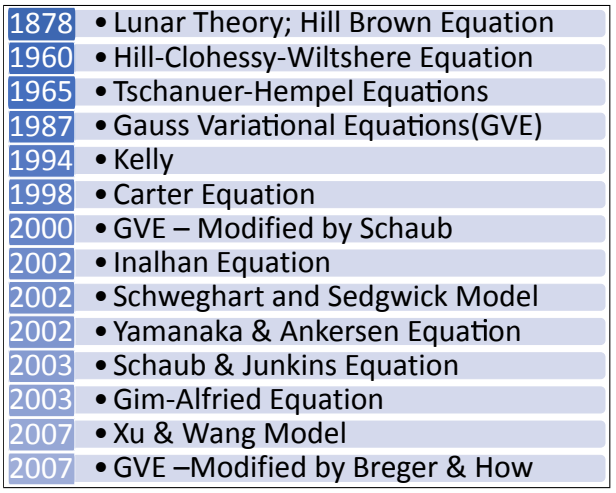

FIGURE 3.1: Most Employed Relative Dynamic Models in Chronological Order [12–14]

The effort behind mathematically explaining the relative motion of two orbiting satellites or objects is exhaustive in order to develop and automate mainly formation flying, RVD missions' design, guidance and control strategies. Initially, in 1878 American mathematician George William Hill came up with an approach explaining the Moon's motion relative to the Earth [149]. After that, in 1960, Hill Equations were further developed by two Mathematician, Clohessy and Wiltshire, for Apollo mission which are called the best and well known model for relative satellite motion [150]. Linearized models were sufficient to complete the mission since the Apollo Crew were also in charge of the critical phases; rendezvous and docking. However, the main disadvantage of HCW Equations is, it is applicable only on circular orbit in other words, can be employed to form a Linear Time-Invariant (LTI) state-space model of relative motion dynamics. In this case, orbital mechanics takes place. HCW Equations are based on the assumption of having a target with *eccentricity(e) = 0*, there are no external forces and the separation between radial and out-of-plane is small. On the other hand, it was proved by Inalhan that the assumption of perfectly circular orbit with *e=0* can cause remarkable prediction errors for cases that has an eccentricity as small as *e=0.005* [151]. That's why, specification of orbit is essential in the relative motion model selection phase.

HCW Equations have kept its popularity as it is a direct ordinary differential equation model. In 1965, Tschauner and Hempel further developed the equations to account for orbital perturbations. Because it was realized that the second-order J_2 effect, acceleration felt by a satellite due to the oblateness of the central body of the orbit (i.e., Earth), is the dominant perturbation especially for long term formation flying missions. Therefore, a number of studies have focused on derivations

that consider the J_2 effect [152–155]. Moreover, today comprehensive mathematical models and algorithms are available to approach nonlinearity of the space missions [156, 157].

In summary, theory comparisons are provided below:

TABLE 3.1: Theory Comparison [29]

Theory	Eccentricity	J_2 Effect	Nonlinearity
Clohessy & Wiltshere	e=0	No	No
Lawden	$0 \leq e < 1$	No	No
Gim-Alfriend	$0 \leq e < 1$	Yes	No
Small Eccentricity	$e \ll 1$	Yes	No
Yan-Alfriend	$0 \leq e < 1$	Yes	Yes

As can be seen from the Table 3.1, after HCW Equations, mathematicians not only derived the mathematical models for eccentric orbit but also included nonlinearities.

Taking all the considerations into account; eventually, formation flying missions has constructed the background for RVD/Berthing missions. The following chart illustrates ways of classifying linearized rendezvous studies which can be found in the literature and the next section will explain RVD/Berthing in detail [156, 157]. The work done by Dan Wei categorizes relative motion dynamics models in three main groups; Ordinary differential equation model, solution-based models & state transition matrix [158]. Yet, in our approach, we classify the models regarding its orbital geometry, whether elliptic or circular orbit, therefore, whether time variant or invariant. In Chapter 4, a case study of a target satellite orbiting in a circular orbit will be investigated. Initial ultimate goal is to demonstrate that our approach is capable of handling input and output constraints. Therefore, it was determined to consider Clohessy-Wiltshere relative motion equations as a starting point and Appendix A.1.1 defines the derivation, linearization, and discritization of the HCW relative motion model. Yet, Fig. 3.1 gives an overview of popular relative motion dynamic models. Later, the formulation of MPC is extended to Linear-Time-Varying form such that the state transition matrix to formulate relative motion in elliptic orbit can be employed as a prediction model.

Now, assuming that the motion is under the effect of gravity field and thruster forces, the original nonlinear equations of motion for chaser spacecraft can be

expressed in the vector form as [159]

$$\ddot{\mathbf{r}} = -\mu \frac{\mathbf{r}}{r^3} + \frac{\mathbf{F}}{m} \tag{3.1}$$

where m is the mass, $\mathbf{r}$ is the position vector and $\mathbf{F}$ is the applied control force to the spacecraft, and μ is the gravitational constant of Earth calculated by $\mu = GM$ where G is the universal gravitational constant and M is the mass of the Earth. Regarding the formulation of the 1-g experimental setup, the translational dynamics is assumed to be expressed with a double integrator and can be written in the inertial frame $\mathbf{N}$ as

$$\frac{\mathbf{F_t}}{m} = \ddot{\mathbf{t}},\ \mathbf{t} \in \{x, y, z\} \tag{3.2}$$

where $\mathbf{F_t}$ is the force input along the direction of $\mathbf{t}$ axis. Because dual quaternions couples translation dynamics with kinematics, expressing them in the same reference frame is needed. Throughout this thesis, the body frame of the Chaser is considered as a base. Hence, Eqn. (3.2) expressed in the Inertial frame can be written in the chaser's rotating body frame with the following $Transport\ Theorem$.

Theorem 1. [160]: Let $\mathcal{N}$ and $\mathcal{C}$ be the Inertial and chaser's body frames with a relative angular velocity vector of $\omega_{\mathcal{C}/\mathcal{N}}$, and let $\mathbf{r}$ be a generic vector; then the derivative of $\mathbf{r}$ in the N frame can be related to the derivative of $\mathbf{r}$ in the C frame as

$$\frac{^{\mathcal{N}}d(\mathbf{r})}{dt} = \frac{^{\mathcal{C}}d(\mathbf{r})}{dt} + \omega_{\mathcal{C}/\mathcal{N}} \times \mathbf{r} \tag{3.3}$$

Proof: [160].

3.2 Rotational Dynamics

Next, the rotational dynamics can be approximated with Euler's equations in Chaser's body frame $\mathbf{C}$ as

$$\mathbf{T} = \frac{d}{dt}(J\omega) + \omega \times J\omega \tag{3.4}$$

where $\mathbf{T}$ is the torque vector expressed in the body frame [161], J is the moment of inertial matrix along with body frame and ω is the angular velocity. In TEAMS5D

simulators, the torque actuation is achieved by the thrusters and the reaction wheels. Eventually, the Eqn. (3.4) evolves into

$$\mathbf{T_{th}} - \mathbf{T_{rw}} = \frac{d}{dt}(J\omega) + \omega \times (\mathbf{I}\omega + h_{rw}) \tag{3.5}$$

where $\mathbf{T_{rw}}$ is the torque commanded by the reaction wheels and h_{rw} is the stored momentum. Eqn. (3.5) is used for initial attitude balancing only whereas for 6-DOF freedom problem, Eqn. (3.4) is employed. If we can now assess the nonlinear attitude dynamics given in Eqn. (3.4). One can note that for a rigid body with a constant angular rate, $\dot{\omega} = 0$, the Eqn. (3.4) becomes

$$\mathbf{T} = \omega \times J\omega \tag{3.6}$$

showing that torque-free constant angular rate can be achieved if and only if $J\omega$ is parallel to ω which occurs when ω is along with the principal axis of the rigid body. This information will be used in the design of a consistent cost function that would allow off-set free tracking or misalignment free RVD operations.

3.3 Reference Frames

It is necessary to define the coordinate frames adopted in this thesis for the description of the orbital motion, for absolute and relative trajectory and attitude motions. Therefore, the relations of these motions to geometric points of interest on the spacecraft, e.g., the sensors, docking ports, can be explained mathematically [8]. Each frame consists of its own origin O_i and set of three orthogonal vectors $x_i,\ y_i,\ z_i$. Throughout this thesis, two types of coordinate frames are employed:

1. **Inertial Frame** is defined to describe the motion relative to a non-accelerating frame and expressed as $\mathcal{N} = (O_\mathcal{N},\ x_\mathcal{N},\ y_\mathcal{N},\ z_\mathcal{N})$ where the origin $O_\mathcal{N}$ is defined in the centre of the granite table.

2. **Spacecraft Body Frame** for both chaser and target ($\mathcal{C}$ & $\mathcal{T}$) satellites are defined to express attitude and motion relative to its centre of mass. If we consider the chaser's body frame $C = (O_\mathcal{C},\ x_\mathcal{C},\ y_\mathcal{C},\ z_\mathcal{C})$, where $O_\mathcal{C}$ is located at the centre of mass and, $(x_\mathcal{C},\ y_\mathcal{C},\ z_\mathcal{C})$ are coincident with the corresponding principal inertia axis of the satellite. The same definition applies to the $\mathcal{T}$.

3.4 Dual Quaternions

In this section, a comprehensive introduction to unit and dual quaternion algebra is given. The mathematical preliminaries that includes all algebraic operations, frame transformations and properties of dual quaternions employed throughout the thesis are explained. One must note that the materials provided are from the field of mathematics and the background is not novel. Nevertheless, for the sake of the completeness of the thesis, the Lemmas & Theorems and corresponding proofs are provided. Then, those background is employed to couple the translational motion with rotational motion. To this end, *dual inertia matrix*, an $8-by-8$ symmetric positive definite matrix is constructed from the mass and moment of inertia of the chaser spacecraft. The corresponding 6-DOF coupled nonlinear equations of motion is provided for actual orbiting simulations and simplified zero-g experiments.

3.4.1 Unit Quaternions

The formulation of spacecraft dynamics and control problems includes considerations of kinematics; description of motions. Quaternions, also known as Euler Parameters consists of 4 elements and can be defined as $q = q_1\hat{i} + q_2\hat{j} + q_3\hat{k} + q_0$, where $q_1,\ q_2,\ q_3,\ q_0\ \in \mathbf{R}$ and satisfies: $\hat{i}^2 = \hat{j}^2 = \hat{k}^2 = -1,\ \hat{i} = \hat{j}\hat{k} = -\hat{k}\hat{j},\ \hat{j} = \hat{k}\hat{i} = -\hat{i}\hat{k}$, and $\hat{k} = \hat{i}\hat{k} = -\hat{k}\hat{i}$. Throughout this thesis, the unit quaternion notation will be denoted as $q = [\mathbf{q}^T, q_0]^T$ where $\mathbf{q} = [q_1\ q_2\ q_3]^T\ \in \mathbf{R}^3$ and $q_0 \in \mathbf{R}$ are the vector and scalar parts of the unit quaternion and, satisfies the constraint $q_0^2 + \mathbf{q}^T\mathbf{q} = 1$. Lastly, a unit quaternion with zero vector part is specified as *scalar quaternion* and a quaternion with zero scalar part is specified as a *vector quaternion*. The four *quaternion* elements can be written in vector notation as

$$q = \begin{bmatrix} e_1 sin(\theta/2) \\ e_2 sin(\theta/2) \\ e_3 sin(\theta/2) \\ cos(\theta/2); \end{bmatrix} \tag{3.7}$$

where $\mathbf{e} = (e_1, e_2, e_3)$ is the eigenaxis vector and θ denotes the rotation angle around that axis such that $\mathbf{q} = \mathbf{e}sin(\theta/2)$. Next, the algebraic properties and operations can be explained.

Quaternion Product: The product of two unit quaternions are given as

$$q \otimes p = \begin{bmatrix} q_0\mathbf{p} + p_0\mathbf{q} + \mathbf{q} \times \mathbf{p} \\ q_0 p_0 - \mathbf{q}^T\mathbf{p} \end{bmatrix} = \underbrace{\begin{bmatrix} S(\mathbf{q}) + q_0\mathbf{I_{3x3}} & \mathbf{q} \\ \mathbf{q}^T & q_0 \end{bmatrix}}_{[q]_\otimes} \underbrace{\begin{bmatrix} \mathbf{p} \\ p_0 \end{bmatrix}}_{p} \triangleq [q]_\otimes p \tag{3.8}$$

where q & p are unit quaternions, $\times$ symbol refers to vector cross product and,

$$S(\mathbf{q}) = \begin{bmatrix} 0 & -q_3 & q_2 \\ q_3 & 0 & -q_1 \\ -q_2 & q_1 & 0 \end{bmatrix} \in SO(3),\ S \in R^{3\times 3}. \tag{3.9}$$

is the skew symmetric matrix.

Quaternion Cross Product: The cross product of two unit quaternions can be given as

$$q \times p = \begin{bmatrix} q_0\mathbf{p} + p_0\mathbf{q} + \mathbf{q} \times \mathbf{p} \\ 0 \end{bmatrix} = \underbrace{\begin{bmatrix} S(\mathbf{q}) + q_0\mathbf{I}_{3x3} & \mathbf{q} \\ 0_{1x3} & 0 \end{bmatrix}}_{[q]_\times} \underbrace{\begin{bmatrix} \mathbf{p} \\ p_0 \end{bmatrix}}_{p} \triangleq [q]_\times p. \tag{3.10}$$

Alternatively, after defining the *conjugate* property of quaternions as $q^* = [-\mathbf{q}^T q_0]^T$, standard quaternion and quaternion cross products can be also written as

$$q \otimes p \triangleq [q]_\otimes p \triangleq [p]^*_\otimes q \tag{3.11}$$

$$\triangleq \underbrace{\begin{bmatrix} S(\mathbf{q}) + q_0\mathbf{I}_{3x3} & \mathbf{q} \\ \mathbf{p}^T & p_0 \end{bmatrix}}_{[p]^*_\otimes} \underbrace{\begin{bmatrix} \mathbf{q} \\ q_0 \end{bmatrix}}_{q} \text{ and,} \tag{3.12}$$

$$q \times p \triangleq [q]_\times p \triangleq [p]^*_\times q \tag{3.13}$$

$$\triangleq \underbrace{\begin{bmatrix} S(\mathbf{q}) + q_0\mathbf{I}_{3x3} & \mathbf{q} \\ 0_{1x3} & 0 \end{bmatrix}}_{[p]^*_\times} \underbrace{\begin{bmatrix} \mathbf{q} \\ q_0 \end{bmatrix}}_{q} \tag{3.14}$$

Finally, the algebraic properties of quaternion operations can be summarized in Table 3.2 below.

TABLE 3.2: Unit Quaternion Operations

Operation	Definition
–	$q = (\mathbf{q}, q_0)$
Addition	$q + r = (\mathbf{q} + \mathbf{r},\ q_0 + r_0)$
Multiplication by a scalar	$\gamma q = (\gamma\mathbf{q},\ \gamma q_0)$
Conjugate	$q* = (-\mathbf{q},\ q_0)$
Quaternion product	$q \otimes r = (\ q_0 r_0 - \mathbf{q}\cdot\mathbf{r},\ q_0\mathbf{r} + r_0\mathbf{q} + \mathbf{q}\times\mathbf{r})$
Dot product	$q \cdot r = (q_0, r_0 + \mathbf{q}\cdot\mathbf{r},\ 0_{3x1})$
Cross product	$q \times r = (q_0\mathbf{r} + r_0\mathbf{q} + \mathbf{q}\times\mathbf{r}, 0)$
Norm	$\|q\| = \sqrt{\mathbf{q}\cdot\mathbf{q}}$

3.4.2 Unit Dual Quaternions

Unit dual quaternions are derived from unit quaternions but can also address the 6-DOF spacecraft motion by including translational motion and couplings with rotational motion. The concept was pioneered by W. Clifford and today mainly used for kinematics of rigid bodies such as robotics [162–164]. A unit dual quaternion consists of two quaternions and can be defined as

$$\tilde{q} = q_1 + \epsilon q_2 \text{ or } \tilde{q} = \begin{bmatrix} q_1 \\ q_2 \end{bmatrix}_{8\times 1} \tag{3.15}$$

where q_1 and q_2 are the real and dual parts constructing the dual number with dual operator ϵ that satisfies

$$\epsilon^2 = 0,\ \epsilon \neq 0,\ 1\cdot\epsilon = \epsilon\cdot 1 = 1 \text{ and, } \epsilon\cdot 0 = 0\cdot\epsilon = 0. \tag{3.16}$$

Throughout the thesis, $\tilde{\mathbf{R}}^{\mathbf{8}}$ is adopted to express the set of dual numbers as given in Eqn. (3.15). Furthermore, it is possible to do reference frame transformation with quaternion algebra. In particular, the dual quaternions can be also expressed in the body frame of Chaser satellite with respect to the inertial frame as

$$\tilde{q}_{\mathcal{C}} = q_{\mathcal{C}} + \epsilon\frac{1}{2} r_{\mathcal{N}} \otimes q = q_{\mathcal{C}} + \epsilon q_{\mathcal{C}} \otimes \frac{1}{2} r_{\mathcal{C}}. \tag{3.17}$$

where $r_{\mathcal{C}}$ is the relative position vector in the chaser's body frame, $r_{\mathcal{N}}$ is the relative position vector in the Inertial frame and $q_{\mathcal{C}}$ is the unit quaternion representing the rotation. Hereafter, the algebraic properties and operations of *unit dual quaternions* can be explained.

Unit Dual Quaternion Product: The product of two unit dual quaternions can be given as

$$\tilde{q}\tilde{\otimes}\tilde{p} = \begin{bmatrix} q_1 \otimes p_1 \\ q_1 \otimes p_2 + q_2 \otimes p_1 \end{bmatrix} = q_1 \otimes p_1 + \epsilon(q_1 \otimes p_2 + q_2 \otimes p_1) \tag{3.18}$$

$$= \underbrace{\begin{bmatrix} [q_1]_{\otimes} & 0_{4\times4} \\ [q_2]_{\otimes} & [q_1]_{\otimes} \end{bmatrix}}_{[\tilde{q}]_{\tilde{\otimes}}} \begin{bmatrix} p_1 \\ p_2 \end{bmatrix} \triangleq [\tilde{q}]_{\tilde{\otimes}}\tilde{p}, \tag{3.19}$$

$$= \underbrace{\begin{bmatrix} [p_1]^*_{\otimes} & 0_{4\times4} \\ [p_2]^*_{\otimes} & [p_1]^*_{\otimes} \end{bmatrix}}_{[\tilde{p}]^*_{\tilde{\otimes}}} \begin{bmatrix} q_1 \\ q_2 \end{bmatrix} \triangleq [\tilde{p}]^*_{\tilde{\otimes}}\tilde{q}. \tag{3.20}$$

Unit Dual Quaternion Cross Product: The cross product of two unit dual quaternions can be given as

$$\tilde{q}\tilde{\times}\tilde{p} = \begin{bmatrix} q_1 \times p_1 \\ q_1 \times p_2 + q_2 \times p_1 \end{bmatrix} = q_1 \times p_1 + \epsilon(q_1 \times p_2 + q_2 \times p_1) \tag{3.21}$$

$$= \underbrace{\begin{bmatrix} [q_1]_{\times} & 0_{4\times4} \\ [q_2]_{\times} & [q_1]_{\times} \end{bmatrix}}_{[\tilde{q}]_{\tilde{\times}}} \begin{bmatrix} p_1 \\ p_2 \end{bmatrix} \triangleq [\tilde{q}]_{\tilde{\times}}\tilde{p}, \tag{3.22}$$

$$= \underbrace{\begin{bmatrix} [p_1]^*_{\times} & 0_{4\times4} \\ [p_2]^*_{\times} & [p_1]^*_{\times} \end{bmatrix}}_{[\tilde{p}]^*_{\tilde{\times}}} \begin{bmatrix} q_1 \\ q_2 \end{bmatrix} \triangleq [\tilde{p}]^*_{\tilde{\times}}\tilde{q}. \tag{3.23}$$

Finally, the algebraic properties of dual quaternion operations can be summarized in Table 3.3 below.

Dual Quaternion Error: The ultimate objective of the chaser satellite is to achieve docking conditions in terms of relative states represented in dual quaternions. Hence, the GN&C objective is to obtain the following relation while ensuring fuel efficient maneuvers and explicit handling of constraints

$$\mathbf{lim}_{k\to\infty}\tilde{q}_{\mathcal{CT},k} = \tilde{q}_d \tag{3.24}$$

TABLE 3.3: Dual Quaternion Operations

Operation	Definition
–	$\tilde{q} = q_1 + \epsilon q_2$
Addition	$\tilde{q} + \tilde{p} = (q_1 + p_1) + \epsilon(q_2 + p_2)$
Multiplication	$(q_1 p_1) + \epsilon(q_2 p_1 + q_1 p_2)$
Multiplication by a scalar	$\gamma\tilde{q} = (\gamma q_1) + \epsilon(\gamma q_2)$
Conjugate	$\tilde{q}* = q_1^* + \epsilon q_2^*$
Dot product	$q \cdot p = (q_1 \cdot p_1) + \epsilon(q_2 \cdot p_1 + q_1 \cdot p_2)$
Cross product	$\tilde{q}\tilde{\times}\tilde{p} = q_1 \times p_1 + \epsilon(q_1 \times p_2 + q_2 \times p_1)$
Quaternion product	$\tilde{q}\tilde{\otimes}\tilde{p} = q_1 \otimes p_1 + \epsilon(q_1 \otimes p_2 + q_2 \otimes p_1)$
Vector Part	$\mathrm{vec}(\tilde{q}) = (\mathbf{q_1}, 0) + \epsilon(\mathbf{q_2}, 0)$
Norm	$\|\tilde{q}\| = \sqrt{q_1 \cdot p_1 + q_2 \cdot p_2}$

where $\tilde{q}_d$ is the corresponding final attitude for successful mechanical docking, $\tilde{q}_{\mathcal{CT},k}$ is the dual quaternion of chaser satellite in chaser's body frame $\mathcal{C}$ with respect to the target's body frame $\mathcal{T}$ at the time instant k. Now, the position vector of the docking port of the target satellite and the final relative position attitude represented in the inertial frame $\mathcal{N}$ can be expressed with r_d and q_d. Eventually, the desired relative pose between the chaser and the target satellite can be given as

$$\tilde{q}_d = q_d + \epsilon\frac{1}{2} r_d^{\mathcal{N}} \otimes q_d. \tag{3.25}$$

Furthermore, the relative quaternion error can be calculated as

$$\tilde{q}_e = q_e + \epsilon\frac{1}{2} q_e \otimes r_e \tag{3.26}$$

with

$$\tilde{q}_e = \begin{bmatrix} q_e \\ r_e \end{bmatrix} = \begin{bmatrix} q_{\mathcal{C}} \otimes q_d \\ r_{\mathcal{C}} - q_{\mathcal{C}}^* \otimes r_d^{\mathcal{N}} \otimes q_{\mathcal{C}} \end{bmatrix} \triangleq \begin{bmatrix} q_d^* \otimes q_{\mathcal{C}} \\ r_{\mathcal{C}} - r_d^{\mathcal{C}} \end{bmatrix} \tag{3.27}$$

where q_e is called the error quaternion whilst, r_e is relative position error.

Consequently, in the desired state, the error quaternion becomes an identity quaternion as $\tilde{q}_e = \tilde{q}_I$; therefore, the relative dual quaternion $\tilde{q}_{\mathcal{C}}$ arrives to the constant desired value as $\tilde{q}_C = \tilde{q}_d \times q_I = q_d$.

3.5 Kinematics and Dynamics with Dual Quaternions

The dual quaternion algebra is explained in Section 3.4. Now, rotational and translational motion can be represented with dual quaternions. The relative motion kinematics of chaser's body frame $\mathcal{C}$ with respect to the target's body frame $\mathcal{T}$ can be given as

$$\dot{\tilde{q}} = \frac{1}{2}\tilde{q} \,\tilde{\otimes}\, \tilde{\omega}_{\mathcal{C}} \ , \text{ or } \dot{\tilde{q}} = \frac{1}{2}\, [\tilde{\omega}_{\mathcal{C}}]^{*}_{\tilde{\otimes}}\, \tilde{q} \tag{3.28}$$

$$\text{with } \tilde{\omega} = \begin{bmatrix} \boldsymbol{\omega}_{\mathcal{B}} \\ \mathbf{v}_{\mathcal{B}} \end{bmatrix}_{8\times 1} \ , \text{ and, } \boldsymbol{\omega}_{\mathcal{B}} = \begin{bmatrix} \omega_{\mathcal{B}} \\ 0 \end{bmatrix}_{4\times 1} \ , \ \mathbf{v}_{\mathcal{B}} = \begin{bmatrix} v_{\mathcal{B}} \\ 0 \end{bmatrix}_{4\times 1} \tag{3.29}$$

Now the dynamics of the translational and rotational motion expressed in the body frame of chaser satellite. If we assume that the rotating frame is fixed to the body frame of the chaser satellite $\mathbf{C}$, the force vector $\mathbf{F}$ and the torque vector $\mathbf{T}$ expressed in the chaser's body frame $\mathcal{C}$ can be given as

$$\mathbf{F} = \frac{^{\mathcal{C}}d}{dt}(mv) = m\dot{v}_{\mathcal{C}} + \omega_{\mathcal{C}} \times mv_{\mathcal{C}}, \tag{3.30}$$

$$\mathbf{T} = \frac{^{\mathcal{C}}d}{dt}(J\omega) = J\dot{\omega}_{\mathcal{C}} + \omega_{\mathcal{C}} \times J\omega_{\mathcal{C}} \tag{3.31}$$

because the translational velocity in the body frame is defined by

$$v_{\mathbf{C}} = \dot{\mathbf{r}}_{\mathcal{C}} + \omega_{\mathcal{C}} \ \times \ \mathbf{r}_{\mathcal{C}} \tag{3.32}$$

we can formulate fully coupled, 6-DOF problem translational and rotational motion dynamics in a compact matrix-vector form as

$$\tilde{\mathbf{F}} = \mathbf{I}\dot{\tilde{\omega}} + \tilde{\omega} \times \mathbf{I}\tilde{\omega} \tag{3.33}$$

with

$$\mathbf{I} = \begin{bmatrix} 0_{3\times3} & 0 & mI_{3\times3} & 0 \\ 0 & 0 & 0 & 1 \\ J & 0 & 0_{3\times3} & 0 \\ 0 & 1 & 0 & 0 \end{bmatrix}_{8\times8} \quad \text{and, } \tilde{\mathbf{F}} = \begin{bmatrix} \mathbf{F} \\ 0 \\ \mathbf{T} \\ 0 \end{bmatrix}_{8\times1} . \tag{3.34}$$

where $\mathbf{I} \in R^{8\times8}$ is an invertible matrix. $Proof$: [144]. Alternatively, the equations of motion can be also expressed in the Inertial frame $\mathcal{N}$. However, for the sake of consistency of the reference frames, all calculations are done in the chaser's body frame $\mathcal{C}$.

Chapter 4

Model Predictive Control for Spacecraft Rendezvous and Docking

This chapter covers the formulation of MPC for spacecraft assuming a full state feedback condition is available. Also, the benefits of MPC paradigm is provided as well as its disadvantages. This includes definitions and use of the three main components: prediction model, objective function and the constraints. The dynamic model is discussed in Chapter 3; the constraints are discussed in Chapter 2 where the challenges are presented. Because MPC paradigm is an optimal control technique, the desired closed loop is reflected in the choice of the objective function. One of the most common critics that MPC faces is the computational demands; thus, in this chapter, MPC using different classes of constrained quadratic optimization algorithms are investigated. This includes the condensing algorithms that are used to transform the original optimal control problem into QP problem in the MPC form and the state of the art QP solvers.

4.1 Introduction

The basic idea of MPC is illustrated in Fig. 4.1. A discrete-time setting is assumed, and the current time is referred as time step k. At the current time, the plant's state is x_k, the input is u_k and the figure shows the state and the input history with grey colour on the "past" side. The green solid line is the "desired set-point" that states should follow.

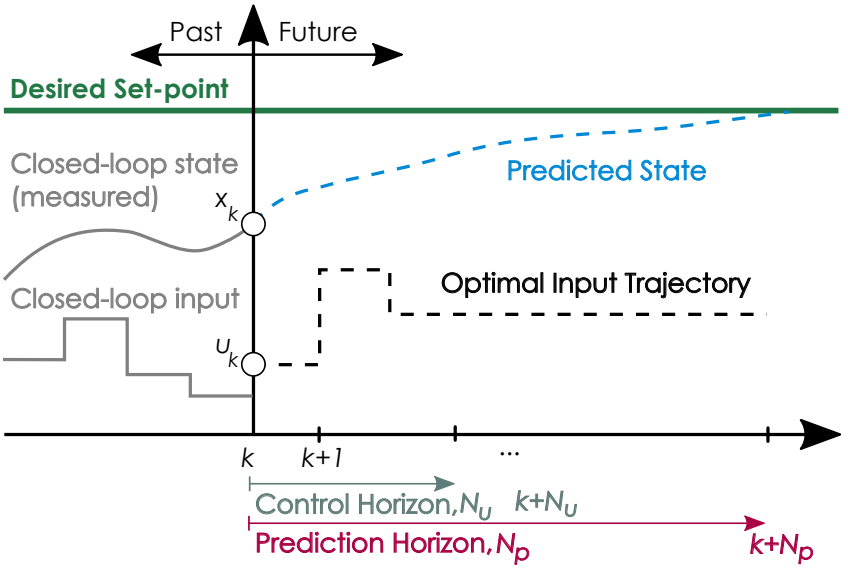

FIGURE 4.1: MPC Overview

MPC has an *internal model* to predict the behaviour of the plant, from the current time, over a future *prediction horizon* denoted with N_p in Fig. 4.1. The predicted trajectory, shown with the blue dashed line, is based on the assumed input trajectory $u_{k+i,k}(i = 0, 1, \ldots, N_p - 1)$ shown with black dashed line.

It is assumed that the sequence of actions at time step k is the following [32] and summarized in Algorithm 1;

1. Obtain the measurements y_k.
2. Predict the future output using system model, regarding the constraints and objectives.
3. Solve the optimization problem
4. Implement the first control action u_k
5. Repeat the calculation at subsequent control intervals

One should note that at each control interval, MPC attempts to optimize the future plant behaviour. This prediction capability provides online solutions to control problems where tracking error is minimized over a future horizon, without violating the constraints on the inputs and outputs.

Algorithm 2.1: Model predictive control

while *controller running* **do**

Solve

$$arg \min_{x,u} F_{N_p}(x_{k+N_p}) + \sum_{i=0}^{N_p-1} l(x_{k+i}, u_{k+i})$$

subject to plant dynamics

$$x_{k+i+1} = f(x_{k+i}, u_{k+i}),\ \forall\ i \in \{0, \ldots, N_p - 1\}$$

and constraints

$$x_{k+i} \in \mathbb{X}\ \forall\ i \in \{0, \ldots, N_p - 1\}$$
$$u_{k+i} \in \mathbb{U}\ \forall\ i \in \{0, \ldots, N_c - 1\}$$
$$x_{k+N_p} \in \mathbb{T}.$$

Apply u_k to plant.

Set $k \leftarrow k + 1$.

end

4.2 MPC as a Quadratic Programming Problem

Consider the discrete-time state-space model

$$x_{k+1} = A_d x_k + B_d u_k, \tag{4.1}$$
$$y_k = C_d x_k \tag{4.2}$$

where x is an n-dimensional state vector, u is an m-dimensional input vector and y is an l-dimensional measured output vector.

We can predict the future outputs by iterating the model,

$$\hat{y}_{k+1} = C_d A_d x_k + C_d B_d \hat{u}_k, \tag{4.3}$$

$$\hat{y}_{k+2} = C_d A_d^2 x_k + A_d B_d \hat{u}_k + C_d B_d \hat{u}_{k+1}, \tag{4.4}$$

$$\vdots \tag{4.5}$$

$$\hat{y}_{k+i} \;=\; C_d A_d^i x_k \;+\; \sum_{j=1}^{i} C_d A_d^{j-1} B_d \hat{u}_{k+i-j} \tag{4.6}$$

If we collect the predicted outputs into a vector, we obtained an expression for the vector of predicted outputs

$$\underbrace{\begin{bmatrix} \hat{y}_k \\ \hat{y}_{k+1} \\ \hat{y}_{k+2} \\ \vdots \\ \hat{y}_{k+N_p-1} \end{bmatrix}}_{\vec{y_k}} = \underbrace{\begin{bmatrix} C_d \\ C_d A_d \\ C_d A_d^2 \\ \vdots \\ C_d A_d^{N_p-1} \end{bmatrix}}_{P \in \mathbb{R}^{lN_p \times n}} x_k + \underbrace{\begin{bmatrix} D_d & 0 & 0 & \cdots \\ C_d B_d & D_d & 0 & \cdots \\ C_d A_d B_d & C_d B_d & D_d & \cdots \\ \vdots & \vdots & \vdots & \ddots \\ C_d A_d^{N_p-2} B_d & C_d A_d^{N_p-3} B_d & C_d A_d^{n_p-4} B_d & \cdots \end{bmatrix}}_{H \in \mathbb{R}^{lN_p \times mN_p}} \cdot \underbrace{\begin{bmatrix} \hat{u}_k \\ \hat{u}_{k+1} \\ \hat{u}_{k+2} \\ \vdots \\ \hat{u}_{k+N_p-1} \end{bmatrix}}_{\vec{u_k}} \tag{4.7}$$

where

P, H *output prediction matrices*
$\vec{y_k}$ *output at time increment* k
$\vec{u_k}$ *control input at time increment* k
N_p *Prediction Horizon*

We can also express Equation 4.7 in a compact form:

$$\vec{y_k} = P x_k + H \vec{u_k} \tag{4.8}$$

The cost function now can be written as

$$J_u = \frac{1}{2} \left(\vec{y_k}^T Q \vec{y_k} + \vec{u_k}^T R \vec{u_k} \right) \tag{4.9}$$

where $Q \in \mathbb{R}^{lN_p \times lN_p}$ is the positive definite matrix of weight for error vector and $R \in \mathbb{R}^{mN_p \times mN_p}$ is the diagonal matrix of weight for input vector. Substituting Eqn. (4.8) into Eqn. (4.9), we get:

$$J_u = \frac{1}{2}((Px_k + H\vec{u_k})^T Q(Px_k + H\vec{u_k}) + \vec{u_k}^T R\vec{u_k}) \tag{4.10}$$

Reorganizing and removing the terms that are independent of $\vec{u_k}$, we obtain:

$$J_u = \frac{1}{2}\vec{u_k}^T \underbrace{(H^T Q H + R)}_{G}\vec{u_k} + \underbrace{(x_k^T P^T)QH}_{W^T}\vec{u_k} \tag{4.11}$$

using matrix G and the vector W, we can write

Cost Function 1

$$J_u = \frac{1}{2}\vec{u_k}^T G\vec{u_k} + W^T\vec{u_k} \tag{4.12}$$

There might be a steady-state error due to the non-zero weight of control inputs in the cost function. This is simply because having a steady-state error is cheaper in cost than eliminating it by increasing the control signals. Let us consider hovering of a drone example at 1m. In order to keep the altitude, there must be a control signal compensating the gravitational force. Hence, if the cost function 1 is used, the cost can never go to zero value but a compromise is to be made by the optimizer between the input use and the steady-state error. An alternative example regarding attitude dynamics is given in Section 3.2. The mentioned problem may be solved by defining the cost function through the rate of change of control inputs rather than control inputs themselves. Control vector components can now be written as

$$\underbrace{\begin{bmatrix} u_k \\ u_{k+1} \\ \vdots \\ u_{k+N_p-1} \end{bmatrix}}_{\vec{u_k} \in \mathbb{R}^{mN_p \times 1}} = \underbrace{\begin{bmatrix} u_{k-1} \\ u_{k-1} \\ \vdots \\ u_{k-1} \end{bmatrix}}_{\vec{u}_{k-1}} + \underbrace{\begin{bmatrix} I & 0 & \cdots \\ I & I & \cdots \\ \vdots & \vdots & \ddots \\ I & I & \cdots \end{bmatrix}}_{\Omega \in \mathbb{R}^{mN_p \times mN_p}} \underbrace{\begin{bmatrix} \Delta u_1 \\ \Delta u_2 \\ \vdots \\ \Delta u_{N_p} \end{bmatrix}}_{\vec{\Delta u_k}} \tag{4.13}$$

where Ω is lower diagonal matrix that consists of identity matrices $I \in \mathbb{R}^{l \times l}$ or zero matrices $0 \in \mathbb{R}^{l \times l}$. Then Eq. 4.8 takes the form:

$$\vec{y_k} = Px_k + H(\vec{u}_{k-1} + \Omega\overrightarrow{\Delta u_k}) \tag{4.14}$$

$\vec{u}_{k-1}$ does not change during the whole horizon.

Cost Function 2 J_u can now be expressed as

$$J_{\Delta u} = \frac{1}{2}\overrightarrow{\Delta u_k}^T G_\Delta \overrightarrow{\Delta u_k} + W_\Delta^T \overrightarrow{\Delta u_k} \tag{4.15}$$

where $G_\Delta = \Omega^T G \Omega$ and $W_\Delta^T = \vec{u}_{k-1}^T G\Omega + W^T\Omega$.

4.2.1 Handling Disturbances and Modeling Uncertainties

To get offset free tracking of a reference in the presence of an unknown but constant disturbance, integral action can be applied to the problem formulation. Surprisingly, this is seldom done or emphasised in the existing literature for spacecraft RVD applications. To include the integral action, we need:

- In steady-state, the minimum of J must be consistent with zero tracking errors. This can be simply achieved by editing the cost function and in our case, **Cost Function 3** to be explained next satisfies the consistency requirement.
- The predictions must be unbiased, i.e., in steady-state, the prediction model should give $\hat{Y} = [I; I; \ldots; I]^T y_{ss}^{real}$, regardless of any differences between the model and the process due to uncertainty and disturbances. This uncertainty could be a modeling uncertainty, e.g., attitude dynamics, knowledge of the mechanical properties, whereas the disturbance could be solar radiation pressure or atmospheric drag. This could be achieved by an incremental state-space model and augmenting it to include output y.

Instead of the state-space model in (4.1) and (4.2), we could also derive the MPC control law by using a state-space model with an incremental input and output

term in the new state vector ensuring the integral action. Below, two examples are given (can be more).

First,

$$\underbrace{\begin{bmatrix}\Delta\hat{x}_{k+1}\\ y_k\end{bmatrix}}_{\hat{\xi}_{k+1}} = \underbrace{\begin{bmatrix}A_d & 0\\ C_d & I\end{bmatrix}}_{A}\underbrace{\begin{bmatrix}\Delta x_k\\ y_{k-1}\end{bmatrix}}_{\xi_k} + \underbrace{\begin{bmatrix}B_d\\ 0\end{bmatrix}}_{B}\Delta\hat{u}_k, \tag{4.16}$$

$$y_k = \underbrace{\begin{bmatrix}C_d & I\end{bmatrix}}_{C}\underbrace{\begin{bmatrix}\Delta x_k\\ y_{k-1}\end{bmatrix}}_{\xi_k} \tag{4.17}$$

Second,

$$\underbrace{\begin{bmatrix}\Delta\hat{x}_{k+1}\\ \hat{y}_{k+1}\end{bmatrix}}_{\hat{\xi}_{k+1}} = \underbrace{\begin{bmatrix}A_d & 0\\ C_dA_d & I\end{bmatrix}}_{A}\underbrace{\begin{bmatrix}\Delta x_k\\ y_k\end{bmatrix}}_{\xi_k} + \underbrace{\begin{bmatrix}B_d\\ C_dB_d\end{bmatrix}}_{B}\Delta\hat{u}_k, \tag{4.18}$$

$$y_k = \underbrace{\begin{bmatrix}0 & I\end{bmatrix}}_{C}\underbrace{\begin{bmatrix}\Delta x_k\\ y_k\end{bmatrix}}_{\xi_k} \tag{4.19}$$

These state-space models can be written in the final compact form

$$\hat{\xi}_{k+1} = A\xi_k + B\Delta\hat{u}_k \tag{4.20}$$

$$y_k = C\xi_k \tag{4.21}$$

where ξ is the new augmented state vector and the matrices A, B & C are defined accordingly. Hence, the output predictions can be written as

$$\underbrace{\begin{bmatrix}\hat{y}_{k+1}\\ \hat{y}_{k+2}\\ \vdots\\ \hat{y}_{k+N_p}\end{bmatrix}}_{\vec{y_k}} = \underbrace{\begin{bmatrix}CA\\ CA^2\\ \vdots\\ CA^{N_p}\end{bmatrix}}_{\Phi}\xi_k + \underbrace{\begin{bmatrix}CB & 0 & \cdots & 0\\ CAB & CB & & \vdots\\ \vdots & & \ddots & \vdots\\ CA^{N_p-1}B & CA^{N_p-2}B & \cdots & CB\end{bmatrix}}_{G}\underbrace{\begin{bmatrix}\Delta\hat{u}_k\\ \Delta\hat{u}_{k+1}\\ \vdots\\ \Delta\hat{u}_{k+N_c-1}\end{bmatrix}}_{\overrightarrow{\Delta\mathbf{u}}} \tag{4.22}$$

Or in a vector-matrix notation

$$\vec{y_k} = \Phi\xi_k + G\overrightarrow{\Delta\mathbf{u}} \tag{4.23}$$

With cost function (4.24) and substituting (4.23), we have

$$J_{\Delta\mathbf{u},\mathcal{I}} = \frac{1}{2}\left(\vec{y_k}^T Q \vec{y_k} + \vec{\Delta\mathbf{u}}^T R \vec{\Delta\mathbf{u}}\right) \tag{4.24}$$

$$J_{\Delta\mathbf{u},\mathcal{I}} = (\Phi\xi_k)^T Q(\Phi\xi_k) + 2\overrightarrow{\Delta\mathbf{u}}^T G^T(\Phi\xi_k) + \overrightarrow{\Delta\mathbf{u}}^T(R + G^T G)\overrightarrow{\Delta\mathbf{u}} \tag{4.25}$$

$$J_{\Delta\mathbf{u},\mathcal{I}} = \frac{1}{2}\vec{\Delta\mathbf{u}}^T \underbrace{(G^T Q G + R)}_{F} \vec{\Delta\mathbf{u}} + \underbrace{(\xi_k^T \Phi^T) Q G}_{V^T} \vec{\Delta\mathbf{u}} \tag{4.26}$$

Cost Function 3 $J_{\Delta u,\mathcal{I}}$ can now be expressed as

$$J_{\Delta\mathbf{u},\mathcal{I}} = \frac{1}{2}\vec{\Delta\mathbf{u}}^T F \vec{\Delta\mathbf{u}} + V^T \vec{\Delta\mathbf{u}} \tag{4.27}$$

4.2.2 Motivational Example

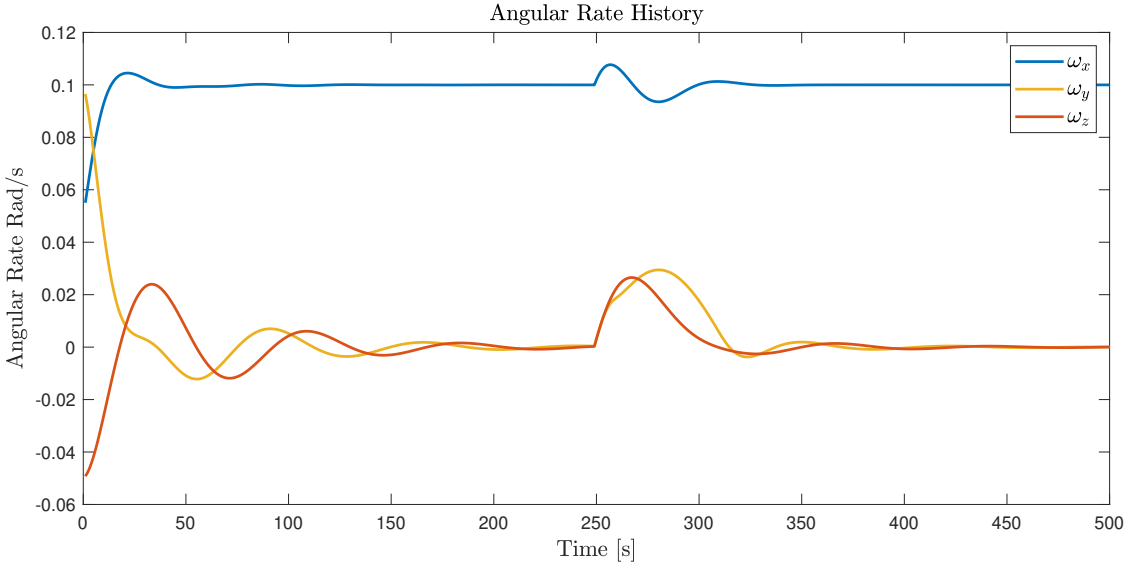

FIGURE 4.2: Integral Action Angular Rate History

It is seen from Fig. 4.2 that the desired spin rate is achieved roughly in 100s around x-axis and when the external disturbance is applied at $t = 250s$, it takes less than 100s to realize and compensate it. Another way of criticising the performance would be screening the torque history which is depicted in Fig. 4.3. After the disturbance, the torque command reaches the values to compensate it. In particular, T_y hits the constraint limit of $T_{max,y} = 0.0075Nm$. Finally, Fig. 4.4 shows that the rate

of change of torque inputs converges to zero. In summary, having a consistent cost function (**Cost Function** 3) together with integral action, not only offset free tracking but also disturbance rejection can be easily achieved.

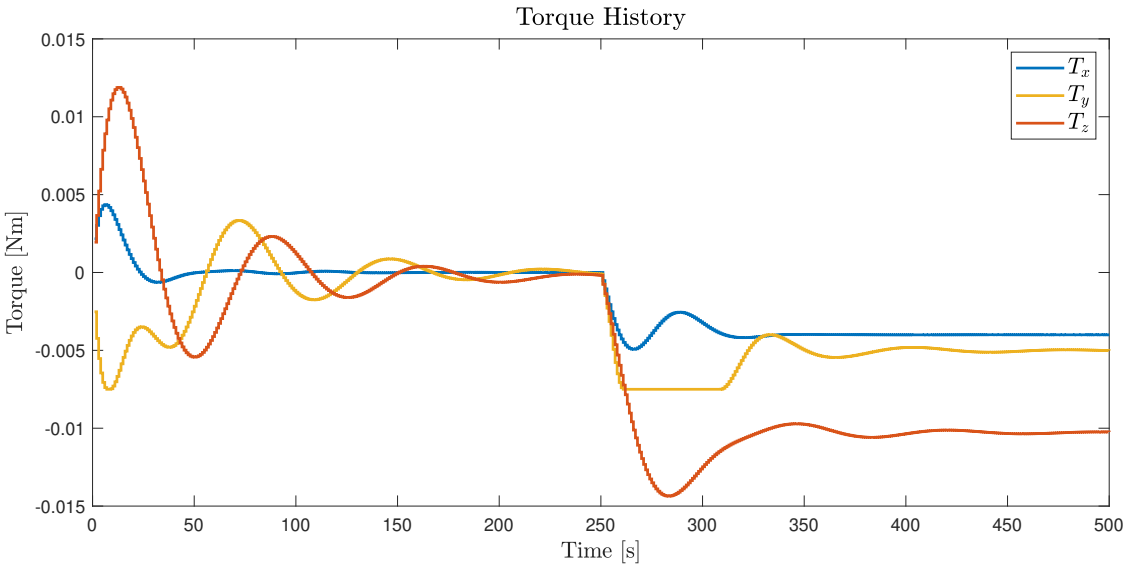

FIGURE 4.3: Integral Action Torque History

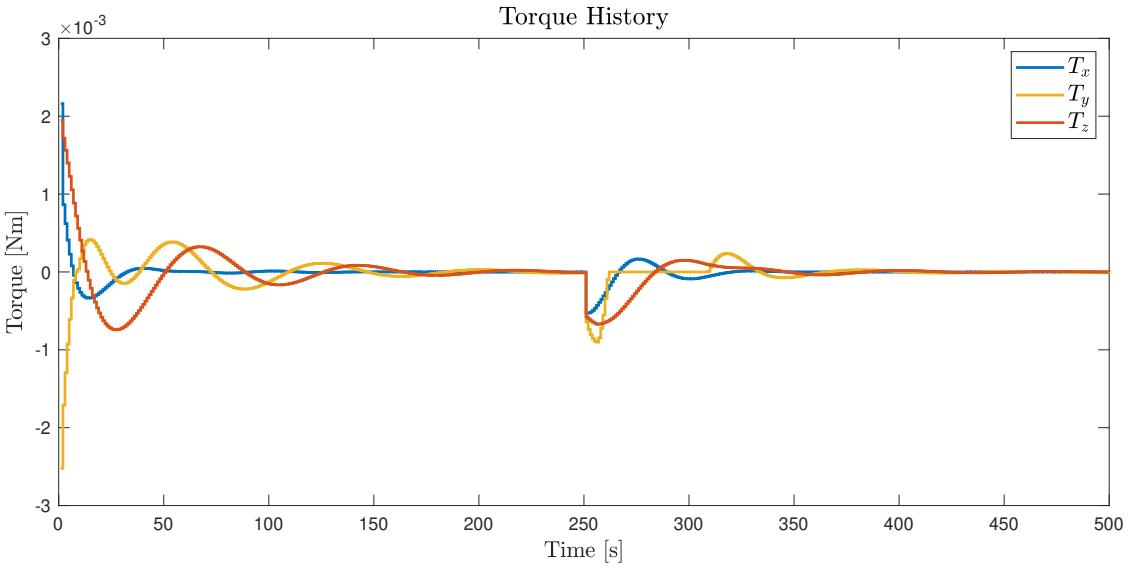

FIGURE 4.4: Integral Action Rate of Change of Torque History

4.2.3 Constraints in MIMO Settings

Because the thesis addresses a MIMO system, the constraints are specified for each input independently. Given m inputs, the upper limit can be written as

$$\mathbf{u}_{\max} = [\ (u_1^{\max})^{\mathrm{T}}\ (u_2^{\max})^{\mathrm{T}}\ \ \dots\ \ (u_m^{\max})^{\mathrm{T}}\ ]^{\mathrm{T}} \tag{4.28}$$

and lower limit as

$$\mathbf{u}_{\min} = [\ (u_1^{\min})^{\mathrm{T}}\ (u_2^{\min})^{\mathrm{T}}\ \ \dots\ \ (u_m^{\min})^{\mathrm{T}}\ ]^{\mathrm{T}} \tag{4.29}$$

Then the magnitude of each control signal must satisfy the constraints in the following inequality form:

$$u_1^{\min} \leq u_{1,k} \leq u_1^{\max} \tag{4.30}$$
$$u_2^{\min} \leq u_{2,k} \leq u_2^{\max} \tag{4.31}$$
$$\vdots \tag{4.32}$$
$$u_m^{\min} \leq u_{m,k} \leq u_m^{\max} \tag{4.33}$$

In general, constant input constraint over the prediction horizon can be written as

$$\underbrace{\begin{bmatrix} \mathbf{u}_{\min} \\ \mathbf{u}_{\min} \\ \mathbf{u}_{\min} \\ \vdots \\ \mathbf{u}_{\min} \end{bmatrix}}_{\overrightarrow{u}_{\min}\ \in\ \mathbb{R}^{mN_p\times 1}} \leq \underbrace{\begin{bmatrix} u_k \\ u_{k+1} \\ u_{k+2} \\ \vdots \\ u_{k+N_p-1} \end{bmatrix}}_{\overrightarrow{u}_{\mathbf{k}}\ \in\ \mathbb{R}^{\mathbf{mN_p}\times \mathbf{1}}} \leq \underbrace{\begin{bmatrix} \mathbf{u}_{\max} \\ \mathbf{u}_{\max} \\ \mathbf{u}_{\max} \\ \vdots \\ \mathbf{u}_{\max} \end{bmatrix}}_{\overrightarrow{u}_{\max}\ \in\ \mathbb{R}^{mN_p\times 1}} \tag{4.34}$$

In compact form,

$$\overrightarrow{\mathbf{u}_{\min}} \leq \overrightarrow{u}_{\mathbf{k}} \leq \overrightarrow{\mathbf{u}_{\max}} \tag{4.35}$$

Similarly, if the decision variable is the rate of change of input, then the inequality constraints can be given as

$$\Delta\mathbf{u}_{\max} = [(\Delta u_1^{\max})^{\mathrm{T}}\ (\Delta u_2^{\max})^{\mathrm{T}}\ \ \dots\ \ (\Delta u_m^{\max})^{\mathrm{T}}\ ]^{T} \tag{4.36}$$

and lower limit as

$$\Delta \mathbf{u}_{\min} = [(\Delta(u_1^{\min})^{\mathrm{T}} \ (\Delta u_2^{\min})^{\mathrm{T}} \ \dots \ (\Delta u_m^{\min})^{\mathrm{T}} \ ]^T \tag{4.37}$$

Then the magnitude of each control signal must satisfy the constraints in the following inequality form:

$$\Delta u_1^{\min} \leq \Delta u_{1,k} \leq \Delta u_1^{\max} \tag{4.38}$$
$$\Delta u_2^{\min} \leq \Delta u_{2,k} \leq \Delta u_2^{\max} \tag{4.39}$$
$$\vdots \tag{4.40}$$
$$\Delta u_m^{\min} \leq \Delta u_{m,k} \leq \Delta u_m^{\max} \tag{4.41}$$

Now, assuming $\Delta u_k = u_k - u_{k-1}$.,

$$\underbrace{\begin{bmatrix} \hat{u}_k \\ \hat{u}_{k+1} \\ \hat{u}_{k+2} \\ \vdots \\ \hat{u}_{k+N_c-1} \end{bmatrix}}_{\overrightarrow{\mathbf{u_k}} \in \mathbb{R}^{mNp \times 1}} = \underbrace{\begin{bmatrix} u_{k-1} \\ u_{k-1} \\ u_{k-1} \\ \vdots \\ u_{k-1} \end{bmatrix}}_{\overrightarrow{\mathbf{u}}_{k-1} \in \mathbb{R}^{mN_p \times 1}} + \underbrace{\begin{bmatrix} I & 0 & 0 & \cdots & 0 \\ I & I & 0 & \cdots & 0 \\ I & I & I & & 0 \\ \vdots & & & \ddots & \\ I & I & \dots & I & I \end{bmatrix}}_{\Upsilon \in \mathbb{R}^{mN_p \times mN_p}} \underbrace{\begin{bmatrix} \Delta\hat{u}_k \\ \Delta\hat{u}_{k+1} \\ \Delta\hat{u}_{k+2} \\ \vdots \\ \Delta\hat{u}_{k+N_c-1} \end{bmatrix}}_{\overrightarrow{\Delta \mathbf{u}} \in \mathbb{R}^{mNp \times 1}} \tag{4.42}$$

where Υ is a lower diagonal matrix and each element is an identity matrix being $I \in \mathbb{R}^{\mathbf{m} \times \mathbf{m}}$. In a compact form,

$$\overrightarrow{\mathbf{u_k}} = \overrightarrow{\mathbf{u}}_{k-1} + \Upsilon \overrightarrow{\Delta \mathbf{u}} \tag{4.43}$$
$$\overrightarrow{\mathbf{u}}_{\min} \leq \overrightarrow{\mathbf{u}}_k \leq \overrightarrow{\mathbf{u}}_{\max} \tag{4.44}$$
$$\overrightarrow{\mathbf{u}}_{\min} \leq \overrightarrow{\mathbf{u}}_{k-1} + \Upsilon \overrightarrow{\Delta \mathbf{u}} \leq \overrightarrow{\mathbf{u}}_{\max} \tag{4.45}$$
$$\underbrace{\overrightarrow{\mathbf{u}}_{\min} - \overrightarrow{\mathbf{u}}_{k-1}}_{u_{lb}} \leq \Upsilon \overrightarrow{\Delta \mathbf{u}} \leq \underbrace{\overrightarrow{\mathbf{u}}_{\max} - \overrightarrow{\mathbf{u}}_{k-1}}_{u_{ub}} \tag{4.46}$$
$$u_{lb} \leq \Upsilon \overrightarrow{\Delta \mathbf{u}} \leq u_{ub} \tag{4.47}$$

Now, the Eqn. (4.47) that consists of u_{lb} & u_{ub} vectors and Υ matrix can be given to QP solver.

4.2.4 LPV Model For Experimentation

For analysis, a nonlinear plant can be transformed into several linear systems via the piecewise-affine approximation method proposed in [49, 144]. Hence, linear MPC can be formulated in a convex optimization framework and real-time implementation becomes feasible thanks to high speed solvers [165, 166]. The continuous time differential equations in Eqns. (3.28-3.33) can be discretized and used as a prediction model of MPC;

$$\mathbf{I}\tilde{\omega}_{k+1} = \mathbf{I}\tilde{\omega}_k - \Delta t[\mathbf{I}\tilde{\omega}_k]_{\tilde{\times}}\tilde{\omega}_k + \Delta t\tilde{\mathbf{F}}_k \tag{4.48}$$

$$\tilde{\mathbf{q}}_{k+1} = \tilde{\mathbf{q}}_k - \frac{\Delta t}{2}[\tilde{\mathbf{q}}_k]_{\tilde{\otimes}}\tilde{\omega}_{k+1} \tag{4.49}$$

where Δt is the sampling period, $\mathbf{I}$ is the inertia tensor defined in Eqn. (3.34), $\tilde{\omega}$ & $\tilde{q}$ are defined in Eqns. (3.17,3.29), finally $[\,\cdot\,]_{\otimes}$ and $[\,\cdot\,]_{\times}$ the dual quaternion operations defined in Eqns. (3.19,3.22). Two different discretizations is done. First, it is assumed that the time sequence of the discretized equations is

$$\tilde{\mathbf{F}} \Longrightarrow \tilde{\omega}_{k+1} \Longrightarrow \tilde{q}_{k+1}, \tag{4.50}$$

and the proof is given in [144]. Now, the state and the input vectors can be summarized as

$$x_k = \begin{bmatrix} \tilde{\omega}_k \\ \tilde{q}_k \end{bmatrix}, \text{ and } u_k = \tilde{\mathbf{F}}_k. \tag{4.51}$$

Subsequently, if the Eqns. (4.49-4.48) are reorganized,

$$\underbrace{\begin{bmatrix} \mathbf{I} & 0_{8\times8} \\ -\frac{\Delta t}{2}[\tilde{q}_k]_{\tilde{\otimes}} & I_{8\times8} \end{bmatrix}}_{M} x_{k+1} = \underbrace{\begin{bmatrix} \mathbf{I} - \Delta t[\mathbf{I}\tilde{\omega}_k]^*_{\tilde{\times}} & 0_{8\times8} \\ 0_{8\times8} & I_{8\times8} \end{bmatrix}}_{N} x_k + \underbrace{\begin{bmatrix} \Delta t I_{8\times8} \\ 0_{8\times8} \end{bmatrix}}_{L} u_k, \ or \tag{4.52}$$

$$x_{k+1} = M^{-1}Nx_k + M^{-1}Lu_k, \ or \tag{4.53}$$

$$x_{k+1} = A_t x_k + B_t u_k \tag{4.54}$$

[49, 144] show that $M_{16\times16}$ matrix in Eqn. (4.52) is invertible and the state-space system in (4.54) can be constructed.

Secondly, if the discretization is done simultaneously;

$$\tilde{\mathbf{F}} \Longrightarrow \tilde{\omega}_{k+1} \ \& \ \tilde{q}_{k+1}, \tag{4.55}$$

$$\underbrace{\begin{bmatrix} \mathbf{I} & 0_{8\times8} \\ 0_{8\times8} & I_{8\times8} \end{bmatrix}}_{M'} x_{k+1} = \underbrace{\begin{bmatrix} \mathbf{I} - \Delta t[\mathbf{I}\tilde{\omega}_k]^*_{\tilde{\times}} & 0_{8\times8} \\ \frac{\Delta t}{2}[\tilde{q}_k]_{\tilde{\otimes}} & I_{8\times8} \end{bmatrix}}_{N'} x_k + \underbrace{\begin{bmatrix} \Delta t I_{8\times8} \\ 0_{8\times8} \end{bmatrix}}_{L'} u_k, \ or \tag{4.56}$$

$$x_{k+1} = (\bar{M})^{-1}(\bar{N})x_k + (\bar{M})^{-1}(\bar{L})u_k, \ or \tag{4.57}$$

$$x_{k+1} = A_t x_k + B_t u_k \tag{4.58}$$

We can now refer to Section 4.2 for derivation of MPC as QP problem.

Remark 10. The PWA modeling method assumes that the states lie in the vicinity of the reference, which is the point of linearisation. Hence, the greater the prediction horizon N_p, the more error in the representation of the nonlinear models given in the compact vector-matrix form in Eqn. (3.33). As a result, the predicted outputs will deviate increasingly from the true outputs and the calculated control action will be far from optimal. On the other hand, for the stability of MPC, the prediction horizons must be sufficiently large. In fact, our results suggest that the larger the prediction horizon, the lower the fuel consumption. Eventually, determination of prediction horizon requires extra care. One potential solution is to decrease the sampling period of PWA strategy. However, this must be also controlled in order not to conflict with other sensors and violate the computation power of on-board PC. The trade-off is explained in detail in the results section.

4.2.5 QP Problem Derivation for LTV Model For Elliptic Orbits

Unlike LTI and LPV, Linear-Time-Varying Models vary by time. Hence, at each time instant k, there exist N_p new models over the prediction horizon. Therefore, the main matrices for the derivation of the QP problem can be accordingly obtained as

$$\underbrace{\begin{bmatrix} y_k \\ y_{k+1} \\ y_{k+2} \\ \vdots \\ y_{k+N_c} \\ y_{k+N_c+1}) \\ \vdots \\ y_{k+N_p} \end{bmatrix}}_{Y(k)} = \underbrace{\begin{bmatrix} C_k \\ C_{k+1}A_k \\ C_{k+2}A_{k+1}A_k \\ \vdots \\ C_{k+N_c}\prod_{i=k}^{k+N_c-1} A_i \\ C_{k+N_c+1}\prod_{i=k}^{k+N_c} A_i \\ \vdots \\ C_{k+N_p}\prod_{i=k}^{k+N_p-1} A_i \end{bmatrix}}_{F_k(x)} x(k) +$$

$$\underbrace{\begin{bmatrix} D_k & 0 & \dots & 0 \\ C_{k+1}B_k & D_{k+1} & \cdots & 0 \\ C_{k+2}A_{k+1}B_k & C_{k+2}B_{k+1} & D_{k+2} & \vdots \\ \vdots & \vdots & \ddots & \ddots \\ C_{k+N_c}\prod_{i=k+1}^{k+N_c-1} A_iB_k & C_{k+N_c}\prod_{i=k+2}^{k+N_c-1} A_iB_{k+1} & \cdots & C_{k+N_c+1}A_{k+N_c}B_{k+N_c}-1 \\ C_{k+N_p}\prod_{i=k+1}^{k+N_p-1} A_iB_k & \vdots & \ddots & \vdots \\ \vdots & C_{k+N_p}\prod_{i=k+2}^{k+N_p-1} A_iB_{k+1} & \cdots & C_{k+N_p}\prod_{i=k+N_c}^{k+N_p-1} A_iB_{k+N_c-1} \end{bmatrix}}_{\Phi_k} \times \underbrace{\begin{bmatrix} \Delta U_k \\ \vdots \\ \Delta U_{k+N_c-1} \end{bmatrix}}_{\Delta U_k} \tag{4.59}$$

From now on, the procedure is similar to the LTI case given in Eqns. (4.8-4.15) and the LTV dynamic matrices are obtained from [167].

4.3 Formulation Of Inscribed Polygon Approach

4.3.1 Line-Of-Sight Constraints

The requirements in spacecraft motion control problems are imposed pointwise-in-time and terminal constraints on both state and control variables. The main ones are Line of Sight (LOS), Field of View (FOV), plume impingement, obstacle avoidance, and physical constraints. In this thesis, we formulate LOS and physical constraints as follows. First, during the proximity maneuvering, it is necessary for controlled spacecraft to stay inside the LOS region if there exists a proximity operation. This region can be represented with a polyhedron and can be in general written as [123, 168]

$$\mathcal{P} \;=\; \{\boldsymbol{x} \;:\; c_\eta \boldsymbol{x} \leq d_\eta\} \tag{4.60}$$

where $\boldsymbol{x}$ denotes the state vector. The inequality constraints are defined as $y \geq c_x(x - x_0),\ y \geq -c_z(z + z_0),\ y \geq -c_x(x + x_0), y \geq c_z(z - z_0)$ where c_x and c_z are the slopes of the tetrahedral cone (i.e., if $c_x = 1$, slope angle is 45 deg), x_0 and z_0 are the docking port 2D dimensions and, $y \geq 0$ ensures that chaser satellite does not crash the docking port.

In Eqn. (4.60),

$$c_\eta \;=\; \begin{bmatrix} 0 & -1 & 0 \\ c_x & -1 & 0 \\ -c_x & -1 & 0 \\ 0 & -1 & c_z \\ 0 & -1 & -c_z \end{bmatrix}, \quad d_\eta \;=\; \begin{bmatrix} 0 \\ c_x x_0 \\ c_x x_0 \\ c_z z_0 \\ c_z z_0 \end{bmatrix} \tag{4.61}$$

The given inequality constraints in Eqn. (4.60) are valid for stable or non-rotating target case where LVHL frame is identical to body-fixed frame. However, for a tumbling target, transformation of A_{LOS} and b_{LOS} dynamic constraints are required to predict future feasible region in order to generate set of inputs that optimizes the RVD problem while respecting the LOS constraints. To this end, LOS constraint matrix can be updated in LVLH frame by using projective geometry in the following

form;

$$c_{\eta,rot} = c_{\eta} R_{Rot} \tag{4.62}$$

where, for a simple scenario, assuming target only rotates around it's z-axis, R_{Rot} can be obtained provided that perfect knowledge of rotation rate is available;

$$R_{Rot-z} = \begin{bmatrix} cos(\alpha) & -sin(\alpha) & 0 \\ sin(\alpha) & cos(\alpha) & 0 \\ 0 & 0 & 1 \end{bmatrix} \tag{4.63}$$

Rotations will be named as yaw, pitch and roll where rotation matrices in the counter-clockwise direction and the other rotation matrices can be obtained by multiplication of the given three matrices.

4.3.2 Physical Constraint

The most commonly employed physical constraint is the following linear inequality constraints which are valid in the presence of the multiple-axis thrusters on-board to fire in every direction;

$$u_{min,\sigma} \leq u_{\sigma} \leq u_{max,\sigma}, \ \sigma \in \{x, y, z\} \tag{4.64}$$

In Eqn. (4.64), it is assumed that each thrust magnitude can be independently fired. However, for a single-axis thruster configuration, the physical limit is on the net thrust and can be expressed as

$$u_x^2 + u_y^2 + u_z^2 \leq u_{\max}^2, \tag{4.65}$$

This results in Quadratically Constrained Quadratic Program (QCQP) where $u_x, \ u_y$ & u_z are the inputs in the $x, \ y$ & z directions respectively.

It is well understood from the relative motion dynamic models, i.e., HCW (Appendix A.1), Inalhan, or Y-A Equations, that in-plane dynamics (x and y) is decoupled from out-of-plane (z) dynamics and can be expressed separately [151, 167]. However, [105] decoupled each thrust direction and formulated them separately

with the following conservative linear inequality constraints:

$$-\frac{u_{\max}}{\sqrt{2}} \leq u_\sigma \leq \frac{u_{\max}}{\sqrt{2}}, \quad \sigma \in \{x, y, z\} \tag{4.66}$$

This technique allows users to obtain QP formulation. However, based on the Eqn. (4.73), the thrust region loss is $\epsilon_{loss}^{\%} \approxeq 36.338\%$, and therefore not desirable for the agile proximity maneuvers in space. Lastly, in the given inequality physical constraints, $u_{\max}$ is characterized by the chaser's thruster performance; F (Newton), mass; m (kg), sampling time; $T_s(s)$ in the following form;

$$u_{\max} = \frac{F}{m} T_s. \tag{4.67}$$

4.3.3 Inscribed Polygon Method

This section presents the main contribution of this Chapter. Inequality relation given in Eqn. (4.81) is quadratic and convex constraint. To our best knowledge, it has been observed that to address single axis thruster configured spacecraft motion planning & control problem, standard decoupled infinity norm constraints given in Eqn. (4.64) or SOCP methods are employed [59, 105, 168, 169].

The inscribed polygon depicted in Fig. 4.5 consists of n number of segments which can be expressed as [170]

$$a_k u_x + b_k u_y = c u_{\max}, \ \forall k \ \in \ \{1, ..., n\} \tag{4.68}$$

where $u_{x,i}$ & $u_{y,i}$ are the optimal inputs at the time instant i; a^k, b^k and c are the constants, calculated based on Eqns. (4.69-4.71) and $u_{\max}$ is user-defined maximum thrust magnitude constant.

$$a_k \ = \sin\Big(\frac{2\pi \times k}{n}\Big) - sin\Big(\frac{2\pi \times (k-1)}{n}\Big) \tag{4.69}$$

$$b_k \ = \ -cos\Big(\frac{2\pi \times k}{n}\Big) + cos\Big(\frac{2\pi \times (k-1)}{n}\Big) \tag{4.70}$$

$$c \ = sin\Big(\frac{2\pi}{n}\Big) \tag{4.71}$$

Having said that, for every time instant, there exist n different inequality constraints therefore, QCQP problem can be now transformed into QP via using the

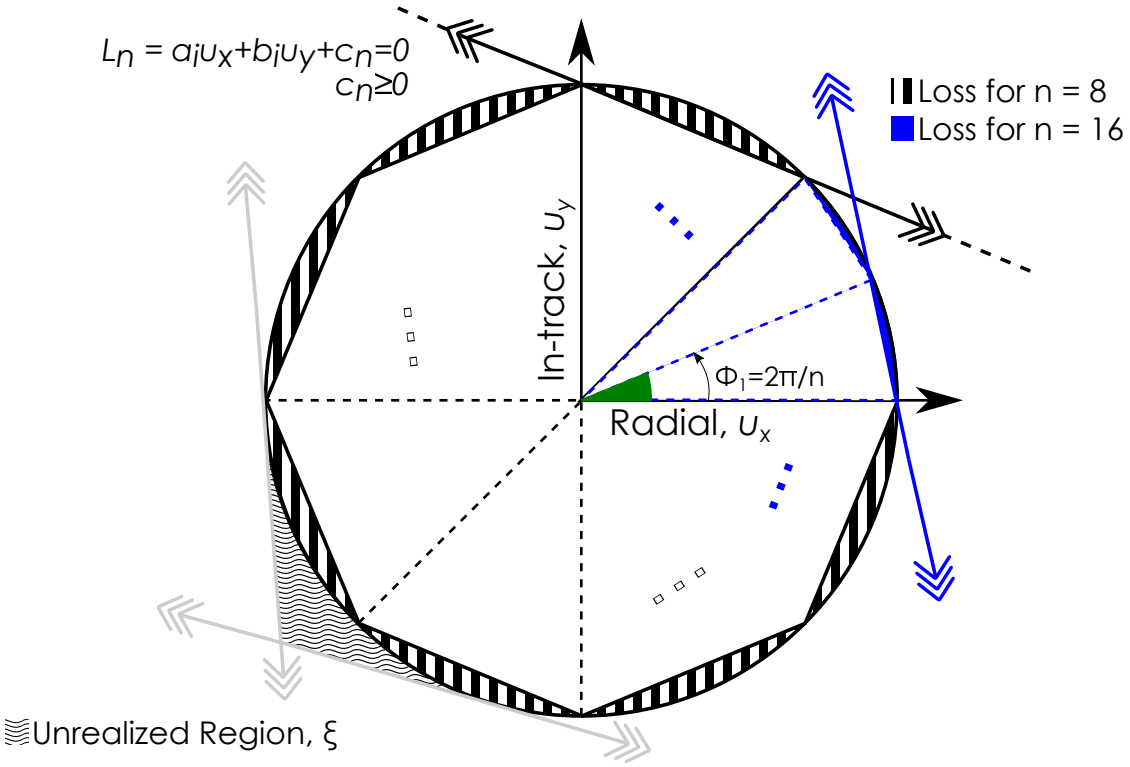

FIGURE 4.5: Illustration of Inscribed Polygon

generalized equation in (4.68) in the following generalized inequality form:

$$G_u \boldsymbol{u} \leq g_u \tag{4.72}$$

Eventually, given inequality constraints (4.60) & (4.72), finally;

Assumption: Let $\mathbb{X} \subseteq \mathbb{R}^{n_x}$, $\mathbb{U} \subseteq \mathbb{R}^{n_u}$, $\mathbb{P} \subseteq \mathbb{X}$ be convex, closed polytopic sets, specified in the form: $\mathbb{X} \triangleq \{\boldsymbol{x} : G_x \boldsymbol{x} \leq g_x\}$, $\mathbb{U} \triangleq \{u : G_u \boldsymbol{u} \leq g_u\}$, $\mathbb{P} \triangleq \{\boldsymbol{x} \ : \ c_\eta \boldsymbol{x} \leq d_\eta\}$

4.3.4 Evaluation Of The Performance

In this section, the overall encapsulated thrust region method is introduced to evaluate the performance of the approximation. In Fig. 4.5, it is clear that for any approximations to a circle there is a loss of control authority. In the area method, one can simply calculate the areas of circle by employing $A_{circle} = \pi R^2$ where R is the radius of the circle. In addition, the area of n-sided convex regular polygon can be calculated by $A_{polygon} = n \times \frac{1}{2} R^2 * sin(\phi)$ where $\phi = 2\pi/n$. The thrust region

loss is denoted with $\epsilon^{\%}_{loss}$ and calculated by

$$\epsilon^{\%}_{loss} = \left| \frac{A_{circle} - A_{polygon}}{A_{circle}} \right| \times 100. \tag{4.73}$$

In addition, in order to evaluate the $T_{Computation}$, the same scenario is simulated for varying n and normalized with a computation time of the original QCQP problem. It is reflected into Table 4.1 that adding more sides to polygon after $n = 24$ leads

TABLE 4.1: Performance Of Different Regular Polygons

Configuration n =	4	8	16	24	32	40	∞ (Circle)
Loss %	36.34	9.97	2.55	1.13	0.64	0.41	0
$T_{Computation}$ %	-6.4	-3.3	-2.3	+0.7	+2	+6.7	-

to diminishing return with extra computation time.

4.3.5 Cost Function

Now, MPC formulation can be finalized. We employ linearized & LTV dynamics motion model (i.e., Y-A Equations), linear constraints (i.e., Input + Line of Sight), and quadratic costs on the states and control input changes. Let $\boldsymbol{x_i}$ and $\boldsymbol{u_i}$ denote the state and input predictions into the future from the current time step i, up to prediction horizon N_p. Define $\Delta\boldsymbol{x} = (\boldsymbol{x_i} - \boldsymbol{x_{i,ref}})$, $\Delta\boldsymbol{u_i} = (\boldsymbol{u_i} - \boldsymbol{u_{i-1}})$, $\mathbf{u} = (\boldsymbol{u_0}, ..., \boldsymbol{u_{N_c-1}})$, $\mathbf{x} = (\boldsymbol{x_0}, ..., \boldsymbol{x_{N_p}})$ where $\boldsymbol{x_{ref}}$ denotes the target, i.e., docking port, and therefore, the cost function

$$J(\mathbf{x}_0, \Delta\mathbf{u}) = \sum_{i=0}^{N_p-1} \left(\left\| \Delta\boldsymbol{x_i} \right\|^2_Q + \left\| \Delta\boldsymbol{u_i} \right\|^2_R \right) \tag{4.74}$$

for matrices $Q \in \mathbb{R}^{n_x \times n_x} \geq 0$ (Positive-Semidefinite (PSD) weight matrix and penalizes the state values), $R \in \mathbb{R}^{n_u \times n_u} \geq 0$ (PSD weight matrix and penalizes the control input change). At each time step i, the designed MPC based controller solves the Problem 1 and applies $\boldsymbol{u_i} = \boldsymbol{u_0^\bullet}(\boldsymbol{x_i})$ where $()^\bullet$ denotes an optimal value. For single-axis thruster configuration, there exists a quadratic input constraint in the form of Eqn. (4.65). Hence, the original LTV QCQP problem is

Problem 1.

$$
\begin{aligned}
(\mathbf{u}^{\bullet},\ \mathbf{x}^{\bullet}(\boldsymbol{x})) &= \min_{(\mathbf{u},\mathbf{x})} J(\mathbf{x},\mathbf{u}) && (4.75)\\
\text{subject to } \boldsymbol{x_0} &= \boldsymbol{x} && (4.76)\\
\boldsymbol{x_{i+1}} &= A_i\boldsymbol{x_i} + B_i\boldsymbol{u_i}, \forall i \in \{0,...,N_p-1\} && (4.77)\\
c_\eta \boldsymbol{x_i} &\leq d_\eta\ \forall i \in \{0,...,N_p-1\} && (4.78)\\
\boldsymbol{x_i} &\in \mathbb{X},\ \forall i \in \{0,...,N_p-1\} && (4.79)\\
\boldsymbol{u_i} &\in \mathbb{U},\ \forall i \in \{0,...,N_c-1\} && (4.80)\\
u_{x,i}^2 + u_{y,i}^2 &\leq u_{\max},\ \forall i \in \{0,...,N_c-1\} && (4.81)
\end{aligned}
$$

Given the inequality constraint in Eqn. (4.81), the problem is no longer a QP representable but is transformed into QCQP. By applying the IPA mentioned in Section 4.3.3, Problem 1 can be approximated with the following formulation

Problem 2.

$$
\begin{aligned}
(\mathbf{u}^{\bullet},\ \mathbf{x}^{\bullet}(\boldsymbol{x})) &= \min_{(\mathbf{u},\mathbf{x})} J(\mathbf{x},\mathbf{u}) && (4.82)\\
\text{subject to } \boldsymbol{x_0} &= \boldsymbol{x} && (4.83)\\
\boldsymbol{x_{i+1}} &= A_i\boldsymbol{x_i} + B_i\boldsymbol{u_i}, \forall i \in \{0,...,N_p-1\} && (4.84)\\
c_\eta \boldsymbol{x_i} &\leq d_\eta\ \forall i \in \{0,...,N_p-1\} && (4.85)\\
\boldsymbol{x_i} &\in \mathbb{X},\ \forall i \in \{0,...,N_p-1\} && (4.86)\\
\boldsymbol{u_i} &\in \mathbb{U},\ \forall i \in \{0,...,N_c-1\} && (4.87)\\
a_1u_{i,x} + b_1u_{i,y} &\leq cu_{\max},\ \forall i \in \{0,...,N_c-1\} && (4.88)\\
a_2u_{i,x} + b_2u_{i,y} &\leq cu_{\max},\ \forall i \in \{0,...,N_c-1\} && (4.89)\\
&\vdots\\
a_nu_{i,x} + b_nu_{i,y} &\leq cu_{\max},\ \forall i \in \{0,...,N_c-1\} && (4.90)
\end{aligned}
$$

where Eqn. (4.81) is approximated by Eqns. (4.88-4.90).

Remark 11. Let $\mathbb{K}$ be the QCQP defined in Problem 1 and $\mathbb{K}(n)$ be the IPA of the QP problem defined in Problem 2. Then, $\mathbb{K}(n) \to \mathbb{K}$ as $n \to \infty$, in other words, $lim_{n\to\infty} \left\|\mathbf{x}(\mathbf{n}) - \mathbf{x} = 0.\right\|$ However, because every piece-wise segments of the IPA linear constraints are written explicitly in the form of Eqns. (4.88-4.90), it comes

with additional computation load. Hence, a trade-off between the performance calculated in Eqn. (4.73) and the computation load is required.

Remark 12. In order to fully utilize the thrusters, it is possible to obtain circumscribed polygon approximation with tangential lines as depicted in Fig. 4.5 with gray lines. However, in this case, the *Unrealized Region*, ξ appears. This is not desirable because after some time, constraints may not be satisfied and the problem can become infeasible. This may end up with catastrophic events in space, i.e., collision. On the other hand, circumscribed polygon allows full realization with a potential loss depicted in the Table 4.1.

Remark 13. Problem 1 is in the form of QCQP due to the Eqn. (4.81) and because it is convex, commercial solvers internally formulate it in the conic form [171, 172]. The main advantages are the mature duality theory for conic optimization problems, direct formulation of conic form for equivalent problem formulation. However, the strategy is to introduce extra variables, linear constraints and quadratic cones to conserve the original variables for equivalent problem but results in a larger problem. On the other hand, in space systems, simplicity is one of the main requirements. One can note that for 3-axes coupled dynamics, i.e., landing on an asteroid, the proposed strategy can be easily implemented by assigning n number of planes instead of lines for intercept polygons. This approximation would result in 3D regular, inscribed polyhedron as depicted in Fig. 4.6

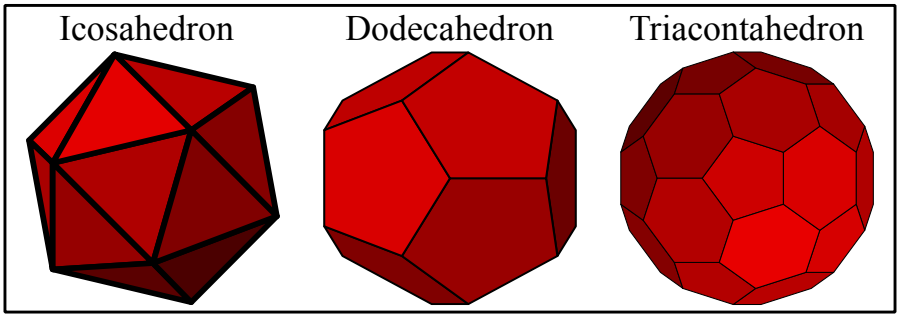

FIGURE 4.6: Illustration Of Polyhedron Approximation To A Sphere

4.4 Simulated Scenarios

In this section, the performance of the proposed approach is evaluated for two challenging scenarios. First, approaching and synchronizing with an uncontrolled

target in a circular orbit. This case is formulated as LTI system explained in Section 4.2 by employing HCW Equations [150]. Second, docking with a stable target in a highly elliptic orbit. This case is formulated as LTV system explained in Section 4.2.5 by employing Y-A Equations [167]. Details about the scenarios are given in Table 4.2 & 4.3. The formulation has been tested by the Nonlinear High Fidelity Engineering Model provided by industrial partner Thales Alenia Space/France. To formulate the optimization Problem 2 (Section 4.3.5), we used CVX, an open source MATLAB based modeling language for convex optimization & MPC [173] and Gurobi as a solver [171].

Table 4.2: MPC Specifications

Parameter	**Case-1**	**Case-2**
X0	[0.25 53 0 0 0 0]	[-20 150 0 -1.5 0 0]
Q	diag([0.01 0.01 0.01 0 0 0])	diag([0.01 0.001 0.01 0.5 0.5 0.5])
R	diag([100 100 100])	diag([10000 10000 10000])
Ts	1[s]	1[s]
Horizon	20	25

In the first scenario, given $53m$ in-track ($y-axis$) separation and $0.25m$ radial ($x-axis$) misalignment as an initial condition, the objective is to approach the uncontrolled satellite up to 20m and synchronize with it for an inspection and/or a robotic operation. Standard linearization (STD-L) could not achieve the objective due to the loss in the thruster utilization, whereas QCQP and IPA successfully obtains the required maneuvers. As illustrated in Figures 4.7 & 4.8, the solution of the Problem 2 becomes infeasible after some time, if the segment number (n) of the IPA approach is not sufficiently selected, i.e., for n=4, there is no feasible solution after 7s.

In the second scenario, docking with a stable target in an elliptic orbit is simulated. In highly elliptic orbits, it is a strong possibility for a controlled satellite to have an initial relative velocity before the execution of the proximity maneuver. Hence, given $-1.5m/s$ initial relative velocity in the radial direction due to high eccentricity, chaser is separated from the target with $-20m$ radial and $150m$ in-track directions. The objective is to compensate the relative velocity and approach the target along in-track axis while respecting LOS constraint mentioned in Eqn. (4.60). Fig. 4.9 shows that for each approach the thruster is fully utilized at the beginning of the maneuver in order to cancel the relative velocity in the radial

direction. However, due to the realization limits, trajectories differ as depicted in Fig. 4.10. It is shown with green triangles that the STD-L trajectory is just able to stay inside the cone. For even slightly higher relative velocity, eccentricity or lower cone angle, STD-L approach is not able to meet with the docking conditions. On the other hand, IPA approach even with insufficient "n" numbers shows a well approximation to the coupling between x-axis & y-axis. In addition, as n increases, the realization is maximized and after $n = 16$, QCQP and IPA results overlap. Eventually, with a sufficiently selected number of n, the IPA approach can address single-axis thruster configuration problem for spacecraft maneuvers.

TABLE 4.3: Scenario Specifications

Parameter	**Case-I**	**Case-II**	**Unit**
$F_{\max}$	40	50	[N]
Chaser Mass	400	500	[kg]
Eccentricity	0	0.7	∅
Perigee Height	590	500	[km]
Inclination	0	0	[deg]
Longitude of the Ascending Node	0	0	[deg]
Argument of Perigee	0	0	[deg]
Initial True Anomaly	0	30	[deg]
LOS Cone Angle	45	15	[deg]
Target Rotation Rate	3	0	[deg/s]

4.5 Lessons Learned

Throughout this section, *Inscribed Polygon Approach* is developed to address the QCQP problem arising in single axis thruster configuration. It has been validated via simulations in NHFEM that proposed method provides quasi circle input constraint realization, in other words, the controller can well approximate to fully utilization of the thruster. In addition, requirements of advanced optimization methods and tools are relaxed, problem can now be solved with mature & reliable QP solvers for fast real-time implementations, i.e., via CVXGEN. In the future, dynamic experiment tests will be conducted to validate simulation results.

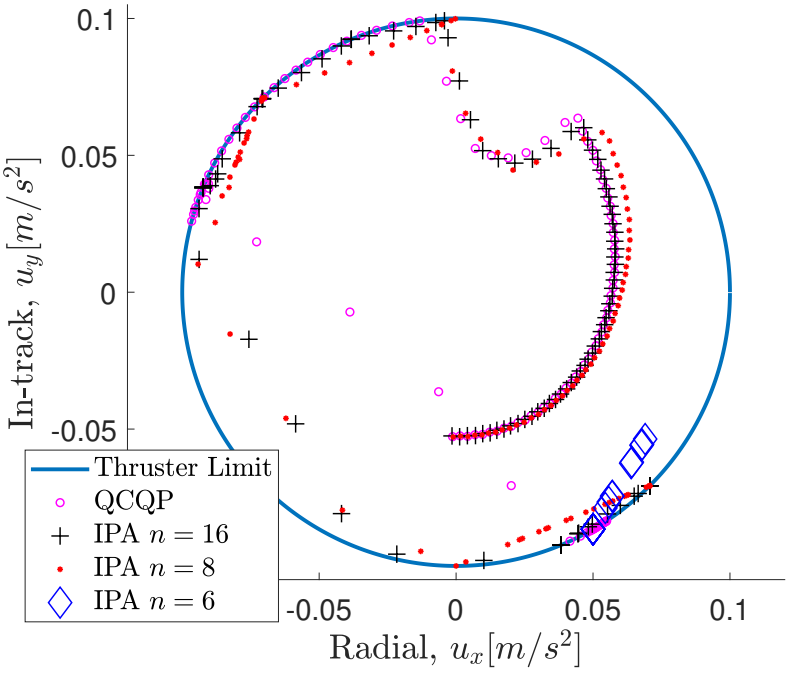

FIGURE 4.7: Scenario 1 - Input History in Circular Orbit

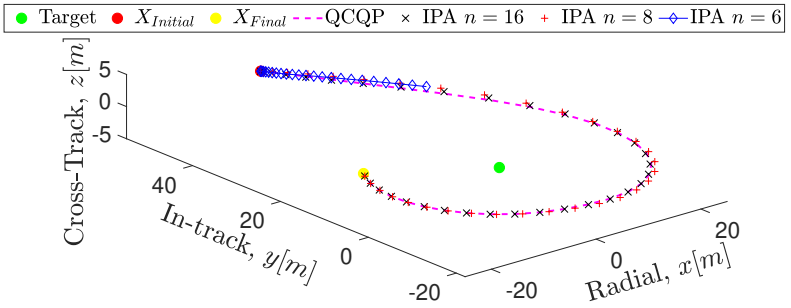

FIGURE 4.8: Scenario 1 - Trajectory History in Circular Orbit

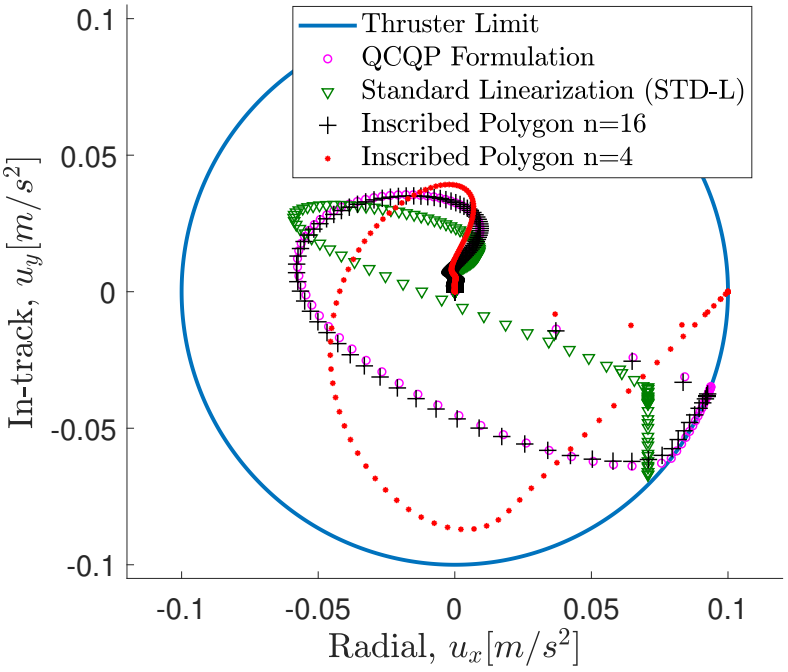

FIGURE 4.9: Scenario 2 - Input History in Elliptic Orbit

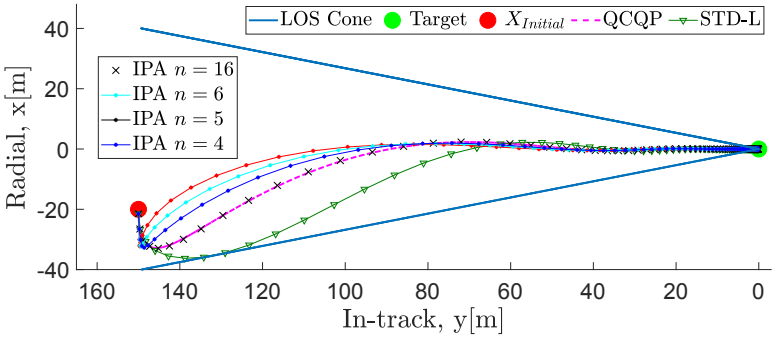

FIGURE 4.10: Scenario 2 - Trajectory History in Elliptic Orbit

Chapter 5

Rendezvous and Docking Problem with Multiple Thruster Configuration

This chapter presents a Guidance and Control (G&C) strategy to address 6-DOF spacecraft attitude and position control for future Rendezvous and Docking (RVD) missions. Future RVD missions, specifically when the target is uncooperative, are challenging as geometric constraints and parameter uncertainties are both present. In addition, due to close proximity and potential angular motion of the target satellite, the point mass approach is no longer sufficient to represent the relative motion dynamics. Hence, throughout this chapter, the coupling between translational and rotational motion of spacecraft relative motion is addressed via Dual Quaternions and Piece-wise Model Predictive Control framework. The algorithm is developed such that the relative position of interest is no longer Centre-Of-Mass (COM) position of the target satellite but can be docking port or a predefined grasping feature. Secondly, physical and geometric constraints are explicitly formulated and respected by formulating a constrained optimization problem. The proposed framework is real-time implementable because the control problem is formulated as a convex optimization problem. Simulation results show that the proposed algorithm is promising because it can respect the physical and geometric constraints and minimize the propellant consumption while coupling translational and rotational motion and still being real-time implementable.

5.1 Guidance & Controller Design

The G&C problem can be posed as an optimal control problem with dynamics describing the motion of the spacecraft subject to constraints on the vehicle state and controls. The generic form is [148]

Problem 3. Generic Autonomous Spacecraft Guidance Problem in Continuous Form

$$\begin{aligned} \min_{t_f,u} \quad & J(x(t),u(t),t) = K(x(t_f),t_f) + \int_{t_0}^{t_f} L(x(t),u(t),t)dt \\ \text{subject to} \quad & \dot{x}(t) = f(x(t),u(t),t) \\ & u(t) \in \mathbb{U}(t) \\ & x(t) \in \mathbb{X}(t), \forall\ t \in [t_0,t_f] \end{aligned}$$

where $x \in \mathbb{R}^n$ is the state of the spacecraft, $u \in \mathbb{R}^m$ is the control input, $t \in \mathbb{R}$ is time, $J : \mathbb{R}^{n+m+1} \to \mathbb{R}$ is the cost-functional (which combines terminal and incremental additive cost functions K and L), $f : \mathbb{R}^{n+m+1} \to \mathbb{R}^n$ defines the dynamics, and $\mathbb{U} : \mathbb{R} \to \mathbb{R}^m$ and $\mathbb{X} : \mathbb{R} \to \mathbb{R}^n$ are set-valued maps defining spacecraft control and state constraints. Due to the existence of system dynamics and constraints, the resulting optimal control problem must be solved numerically via an optimization algorithm after a proper discretization [174–177]. Hence, the generic problem can be written in the following discrete form:

Problem 4. Generic Autonomous Spacecraft Guidance Problem in Discrete Form

$$\begin{aligned} \min \quad & J(x_k,u_k,k) = F_{N_p}(x_{k+N_p}) + \sum_{i=0}^{N_p-1} l(x_{k+i},u_{k+i}) \\ \text{subject to} \quad & x_{k+i+1} = f(x_{k+i},u_{k+i}), \forall\ i \in \{0,\dots,N_p-1\} \\ & x_{k+i} \in \mathbb{X}\ \forall\ i \in \{0,\dots,N_p-1\} \\ & u_{k+i} \in \mathbb{U}\ \forall\ i \in \{0,\dots,N_p-1\} \\ & x_{k+N_p} \in \mathbb{T}. \end{aligned}$$

where x_k is the state of the spacecraft at time k and x_{k+i} is the state of the spacecraft at time $k+i$, predicted at time k obtained by starting from the current state x_k and applying to the system model the input sequence $u_k, u_{k+1}, ..., u_{k+i-1}$. Further, $\mathbb{T} : \mathbb{R} \to \mathbb{R}^n$ is set-valued maps defining spacecraft terminal state constraint.

5.1.1 Linear Parameter Varying Model Predictive Control

In this section, we discuss the dynamic equality constraint of the optimization problem. MPC paradigm closes the loop by simply re-planning the maneuver at each time step, after applying the set of control inputs corresponding to the first time step, and keeps looking ahead N_p time steps, i.e., the so-called receding horizon strategy. Unlike standard linear time-invariant MPC formulation, the LPV model must be updated when parameters of the model change and therefore, the QP matrices to be constructed online in accordance. Hence, the re-planning is done with the updated model that is obtained from the actual states at each time step. This scheme brings feedback action that can compensate for the disturbances and modeling uncertainties to some level. We can now provide the following LPV system sampled and updated at time instant k as

$$x_{k+1} = A_k x_k + B_k u_k, \tag{5.1}$$

Unlike standard linear time-invariant MPC formulation, the LPV model must be updated at every instant k and therefore, the matrices that constructs the special type of resulting optimization problem: Quadratic Programming (QP) to be constructed online in accordance. Hence, the re-planning is done with the updated model that is obtained from the actual states at each time step where $x_k \in \mathbf{R}^n$ and $u_k \in \mathbf{R}^m$ are the state and the control vectors, respectively. This LPV system is subject to the following state and input constraints

$$x_k \in \mathcal{X}, \text{ and } u_k \in \mathcal{U} \tag{5.2}$$

where $\mathcal{X}$ and $\mathcal{U}$ are assumed to be the convex sets. Lastly, the dynamic and input matrices A_k and B_k are obtained at time instant k and, remain constant in the interval of $[k, k + \Delta t]$. In other words, the PWA linearization technique is applied at every time step and resulting matrices are employed in the equality constraint till the end of prediction horizon N_p.

5.1.2 Objective Function

In [49], the cost function $J_t^\dagger$ to be minimized is selected as

$$J_t^\dagger(x_0, \mathbf{U}) = \sum_{k=0}^{N_p-1} \left(\left\| \mathbf{x_k} \right\|_Q^2 + \left\| \mathbf{u_k} \right\|_R^2 \right) + \left\| \mathbf{x}_{N_p} \right\|_{Q_p}^2 \quad \text{s. t. constraints} \tag{5.3}$$

where $Q \succeq 0$ and $R \succ 0$ are the penalty weights on the states and inputs, $Q_p \succeq 0$ is the terminal state penalty weight. The cost function given in Eqn. (5.3) is beneficial when the problem is a stabilizing or a regulation problem as it penalizes the states and input values while terminal penalty ensures stability of the system. However, upon the discussion held in Chapter 3, the cost function is not suitable even when the problem is simply keeping a satellite with a constant rotation rate. Furthermore, the RVD problem has additional complexities due to the following arguments: Traditionally, Center-Of-Mass (COM) is the position of interest for close proximity maneuvers [150, 151, 167]. However, docking ports are located elsewhere on the spacecraft and the relative position, as well as velocity in between, maybe time-varying despite the fact that relativity of COM stays still. Therefore, first, the relative motion dynamics and kinematics models must account for the couplings in the system second, the control must be able to derive the states to a desired state vector based on the location & direction of the docking port when the mechanical connection to be achieved. Thanks to dual quaternion, similar to [49], the couplings can be addressed. However, for off-set free tracking of target satellite and misalignment free RVD operation, the desired docking port relative states must be known and included in the problem formulation. In our use case, the target is assumed to be non-cooperative and shares no information about its states. Hence, the chaser satellite must have the required information of docking port-to-port motion information in order to consistently formulate the optimization problem. Throughout this work, it is assumed that the instantaneous relative states are known. Hence, it is a matter of modeling the attitude modes of the target as it results in the docking port motion. To get offset free tracking of a reference in the presence of an unknown but constant disturbance, we need:

- In steady-state, the minimum of J must be consistent with zero tracking errors. This can be simply achieved by editing the cost function and in our

case, *Cost Function* 3 satisfies the consistency requirement.

- The predictions must be unbiased, i.e., in steady state, the prediction model should give $\hat{Y} = [I; I; \ldots; I]^T y_{ss}^{real}$, regardless of any differences between the model and the process due to uncertainty and disturbances. This uncertainty could be a modelling uncertainty, e.g., attitude dynamics, knowledge of the mechanical properties, whereas the disturbance could be solar radiation pressure or atmospheric drag. This could be achieved by augmenting the state space model that includes output term, y.

Instead of the state space model (1), we could also derive the MPC control law by using a state space model with an incremental input and output term in the new state vector ensuring the integral action. Below, two examples are given (can be more).

First,

$$\underbrace{\begin{bmatrix}\Delta x_{k+1}\\ y_k\end{bmatrix}}_{\xi_{k+1}} = \underbrace{\begin{bmatrix}A_d & 0\\ C_d & I\end{bmatrix}}_{A}\underbrace{\begin{bmatrix}\Delta x_k\\ y_{k-1}\end{bmatrix}}_{\xi_k} + \underbrace{\begin{bmatrix}B_d\\ 0\end{bmatrix}}_{B}\Delta u_k, \tag{5.4}$$

$$y_k = \underbrace{\begin{bmatrix}C_d & I\end{bmatrix}}_{C}\underbrace{\begin{bmatrix}\Delta x_k\\ y_{k-1}\end{bmatrix}}_{\xi_k} \tag{5.5}$$

Second,

$$\begin{bmatrix}\Delta x_{k+1}\\ y_{k+1}\end{bmatrix} = \begin{bmatrix}A_d & 0\\ C_d A_d & I\end{bmatrix}\begin{bmatrix}\Delta x_k\\ y_k\end{bmatrix} + \begin{bmatrix}B_d\\ C_d B_d\end{bmatrix}\Delta u_k, \tag{5.6}$$

$$y_k = \begin{bmatrix}0 & I\end{bmatrix}\begin{bmatrix}\Delta x_k\\ y_k\end{bmatrix} \tag{5.7}$$

These state space models can be written in the final compact form

$$\xi_{k+1} = A\xi_k + B\Delta u_k \tag{5.8}$$

$$y_k = C\xi_k \tag{5.9}$$

where ξ is the new augmented state vector and the matrices A, B & C are defined in (5.4-5.5). Now, let the Eqn. (3.27) define the dual quaternion errors to be

minimized and $\Delta\tilde{\mathbf{F}}$ be the rate of change of inputs in dual quaternion format. The cost function can be written as

$$J^{\ddagger}(x_0, \Delta\mathbf{U}) = \sum_{i=1}^{N_p} \left(\left\| \begin{bmatrix} \tilde{q}_e \\ \tilde{\omega}_e \end{bmatrix} \right\|_Q^2 + \left\| \Delta\tilde{\mathbf{F}} \right\|_R^2 \right) \tag{5.10}$$

where $Q \succeq 0$ and $R \succ 0$ are the block diagonal penalty weights on the output errors and rate of change of inputs. In addition, $[\tilde{\omega}_k^T \ \tilde{q}_k^T]^T$ is the state vector and $\Delta\mathbf{F}$ is the rate of change of control inputs. As explained in Section 4.2.4, new state vector $x_k = [\tilde{\omega}_k^T \ \tilde{q}_k^T]_{16\times1}^T$, $\mathbf{U} = \tilde{\mathbf{F}}$ and, $\boldsymbol{\Delta}\mathbf{U} = \Delta\mathbf{F}$ can be defined to write the general optimization problem in the following section.

5.1.3 Optimization Problem

This section introduces the algorithm developed throughout this thesis to address 6-DOF fuel optimal rendezvous and docking with uncooperative targets problem. The problem formulation consists of three key elements: cost function, constraints, and the prediction model. Without the loss of generality, the problem formulation is as follows:

Problem 5.

$$\min \ J^{\ddagger}(x_0, \Delta\mathbf{U}) \tag{5.11a}$$

$$\text{subject to } \ x_0 = x \tag{5.11b}$$

$$x_{k+1} = A_t x_k + B_t u_k, \forall k \ \in \ \{0, ..., N_p - 1\} \tag{5.11c}$$

$$y_k = C_t x_k, \forall k \ \in \ \{0, ..., N_p - 1\} \tag{5.11d}$$

$$u_k \in \mathbf{U}, \ \forall k \in \ \{0, ..., N_c - 1\} \tag{5.11e}$$

$$\Delta u_k \in \Delta\mathbf{U}, \ \forall k \in \ \{0, ..., N_c - 1\} \tag{5.11f}$$

$$y_k \in \mathbf{Y}, \ \forall k \in \ \{0, ..., N_p\} \tag{5.11g}$$

First, the cost function which is given in Eqn. (5.10) penalizes the state errors and rate of change of control inputs. Next, the equality state constraints given in Eqn. (4.58) is augmented with Eqn. (5.6). Hence, the constraints on states are enforced to the outputs to achieve integral action for disturbance rejection and robustness to the modelling uncertainties. This includes the output constraints on the angular

rates and velocity of the target satellite to ensure safety. Further, the input and rate of change of input constraints are enforced in Equations (5.11e-5.11g). Finally, regarding the experimental setup, it is fairly assumed that the states are measured and full state feedback is available at all time instants as given in Eqn. (5.11b).

FIGURE 5.1: Block Diagram

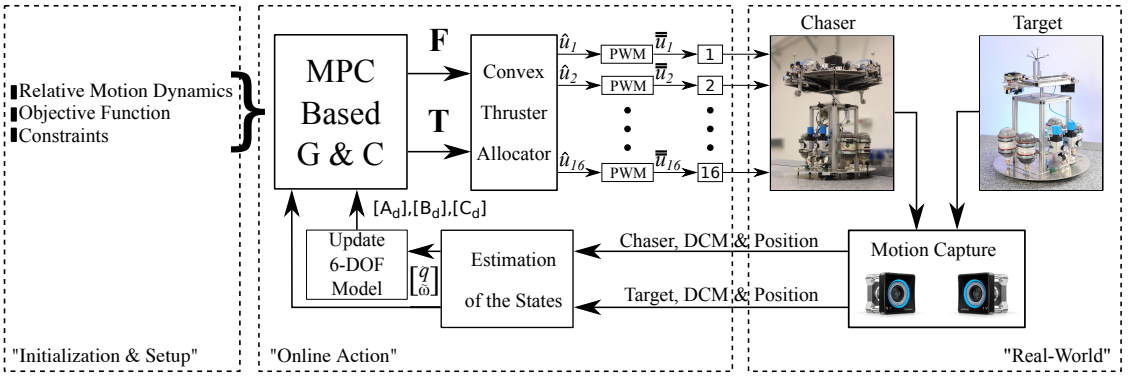

5.1.4 Constraints

A number of constraints exist in the spacecraft maneuvering problem. These constraints may be respected by tuning the weight parameters. However, mentioned method provides no guarantee of constraint satisfaction. Hence, the controller either becomes unaware of being unable to deliver the commanded for instance input values, or for conservative tuning, thrusters may never be fully utilized. This results in excessive input use or violation of state constraints. To address this section discusses the input & output constraints and, the procedure to address them within QP formulation.

5.1.4.1 Rate Of Change Of Input Constraint

The valve opening time or the gimbaled thruster to direct towards the commanded direction takes time. This duration can be explicitly handled by formulating the rate of change of input constraints.

Remark 14. Recall that $\Delta u_k = u_k - u_{k-1}$. and $u_k = [u_{k,T}^T, u_{k,F}^T]_{6\times 1}^T$ where k is the sampling instant.

As explained in the Problem #2 (Section 4.3.5), the decision variable is the rate of change of control inputs. Hence $\mathbf{\Delta U}$, the constraints on the rate of change of force and torque values can be given by:

$$\Delta\mathbf{U} = \left\{ \Delta u_k \in \mathbf{R}^6 \middle| \underbrace{\begin{bmatrix} \Delta u_{\mathbf{Fmin}} \\ \Delta u_{\mathbf{Tmin}} \end{bmatrix}}_{\Delta u_{min}} \leq \Delta u_k \leq \underbrace{\begin{bmatrix} \Delta u_{\mathbf{Fmax}} \\ \Delta u_{\mathbf{Tmax}} \end{bmatrix}}_{\Delta u_{max}} \right\} \tag{5.12}$$

where, Δu_k is the rate of change of input at time instant k, Δu_{min} and Δu_{max} are the lower and upper rate of change of input limits.

5.1.4.2 Input Constraint

The maximum thrust force and torque that can be delivered is limited to the capacity of the thrusters. $\mathbf{U}$ is the constraints on the deliverable force and torque values can be given by:

$$\mathbf{U} = \left\{ u_k \in \mathbf{R}^6 \middle| \underbrace{\begin{bmatrix} u_{\mathbf{Fmin}} \\ u_{\mathbf{Tmin}} \end{bmatrix}}_{u_{min}} \leq u_k \leq \underbrace{\begin{bmatrix} u_{\mathbf{Fmax}} \\ u_{\mathbf{Tmax}} \end{bmatrix}}_{u_{max}} \right\} \tag{5.13}$$

where, u_k is the input at time instant k, u_{min} and u_{max} are the lower and upper input limits.

Remark 15. Each thruster can produce maximum thrust of 65 mN. Regarding to the thruster configuration, 0.26 N thrust can be generated in each direction and 6 mNm torque can be generated.

5.1.4.3 Output Constraints

Due to the safety reasons, constraints on angular rates ω and velocity $\mathbf{v}$ are enforced as

$$\mathbf{Y} = \left\{ \tilde{\omega}_k \in \mathbf{R}^8 \middle| \underbrace{\begin{bmatrix} \tilde{\omega}_{\omega-\mathbf{min}} \\ - \\ \tilde{\omega}_{\mathbf{v}-\mathbf{min}} \\ - \end{bmatrix}}_{\tilde{\omega}_{min}} \leq \tilde{\omega}_k \leq \underbrace{\begin{bmatrix} \tilde{\omega}_{\omega-\mathbf{max}} \\ - \\ \tilde{\omega}_{\mathbf{v}-\mathbf{max}} \\ - \end{bmatrix}}_{\tilde{\omega}_{max}} \right\} \tag{5.14}$$

This is mainly to ensure that the spacecraft will not be shortsighted and therefore the problem becomes infeasible because there is also a limit in the available input force and torque values. In addition, increased rotation rate will result in higher non-linearity; therefore, higher error when PWA based modeling approach is applied.

5.1.4.4 Conic Constraints

For real-time implementation capability, the problem is cast as a QP problem with quadratic cost and linear constraints. On the other hand [49] formulated the so-called Field-of-view and line-of-sight constraints. FOV is the limit of the sensors and LOS is the allowed safe cone for proximity maneuver and both can be formulated as conic constraints. However, as can be seen from the hierarchy below, including conic constraints increases the complexity of the optimization problem to Second Order Cone Programming (SOCP) form in which the available processing power fails to meet with the computation time requirements [178]

$$\underbrace{LP \subseteq QP \subseteq QCQP \subseteq SOCP \subseteq SDP}_{Convex} \subseteq \underbrace{NP}_{Non-convex} \tag{5.15}$$

where LP is "Linear Programming", SDP is "Semi-definite Programming" and finally NP is "Nonlinear Programming". Hence, although it is a convex optimization problem, due to the average solution time, conic constraints are left as future work.

5.2 Thruster Types & Allocation Problem

In the literature, the three main thruster firing cases are referred as Pulse Width-Modulated (PWM), Pulse Amplitude-Modulated (PAM) and impulsive control approaches. This section introduces different thruster characteristics, the motivation of our selection, as well as the theory, developed to address the thruster allocation problem.

5.2.1 Pulse Width-Modulated (PWM)

In the PWM type, the actuators' output level is fixed to the F_{max} which is the maximum thrust force that can be generated by that particular thruster. The binary switch is the only parameter that can be controlled; therefore, thrusters can be turned on or off only. Eventually, the control problem becomes nonlinear in switching times despite the linear dynamics. The mathematical formulation can be given as

$$u_i(t) = \begin{cases} 0, t \in [t_k, t_k + \tau_{k,i}), \\ u^w_{k,i}, t \in [t_k + \tau_{k,i}, t_k + \tau_{k,i} + \kappa_{k,i}), \\ 0, t \in [t_k + \tau_{k,i} + \kappa_{k,i}, t_{k+1}], \end{cases} \tag{5.16}$$

with $\kappa_{k,i} > 0,\ \tau_{k,i} > 0$ and $\kappa_{k,i} + \tau_{k,i} < T$ where T is the sample time and k denotes the sampling step of each term. In each sampling step, each input u_i is the input pulse which starts at a time $\tau_{k,i}$ with a pulse width $\kappa_{k,i}$ and with a maximum thrust magnitude of $u_{max} = i^w_{k,i}$, and the last constraint ensures that the PWM signal is cut at the end of the current time step [169].

5.2.2 Pulse Amplitude Modulated (PAM) Type Thruster

Unlike PWM, PAM type thrusters can generate any input signal within the physical limits. In the mathematical framework,

$$u_i(t) = \Big\{ u^A_{k,i}, t \in [t_k, t_k + \tau_{k,i}], \tag{5.17}$$

5.2.3 Impulsive Control

Impulsive thrust configuration, usually also known as ΔV's, to obtain a maneuver in space is widely used where initial and final impulses are computed to achieve the rendezvous. In this model, it is also assumed that the impulse $u_i(t)$ can be applied at any sample interval in any direction. However, the dynamic equality constraint differs and can be written as

$$x_{k+1} = A(t_{k+1}, t_k)x_k + B(t_{k+1}, t_k)u_k, \tag{5.18}$$

where u_k is the input vector at time instant k and,

$$B(t_{k+1}, t_k) = A(t_{k+1}, t_k)B_d \tag{5.19}$$

where B_d is the input matrix.

5.2.4 Thruster Allocation Cost Function

Given the required background above, we can now describe the solution to the spacecraft thruster allocation problem arising from 16-PWM type thrusters on the chaser TEAMS5D robot. Those thrusters are used for both translational and rotational motion of the simulators. In the literature, the problem is investigated for space and underwater vehicles via optimization based and analytical solutions [138, 179, 180]. Consequently, the objective is to design an allocator that minimizes the fuel expenditure while meeting with the commanded force and torque values. It is commonly 1-norm of the control signal, proven that the most effective way to save fuel use [123]. Hence the corresponding cost functions can be given as

$$J_{PAM} = \sum_{k=0}^{N_p-1} \|u^T(k)\|_1 = \|u_s\|_1 \tag{5.20}$$

$$J_{PWM} = \sum_{k=0}^{N_p-1} \sum_{i=1}^{3} (u^+_{i_{max}} \kappa^+_i(k) + u^-_{i_{max}}(k)) \tag{5.21}$$

Nevertheless, the literature of thruster selection strategies for spacecraft control purpose is limited. Namely, [179] proposed a method for 6-DOF spacecraft control by on-off thrusters with guaranteed Lyapunov-stable tracking of linear dynamic models. The approach minimizes the number of thrusters utilized and reduces the computational effort of the on-board computers when compered to the classical thruster mapping algorithms that involves iterative matrix operations. On the other hand, trajectory planning for spacecraft rendezvous and docking missions with PWM type thrusters are studied in [104]. This method is based on iterative solutions. [104] requires an initial solution of the problem based on PAM type thruster which is then converted into PWM signals and used as a starting guess. The solution is iterated until the optimal value is reached. It was proven that after few iterations the required convergence can be achieved and therefore implemented in real-time in circular orbit. This formulation is extended by developing

the Linear-Time-Varying (LTV) MPC formulation to incorporate with transition matrix for RVD in elliptic orbits in [169]. Aside from the spacecraft maneuvering problem, over-actuated underwater vehicles face the same thruster allocation challenge. For example, [180] develops QP formulation to address thruster allocation problem in the presence of constraints and thruster failure.

In summary, Lyapunov based approach can provide the fastest solution and proven to be real-time implementable, however, iterative matrix operations can be an alternative method as it can also address the non-linearity caused by the PWM model. Still, it is derived for translational motion purposes whilst in our case, the G & C block provides six inputs namely the force and torque values and sixteen decision variables are in the real-time implementation due to the number of thrusters. This complicates the actuation problem and therefore would increase the solution time in the order of magnitude if the iterative method is used. Before starting our formulation, it is important to note that the thrusters mounted on the $TEAMS5D$ robots are *unilateral*. In other words, they can produce only positive thrust forces. Each robot carries 16 proportional thrusters on the upper stage, attitude platform. The real-time convex optimization-based approach is used and presented in this work determines the thruster allocation commands in order to generate commanded force and torque values. Hence, the solver provides a thruster vector, $\mathbf{u}$ that contains the individual thrust commands of all 16 thrusters. Despite the fact that the thrusters are PWA type, the valves can instantly adjust the commanded opening of each thruster. Hence, each element in $\mathbf{u}$ must be in the interval of [0,1]. Recall that $\tilde{\mathbf{F}}$ is the augmented input vector that consists of commanded torque $\mathbf{T}$ and force $\mathbf{F}$ values. The relation between the thruster allocation vector and the augmented input vector can be given as

$$\tilde{\mathbf{F}} = \begin{bmatrix} \mathbf{F} \\ \mathbf{T} \end{bmatrix} = \begin{bmatrix} \mathbb{F} \\ \mathbb{T} \end{bmatrix} \mathbf{u} = \mathbb{A}\mathbf{u} \tag{5.22}$$

where $\mathbb{A} \in \mathbf{R}^{6\times 16}$ is the thruster mapping matrix representing the geometry of the thruster configuration in terms of thrust direction and position as depicted in Fig. 6.3. If robots are fully actuated, they can always provide directional forces and attitude torques. Moreover, geometry would guarantee that there exists a firing configuration, $\mathbf{u}$, that guarantees only torques without any force and vice versa.

This can be summarized in the following two lines;

$$\exists\ \mathbf{u_f}\ |\ \mathbb{F}\mathbf{u_f}\ \neq\ 0\ \&\ \mathbb{T}\mathbf{u_f}\ =\ 0 \tag{5.23}$$

$$\exists\ \mathbf{u_m}\ |\ \mathbb{T}\mathbf{u_m}\ \neq\ 0\ \&\ \mathbb{F}\mathbf{u_m}\ =\ 0 \tag{5.24}$$

Given the background, the thruster vector $\mathbf{u}$ for a commanded $\tilde{\mathbf{F}}$ can be formulated as a convex optimization problem:

Problem 6.

$$min\ J = \sum_{i}^{16} \mathbf{u_i} + \lambda \left\| \mathbb{A}\mathbf{u} - \tilde{\mathbf{F}} \right\|_1 \tag{5.25a}$$

$$\text{subject to } \mathbb{C}\mathbb{A}\mathbf{u} = 0 \tag{5.25b}$$

$$\mathbf{u} \in \mathbb{U}, \tag{5.25c}$$

where,

$$\mathbb{C} = \begin{bmatrix} -\mathbf{F}_y & \mathbf{F}_x & 0 & 0 & 0 & 0 \\ -\mathbf{F}_z & 0 & \mathbf{F}_x & 0 & 0 & 0 \\ \vdots & -\mathbf{F}_z & \mathbf{F}_y & 0 & 0 & 0 \\ 0 & -\mathbf{T}_x & 0 & \mathbf{F}_y & 0 & 0 \\ \vdots & \vdots & 0 & \dots & \ddots & \ddots \end{bmatrix} \tag{5.26}$$

with $\mathbf{F} = [F_x,\ F_y,\ F_z]^T$ and $\mathbf{T} = [T_x,\ T_y,\ T_z]^T$. The optimizer searches for the minimum of the sum of all elements of $\mathbf{u}$ and thus minimizes the air consumption of the thruster system. The constraint (5.25c) guarantees that $A\mathbf{u} \sim \tilde{\mathbf{F}}$, even if the thruster system can not fulfill the commanded force/torque. In that case, the second term of the cost function causes $\mathbb{A}\mathbf{u}$ to be as near to $\tilde{\mathbf{F}}$ as possible, if λ is large enough, while still minimizing $\sum \mathbf{u}$. If the thruster system can fulfill the commanded force/torque, the second term of the cost function can be minimized to 0 and the optimizer only minimizes the air consumption. To solve the optimization problem on the on-board computer and in real-time the code generator for convex optimization CVXGEN has been used [165].

In summary, at each time step k, the designed MPC based controller solves the Problem #5 (Section 5.1.3) and applies $\mathbf{u_k} = \mathbf{u_0}^*(\mathbf{x_k})$ where $()^*$ denotes sub-optimal value. Next, the thruster allocation vector $\mathbf{u}$ is obtained by solving the

Problem #6 (Section 5.2.4) to be implemented into real-dynamics. Subsequently, the states are measured and estimated, and the next dynamic matrices are obtained for the trajectory and attitude planning of the chaser satellite via LPV-MPC formulation.

5.3 Simulation Results

5.3.1 Inspection Operation In Space: Bird-Eye View

In this simulation, given an initial condition in the vicinity of the target satellite, 1.2m separation in x direction, the objective is to insert the satellite into a pseudo orbit that has 1m radius, synchronize with the rotating target and lastly point at the target while inspecting it in the pseudo orbit. This is known as the *Inspection* operation [181] and will be called *bird-eye view*. It is assumed that the rotation rate is known. Hence, the corresponding future trajectory is calculated both for positions and rotations.

The results shown in Fig. 5.2 overlaps with the pseudo orbit reference. Hence, the reference is not given. There are two major points to be addressed in the simulation results of this section. First, the constant rotation rate of the chaser satellite can be achieved thanks to the cost function that includes the rate of change of inputs which can satisfy the Eqn. (3.4). Secondly, the preview capability of MPC results in the smoothest state history without any overshoot except the initialization.

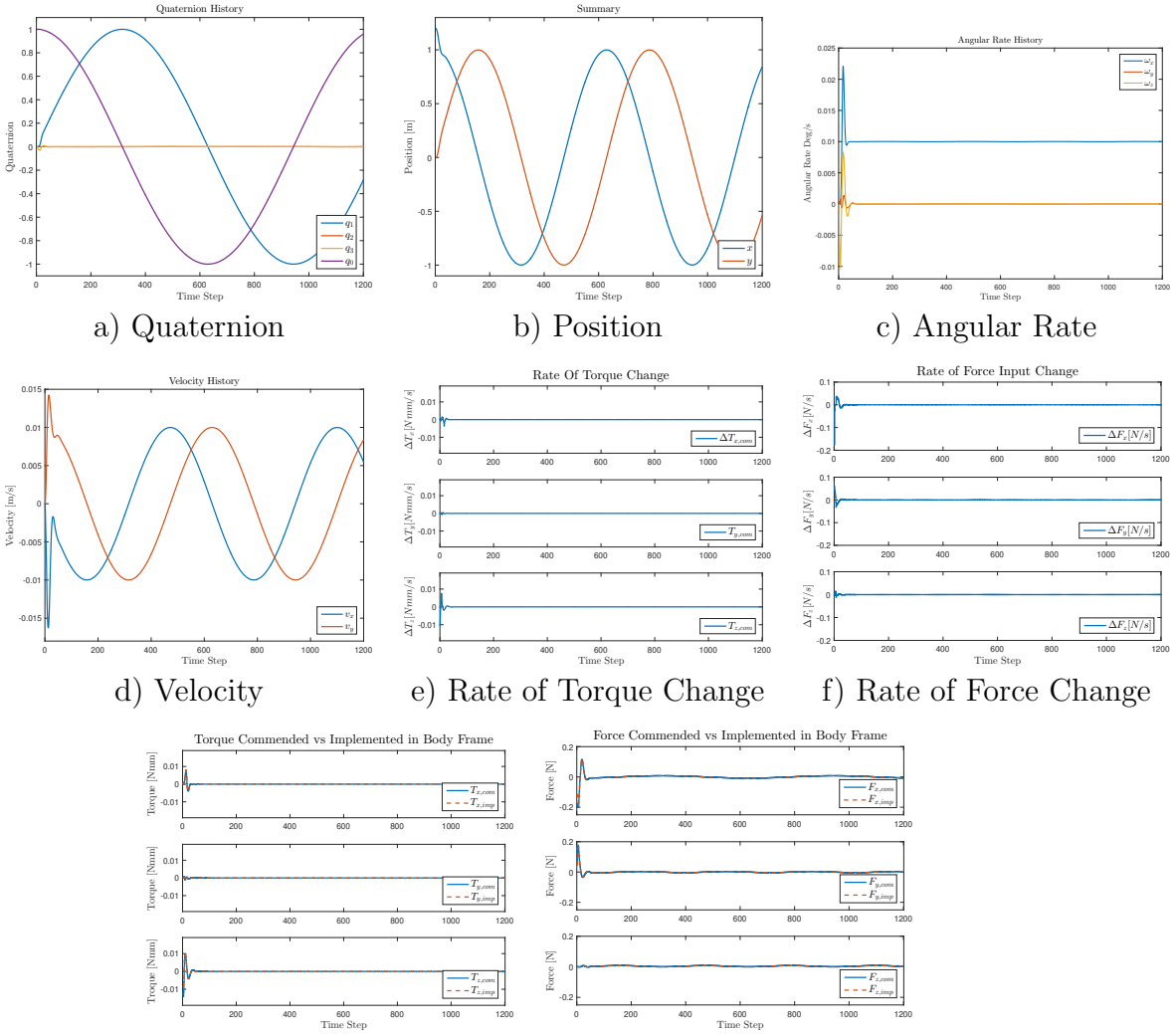

a) Quaternion b) Position c) Angular Rate

d) Velocity e) Rate of Torque Change f) Rate of Force Change

g) Torque History h) Force History

FIGURE 5.2: Simulation: Bird-Eye View

5.3.2 Thruster Failure

As mentioned in the earlier sections, the same thruster might be used to contribute net torque and force value due to the coupling. Therefore, when failed, both attitude and translational motion control are affected. This incidence is studied under Fault-Detection-Isolation and Recovery (FDIR) framework. The possible way of addressing failure is designing a re-configurable algorithm that updates the mapping matrix and hence, the faulty thruster is never actuated. In this thesis, FDIR is kept out of the scope but the response of the Offset-Free MPC approach is evaluated by the failing number of thrusters. Briefly, when a single thruster fails out of 16, MPC is able to take it as a disturbance and compensate for the missing actuation by integral action via increasing the load of the thrusters; therefore, gradually overloading the complementary thrusters. However, more than two thruster failures, as shown in Fig. 5.3, result in the first conflict of torque-force values and losing the control authority as a consequence. In this case, it is concluded that an explicit constraint handling capability of MPC can be easily adapted to take into account the thruster configuration. What is more, the mapping matrix can be also updated online provided that fault detection is available. This part is left as future work.

Remark 16. Based on the simulations and experimental results, it can be concluded that the thruster configuration geometry is one of the most critical design challenges of spacecrafts equipped with multiple thrusters for both attitude and translational control. In addition, preliminary results based on simplified thruster geometry constraints shows the effectiveness of constrained optimization based G&C approaches. The results illustrates that when coupled constraints are enforced, the rate of implemented inputs over commanded inputs can be maximized. The complete thruster geometry formulation into the optimization problem is left as a future work but keeps its novelty to be explored. Lastly, when the configuration is realised by the G&C approach, the fault tolerance can be maximized provided that the failed thruster is detected.

Remark 17. Solving two consecutive optimization problem rises questions on the global optimality of the formulated G&C problem. Even though, optimality is sufficiently studied for instance by [182–185], the suggested methods are not applicable to check the optimality. However, it should be noted that the process of obtaining the input vector for the thrusters' allocation are not guaranteed to be

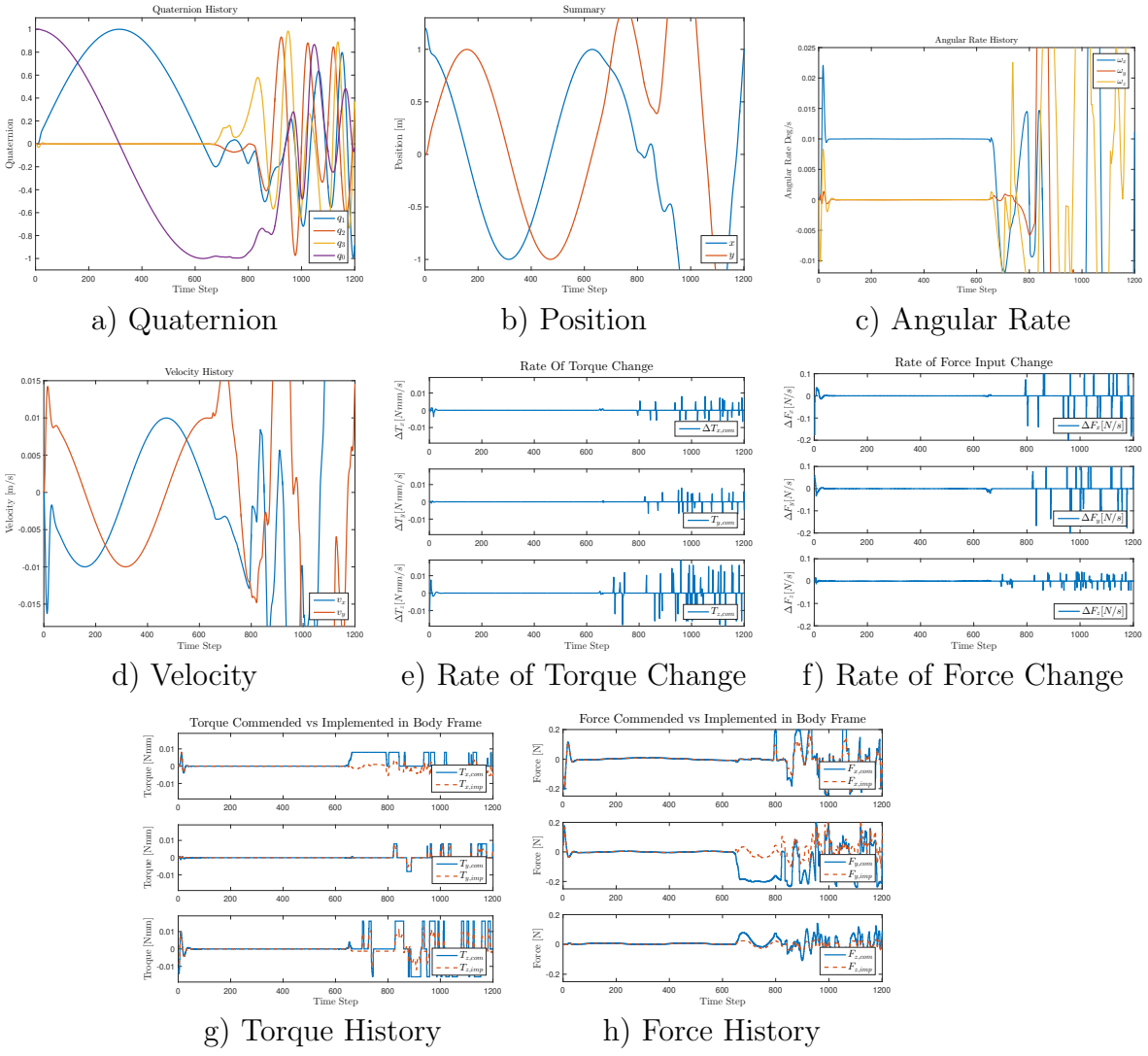

a) Quaternion b) Position c) Angular Rate

d) Velocity e) Rate of Torque Change f) Rate of Force Change

g) Torque History h) Force History

FIGURE 5.3: Simulation: Double Thruster Failure

feasible. To address this issue, the thruster allocation will be formulated as an inequality constraint and left as a future work. Details are explained in Chapter 7 under the "Future Work". Later, optimality will concern will be revisited.

5.4 Highlights

In the simulations, Guidance and Control (G&C) strategy to address 6-DOF spacecraft attitude and position control for future Rendezvous and Docking (RVD) missions are presented. Highlights can be summarised as

1. Due to close proximity and potential angular motion of the target satellite, the point mass approach is no longer sufficient to represent the relative motion dynamics. In the literature, the 6-DOF problem formulation is available; however, limited with regulation problems. Results show that the RendezVous and Docking (RVD) problem can be addressed to extended problem formulation. The RVD capability is acquired by formulating a consistent optimization problem that regards target-chaser docking port-to-port relative motion control instead of regulating the angular rates of controlled lander/spacecraft strategy available in the literature. The details are discussed in Subsection 5.2.4 *Objective Function*.

2. In the literature, the net commanded thrust is assumed to be delivered without any loss. In reality, multiple thruster configurations might be selected where there might exist a loss between commanded versus implemented thrust (and torque) values. Simulations took into account the thruster configuration with a generalized, convex optimization based thruster allocation approach which was previously ignored by other simulation work presented in Chapter 2. Furthermore, in the literature, external disturbances, modeling uncertainties, and actuator failures are neglected aside from some exceptional work. The simulation results demonstrate that more advanced strategies are required to address multiple thruster failures during the proximity maneuver while the proposed approach can inherently address a single thruster failure.

3. Lastly, simulation results show that the proposed algorithm is promising because it can respect the physical and geometric constraints, and minimize the propellant consumption while coupling translational and rotational motion, and still being real-time implementable.

Further simulations to demonstrate the efficacy of the proposed approach is presented in Chapter 6, and results are shown in parallel to experimental results.

Chapter 6

Dynamic Experiments

This chapter presents pioneer and novel dynamics experiments to test the Guidance and Control (G&C) strategy to address spacecraft maneuvering problems for future Rendezvous and Docking (RVD) missions. We formulated an offset-free 6-DOF RVD problem and thruster allocation problem as two separate convex optimization problem and, solved them with active set and standard primal-dual interior-point methods. The proposed strategy allows safe and propellant efficient trajectories for space servicing missions including tasks such as approaching, inspecting and capturing. This work provides the validation test results of the G&C laws using a hardware-in-the-loop (HIL) setup with two robotic mock-ups representing the chaser and the target spacecraft. Through this chapter, the laboratory and the robots are introduced. Besides the challenges presented in Chapter 2, the thruster characteristics and sensor errors are presented in detail. The distinctive challenge is the allocation of the thrusters. The experimental setup has 16 unilateral thrusters that generate both force and torque values. Due to the multiplicative nonlinear coupling, the convex programming approach is posed to achieve the commanded force and torque values as a result of a 6-DOF motion planning algorithm. The results also cover a comparison between the proposed algorithms with the PD controller highlight the clear advantages of the MPC formulation.

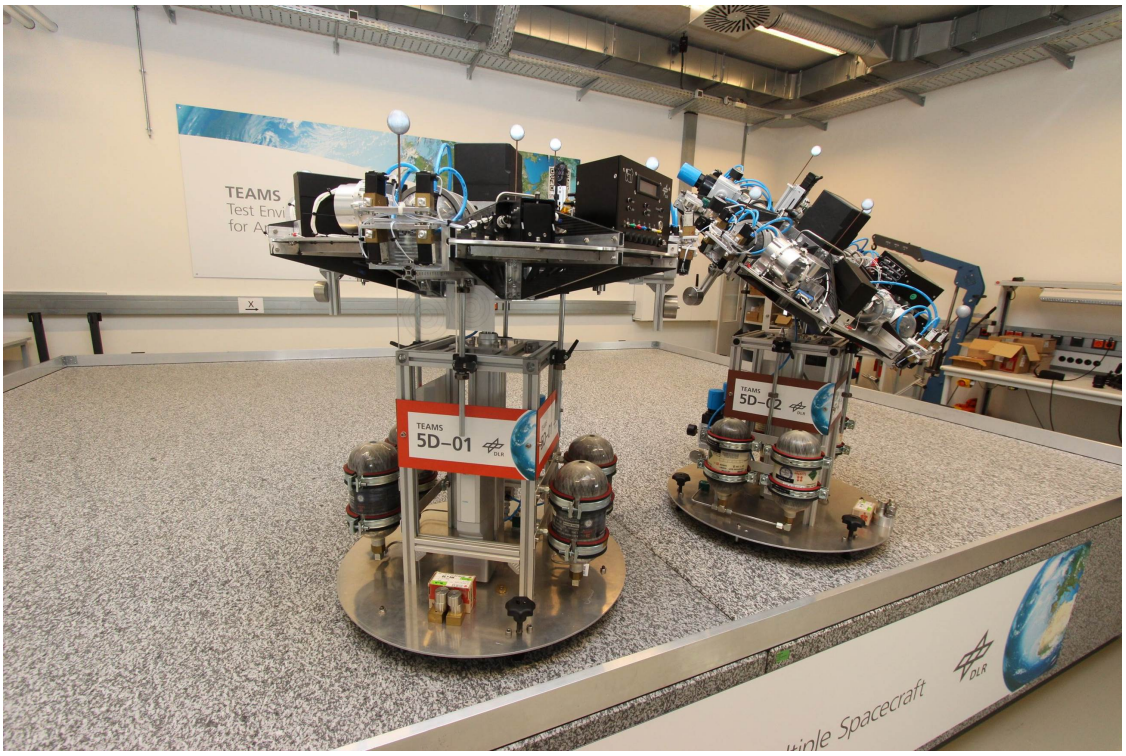

FIGURE 6.1: TEAMS5D Robots

FIGURE 6.2: TEAMS Family

6.1 Experimental Facility

The experimental work for dynamic validation took place and was supported by the Institute of Space Systems of the German Aerospace Center (in German: Deutsches Zentrum für Luft- und Raumfahrt e.V.), abbreviated DLR [44]. The experiments have been conducted in the Test Environment for Applications of Multiple Spacecraft (TEAMS) [45]. The TEAMS facility consists of test-bed, robots and motion capture system. The size of the test-bed is 4 m x 2.5 m. The test-bed is made of a granite table and the accuracy of the surface manufacturing is $3\mu m$ that allows an air cushion for free floating quasi 0-g simulations on Earth. However, there is still residual friction as expected. The spacecrafts are simulated by air cushioned robots of various designs (See Fig. 6.1 and Fig. 6.2). Throughout this work, robots with 5-DOF motion capacity is used (Fig. 6.1). These robots are named TEAMS5D and consist of a lower part called "*Translational Stage*" and upper part so-called "*Attitude Stage*". In between, there is a spherical air bearing connecting two parts without any physical interaction, through pressurized air allowing quasi frictionless motion. Both stages have air tanks and pressure regulators and thrusters are used as main actuators: *Translational Stage* to create a cushion between granite table and the TEAMS5D robot in order to cancel the friction force with the granite table; *Attitude Stage* to facilitate closed loop control commands. Hence, the *Attitude Stage* includes 16 thrusters for testing Guidance & Control (G&C) laws. Each thruster can produce a maximum thrust of 65 mN and can be individually throttled by Pulse Width Modulation (PWM), on a 2 kHz modulation frequency, from 0 % to 100 % in 256 steps. Besides, 3 reaction wheels are used for initial attitude balancing operation. Aside from G&C, for navigation, infrared-based motion capture system is used to localize and provide the instantaneous attitude for feedback control, Inertial Measurement Unit (IMU) is used to measure acceleration and angular rate with 3 accelerometers and 3 gyroscopes for the x, y, and z axes.

Remark 18. The experimental facility comes with its own challenges. One of the practical challenge is the consistency of the sampling time of each block, e.g., MPC, Convex Optimizer, motion capture blocks, etc. To this end, for simplicity, the sampling time is set to 1s and some experiments are run at 0.5s.

Remark 19. Each controller has been associated with its own unique domain of attraction such that if the spacecraft starts within this region, the controller will stabilize the system to equilibrium [186]. In the literature, different methods are available to estimate these regions. For example, for the linearized systems, regions can be estimated by using a scaled sub-level set of the Lyapunov function [187]. Alternatively, in [188], nonlinear simulations are used to approximate the region of attraction for a cuboid spacecraft using the Linear Quadratic (LQ) and the pole placement controllers. Furthermore, there are advanced tools to do the calculations systematically by such as Multi-Parametric Toolbox [189]. It was shown in [186] that the horizon can enlarge the domain of attraction whilst [190] shows that the region can be enlarged by without computational complexity of increasing the prediction horizon by changing the terminal constraint set. Given the background, in our case, the domain of attraction cannot be easily calculated by the available tools due to the complexity of the problem; however, lots of simulations have been run and observed that in close proximity (less than a few km) systems converges. Also, we take note of the advances in the literature, limit our work to the experimental platform size (4m by 2.5m), and leave estimation of the domain of attraction as future work.

The 5-DOF motion of chaser's spacecraft is assumed to be controlled by thrusters only and they are used to provide both the needed force and torques for translational and rotational motions. The net force can be simply calculated by summing the forces along the same direction and therefore the force input vector is expressed as $\mathbf{F} = [F_x \ F_y \ F_z]^T$. However, the torque value is calculated by the vector cross product of the position vector and the force vector as

$$\boldsymbol{\tau} = \mathbf{r} \times \mathbf{F}.$$

where $\boldsymbol{\tau}$ is the torque vector (τ is the magnitude), $\mathbf{r}$ is the moment arm and finally, $\mathbf{F}$ is the force vector. We can now define the torque input vector as $\mathbf{T} = [\tau_x \ \tau_y \ \tau_z]^T$. Hence, the controller generates the input vector $\tilde{\mathbf{F}} = [\mathbf{F}^T \quad \mathbf{T}^T]^T$.

Because the same thruster on-board spacecraft can generate torque or force, let us now define the thruster allocation vector as

$$\mathbf{u} = [\hat{u}_1, \ \hat{u}_2, \ \cdots \ \hat{u}_{16}]^T \tag{6.1}$$

where **u** consists of the thruster activity commands to the 16 thrusters.

Remark 20. One must note that these thrusters can generate only positive thrust values in Newtons; therefore *unilateral* and can be expressed as

$$\hat{u}_i \geq 0,\ i \in \{1, 2, \cdots, 16\}. \tag{6.2}$$

or,

$$\mathbb{U} = \left\{ \mathbf{u} \in \mathbf{R}^{16} \;\middle|\; 0 \leq \mathbf{u} \leq u_{max} \right\} \tag{6.3}$$

The resulting force and torque can be calculated as

$$\tilde{\mathbf{F}} = \begin{bmatrix} \mathbf{F} \\ \mathbf{T} \end{bmatrix} = \begin{bmatrix} \mathbb{F} \\ \mathbb{T} \end{bmatrix} \mathbf{u} \tag{6.4}$$

where $\mathbb{F}$ and $\mathbb{T}$ are the thruster mapping matrices obtained from the thruster configuration geometry illustrated in Fig. 6.3 and can be given as

$$\mathbb{F} = \begin{bmatrix} +\kappa & +\kappa & +\kappa & +\kappa & -\sigma & +\sigma & -\sigma & +\sigma & -\kappa & -\kappa & -\kappa & -\kappa & -\sigma & +\sigma & -\sigma & +\sigma \\ -\sigma & +\sigma & -\sigma & +\sigma & +\kappa & +\kappa & +\kappa & +\kappa & -\sigma & +\sigma & -\sigma & +\sigma & -\kappa & -\kappa & -\kappa & -\kappa \\ +\rho & +\rho & -\rho & -\rho & +\rho & +\rho & -\rho & -\rho & +\rho & +\rho & -\rho & -\rho & +\rho & +\rho & -\rho & -\rho \end{bmatrix} \tag{6.5}$$

with $cos(\beta)cos(\alpha) = \kappa$, $cos(\beta)sin(\alpha) = \sigma$ and $sin(\beta) = \rho$. Each thruster has their own reference frame where x is along the radial direction of the upper platform, y is parallel to the Earth surface and z axis completes the right hand rule. The angles β and α are the rotations around z and y axes as shown in Fig. 6.3. Next,

$$\mathbb{T} = \begin{bmatrix} -r & -r & -r & -r & +\varkappa & -\varkappa & +\varkappa & -\varkappa & +r & +r & +r & +r & -\varkappa & +\varkappa & -\varkappa & +\varkappa \\ +\varkappa & -\varkappa & +\varkappa & -\varkappa & +r & +r & +r & +r & -\varkappa & +\varkappa & -\varkappa & +\varkappa & -r & -r & -r & -r \\ +\nu & +\nu & -\nu & -\nu & +\nu & +\nu & -\nu & -\nu & +\nu & +\nu & -\nu & -\nu & +\nu & +\nu & -\nu & -\nu \end{bmatrix} \tag{6.6}$$

with $r \approx 44$ cm (radius of the upper stage), $\varkappa \approx 4$cm, the vertical displacement of the thrusters along z-axis $\nu \approx 2$cm, the horizontal displacement from the center of rotation to each thrusters.

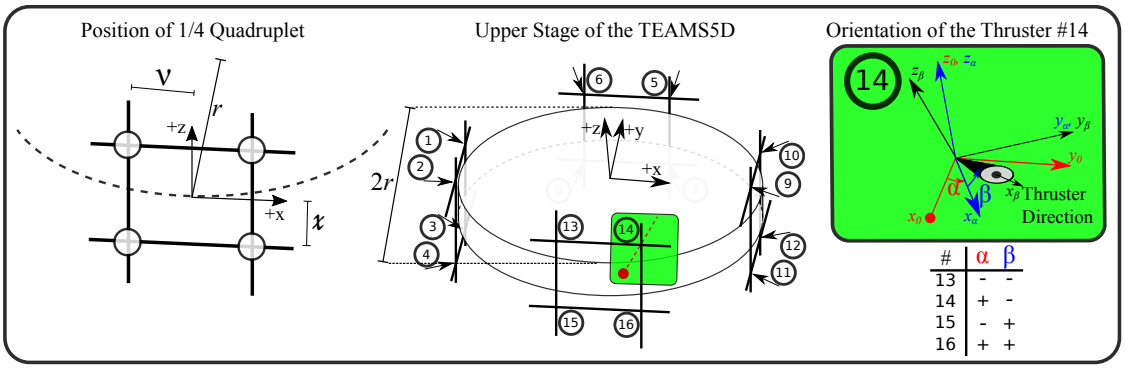

FIGURE 6.3: TEAMS5D Attitude Stage Illustration & Thruster Configuration

As formulated in Section Problem #6 (Section 5.2.4), the 16 decision variables can be obtained via convex optimization that minimizes the fuel consumption and respects the thruster configuration geometry as depicted in Fig. 6.3.

6.1.1 On-board Processing & Software

The on-board computer executes the G&C and Thruster Allocator algorithms in real-time. The MATLAB/Simulink coder generates C code from the model, which can be compiled and uploaded to the on-board-computer. During the test, the external mode of MATLAB/Simulink is used to receive data from the model running on the on-board computer. Infrared beacons mounted on the attitude platform are tracked by the laboratory's position and attitude tracking system and hence, the whole Guidance, Navigation, and Control (GN&C) loop can be closed and real-time, on-board MPC experiments can be conducted. Real-time implementation capability of MPC has been proven in various fields namely, energy, aeronautics, and space [191]. In the space applications however, the two main criteria are critical: real-time implementation capability in the presence of computation power constraints and the reliability (guarantee to solve the optimization problem in real-time) of the problem formulation. To address these two issues, MPC must be modeled with a linear prediction model, quadratic costs and conic or linear constraints in order to cast the convex optimization problem and solve it via high-speed solvers. The linearization of the coupled 6-DOF spacecraft model is explained in Section 4.2.4, the quadratic cost function and linear constraints are introduced in Problem #5 (Section 5.1.3). One must note that the constraints can be formulated in a conic form similar to [49]; however, the limitations of on-board processing power

do not allow hence the final problem is fit into the QP problem category. The code-generation CVXGEN employs interior-point method but limited with problem size. Hence, CVXGEN is employed only in the thruster allocation Convex Optimization Problem #6 (Section 5.2.4) [165]. In order to solve the main 6-DOF spacecraft maneuvering problem, qpOASES solver is used [166]. qpOASES is a parametric active-set algorithm for quadratic programming that provides the solution to our QP problem in few milliseconds. The on-board computer is an embedded x86 Atom Z530 on a PC/104 stack and runs the QNC real-time operating system. The code is developed in MATLAB/Simulink. The automatic C code generation of Simulink coder is used and for solving the optimization problem, qpOASES and CVXGEN are compiled into a so-called S-function.

6.2 Experimental Results

In this section, we present the experimental results obtained with the TEAMS5D spacecraft simulators. The chaser's maneuver is the basis for on-orbit servicing missions and docking/berthing with uncooperative target scenario is considered as a use case. In the literature, it can be seen that the problem is also studied as robotic capture of uncooperative targets and has three major challenges: image processing for pose estimation, the agility of the chaser spacecraft and versatile gripper to grasp fixtures of varying shapes. Throughout this study, we assumed that the target's states are known thanks to the motion capture system. Hence, the ultimate objective is to guide and control the chaser satellite from an relative initial condition within the experimental setup to the docking port.

6.2.1 Summary of the Experiments: Novelties & Technical Innovations

An important contribution of this thesis is the validation that the proposed controller can be implemented real-time on an experimental test bench in German Aerospace Center (DLR) [44, 45]. Therefore, this thesis bridges the gap between theory and real practice with hardware-in-the-loop tests. The work presented is a pioneering work which addresses the practical implementation of MPC using models that handles the coupling between translational and rotational dynamics via dual quaternions, multiple thruster allocation problem and constraints. The technical challenges of solving two separate optimization problem online & on-board and actuating the spacecraft with only thrusters are explained in Chapter 5. The work paves the way for future satellite servicing missions as it can save fuel & address safety concerns due to constrained optimization-based formulation. In addition, this work can enable agile maneuvers due to the thruster allocation strategy and full utilization capability thanks to the optimization theory behind.

The experiments, their novelties & technical innovations can be summarised in Table 6.1 and in the following sentences.

Table 6.1: Summary of the Experiments

Experiment	Implementation
1	Balancing
2	Comparison: Observe the Effect of Sampling Time
3	Comparison: Attitude Control with balanced Platform Additional Output Disturbance (Coin Experiment)
4	Attitude Control with Imbalanced Platform Additional Unknown Input Disturbance
5	Translational Motion Control
6	5-DOF Control: Simultaneous Discretization
7	5-DOF Control: Sequential Discretization

The experiments start with balancing the upper attitude stage of the spacecraft simulator. The balancing procedure and motivation are introduced in Section 6.2.2. In the experiment #2, the effect of sampling time on the attitude control as well as the pointing accuracy is observed for sampling time Ts = 0.5s & 1s. In the experiment #3, control of nonlinear attitude dynamics in the presence of output disturbance, i.e. atmospheric drag, is considered and a comparison study with

PD controller is demonstrated. Next, the experiment of #4 started without the balancing of the attitude stage in order to simulate uncertainties of the spacecraft dynamics, i.e. fuel sloshing, flexible modes, or modeling errors, are studied. Furthermore, an input disturbance is added to the simulated scenario in order to simulate, i.e. thruster mismatch, during the spacecraft maneuvers. After experiment #3 and #4, robustness to modeling uncertainty, input, and output disturbances are intended to be demonstrated with a simple comparison. Subsequently, in experiment #5, translational motion control is conducted. Next, in the experiment #6 & #7, two different discretization strategy, namely simultaneous and sequential discretization is demonstrated for 5-DOF spacecraft motion control towards rendezvous and docking with uncooperative targets.

6.2.2 Balancing

Balancing and the experiment #1 is the process of positioning the attitude platform's center of gravity on the air bearing's center of rotation, in order to diminish gravity disturbance torques. It's important to perform the balancing procedure before every test, to guarantee the best performance possible. The balancing start with a closed-loop attitude control of the upper platform by PID controller with reaction wheels. Hence, imbalance torque should not be larger than the torque capacity of the wheels for each axes. Subsequently, once the platform is controlled, the balancing weights can move to relax the torque required by the reaction wheels before they saturate. The counter weights highlighted in Fig. 6.4 are slowly moved to balance the attitude platform. The idea behind is similar to balancing a see saw where in 2D the objective is to make sure the that sum of the moments about some point to be equal to zero, hence balanced. In the platform, imbalance is caused because of the mounting configuration of the hardware, i.e. thrusters, and the fuel inside the tanks which depleted over time non-uniformly. Fig. 6.5-a) illustrates the Torque history, and Fig. 6.5-b) & Fig. 6.5-c) show the corresponding quaternion and angular rate history during a balancing practice. As can be seen from Fig. 6.5-a), roughly after 25s (at 250 time step since the time step is 0.1 second), the torque values depicted with red and blue colors gradually decrease. This is because, the balancing mechanism is activated to compensate the error by moving the weights attached to the spring mechanism highlighted in Fig. 6.6.4. Following

that the other axis is balanced and after 400s, the balancing procedure is finalized.

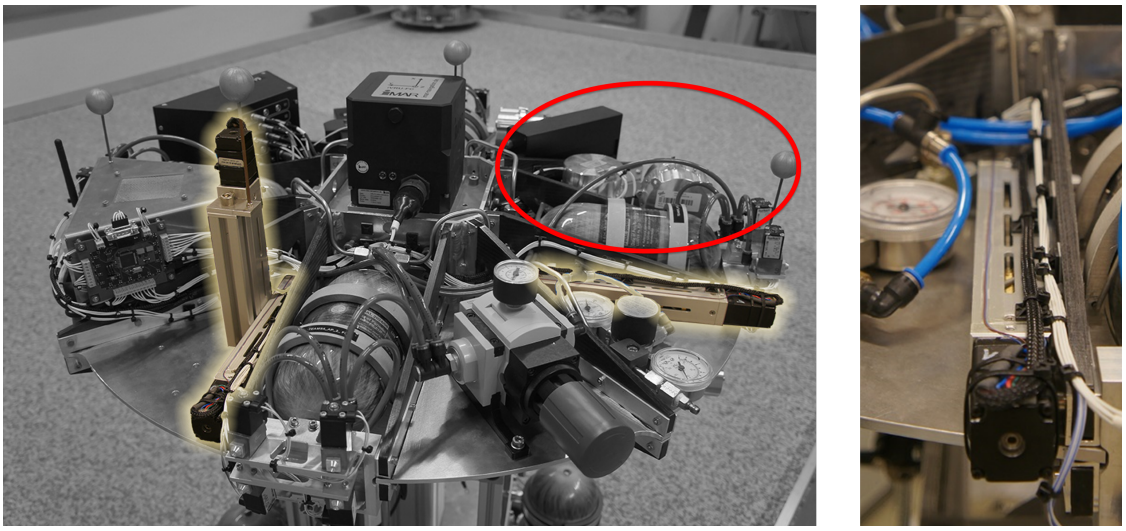

FIGURE 6.4: Balancing Mechanism & Reaction Wheels Highlighted

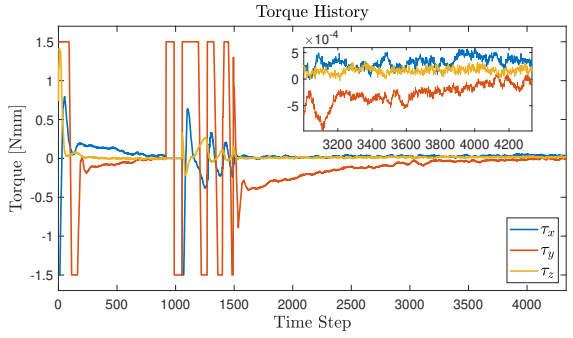

a) Initial Balancing - Torque History

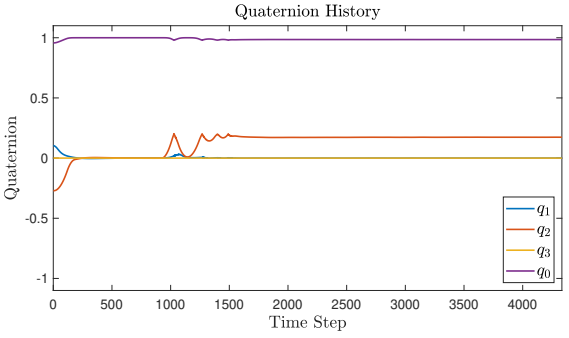

b) Initial Balancing - Quaternion History

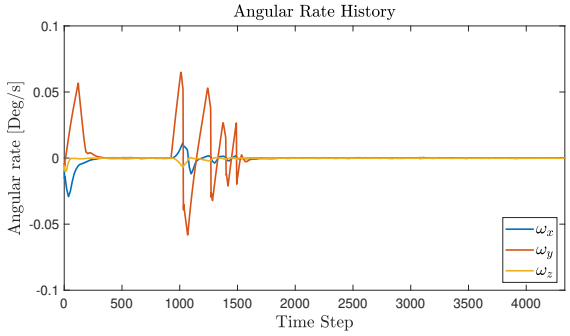

c) Initial Balancing - Angular Rate History

FIGURE 6.5: Exp 1 - Initial Balancing

Remark 21. In the **experiment #2**, the effect of sampling time on the attitude control as well as the pointing accuracy is observed for sampling time Ts = 0.5s & 1s.

After running two experiments to compare the effect of sampling time on the attitude pointing error, it can be concluded that sampling times, $T_s = 0.5s$ & $1s$ show similar satisfactory performance whilst $T_s = 0.5s$ is slightly better performance in terms of error. This conclusion is obtained from Figures 6.6-b) and 6.6-a) which illustrate quaternion and angular rate history comparisons. The figures show that the shorter the sampling time, the lesser the oscillation. However, we selected $T_s = 1s$ in order to have more time for computation.

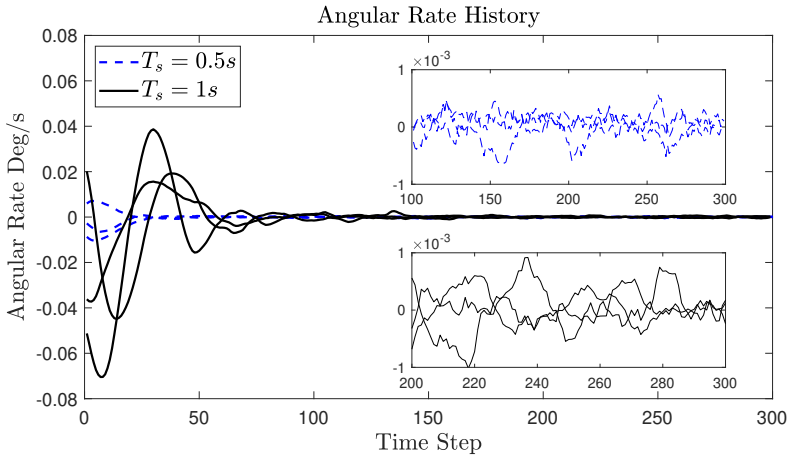

a) Angular Rate History Comparison

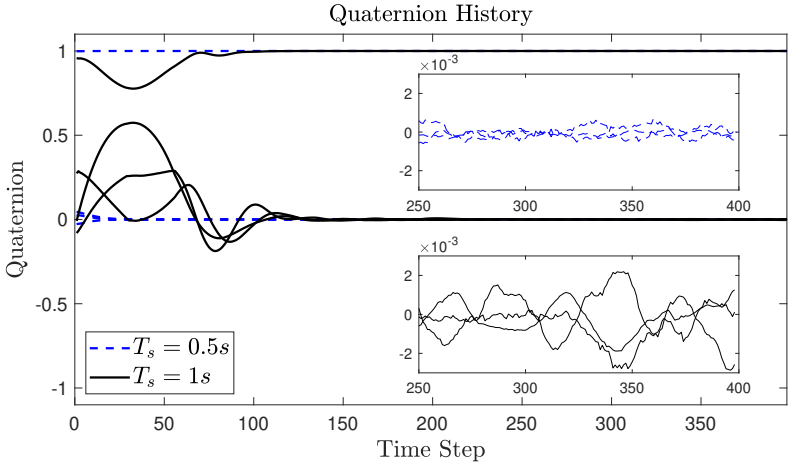

b) Quaternion History Comparison

FIGURE 6.6: Exp 2: - Sampling Time Comparison

6.2.3 Uncertainties and Unknown Disturbances

The actual orbit is influenced over time by other phenomena called orbital perturbations, such as the third body gravitational force, atmospheric drag, solar radiation pressure, and the non-spherical shape and non-uniform mass distribution of the Earth [192]. Hence, it is a necessity of the controller to address uncertainties and disturbances in space. Because the aforementioned perturbations are negligible regarding the duration of the experiment, i.e. two minutes, an alternative perturbation is artificially posed to the experimental platform by starting the experiment with an imbalanced attitude platform and adding external disturbance by simply putting a coin at the tip of the platform. The deterioration caused is completely random. First, we will evaluate the performance of the proposed approach for controlling the attitude only. In **experiment #3** and #**4**, the Cost function 3, presented in Chapter 4-page 58, is employed. Briefly, the important parts to recall are the integral action and penalizing the rate of change of torque inputs to compensate the external disturbances and modelling uncertainties.

Remark 22. In **experiment #3**, control of nonlinear attitude dynamics in the presence of output disturbance, i.e. atmospheric drag, is considered and a comparison study with PD controller is demonstrated.

As explained in Chapter 3, dual quaternions can be used as two separate unit quaternions. First, we will evaluate the performance of the formulated approach for controlling the attitude only. The objective is to robustness of the proposed Quasi LPV Based MPC approach and compare it with the existing PD design presented in [193]. In the nominal conditions, no external disturbance and well-balanced platform, proposed MPC approach attitude pointing accuracy is 5 times better than traditional PD controller. Specifically, proposed accuracy is +/- 0.1 deg whilst the traditional approach is +/- 0.5 deg as can be seen in Fig. 6.7- b) & d) inside the zoomed boxes on the left. Secondly, when an external disturbance is applied, the proposed approach is capable rejecting the disturbance. The output disturbance is experimented by adding a coin as illustrated in Fig. 6.8. Fig. 6.8 shows that after the attitude is controlled and stabilized, a 1 cent coin is put roughly at the end of the y-axis in the body frame on the attitude stage at t=70s. The attitude stage became imbalance and the PD controller took more than 200 seconds to re-balance the attitude due to the external disturbance introduced by the 1 cent

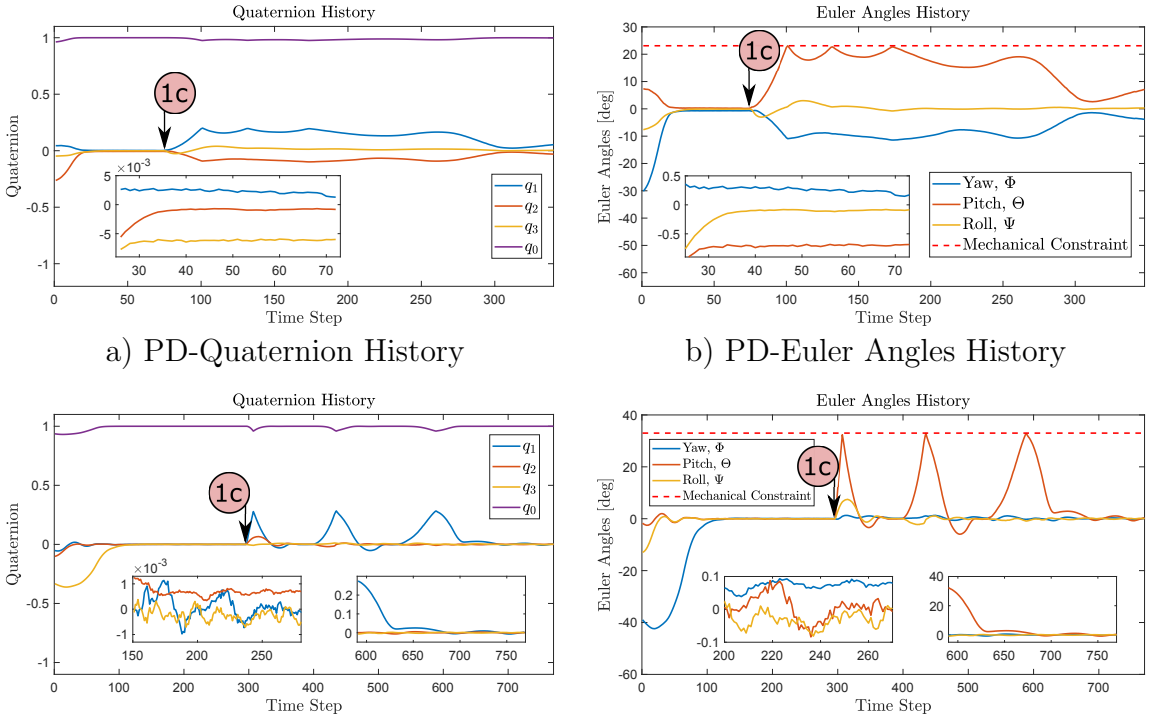

FIGURE 6.7: Exp 3 - Output Disturbance: Comparison of MPC and PD Results

coin; nevertheless, the +/-10 deg. offset remains as can be seen from Fig. 6.7-b) PD-Euler Angles History. When the "1 cent coin" test is applied to the proposed MPC, it took around 100 seconds to compensate the disturbance and the pointing accuracy stays within +/- 0.15 deg. One can note that multiple discrete peaks are observed in MPC (Fig. 6.7-d) and PD (Fig. 6.7-b) experiments. The reason of the peaks is the mechanical constraints depicted in the "Euler Angles History" plots with red dashed lines. Those mechanical constraints are the limitations of the upper attitude stage on its pitch motion. 2D illustration of the dynamic components of the upper/attitude stage & its limitations are depicted in Fig. 6.9. One must note that the physical limitations are not uniform. In other words, the tilting limit varies. Therefore, depending on the yaw angle, the limitation can be up to 35 degrees and hence, when an external disturbance is applied, before the compensation, the attitude stage hits its limit, bounces back, tilts slowly towards the imbalance, and thrusters slowly demonstrates successful disturbance handling as depicted in Fig. 6.7 – d) and Fig. 6.8. It might be logically suggested to use integral action in the PD controller to compensate this error. However, the external disturbances, as well as the dynamic uncertainties for space missions, are indispensable and integral action may lead instability of the system. The instability is caused by

the windup of integrator where a large change in set-point occurs and the integral terms accumulates a significant error during the rise (windup) [194] although there are techniques to handle integral windup. On the other hand, the proposed MPC based approach can inherently address the external disturbance with embedded integral action capability as explained in Chapter 5.

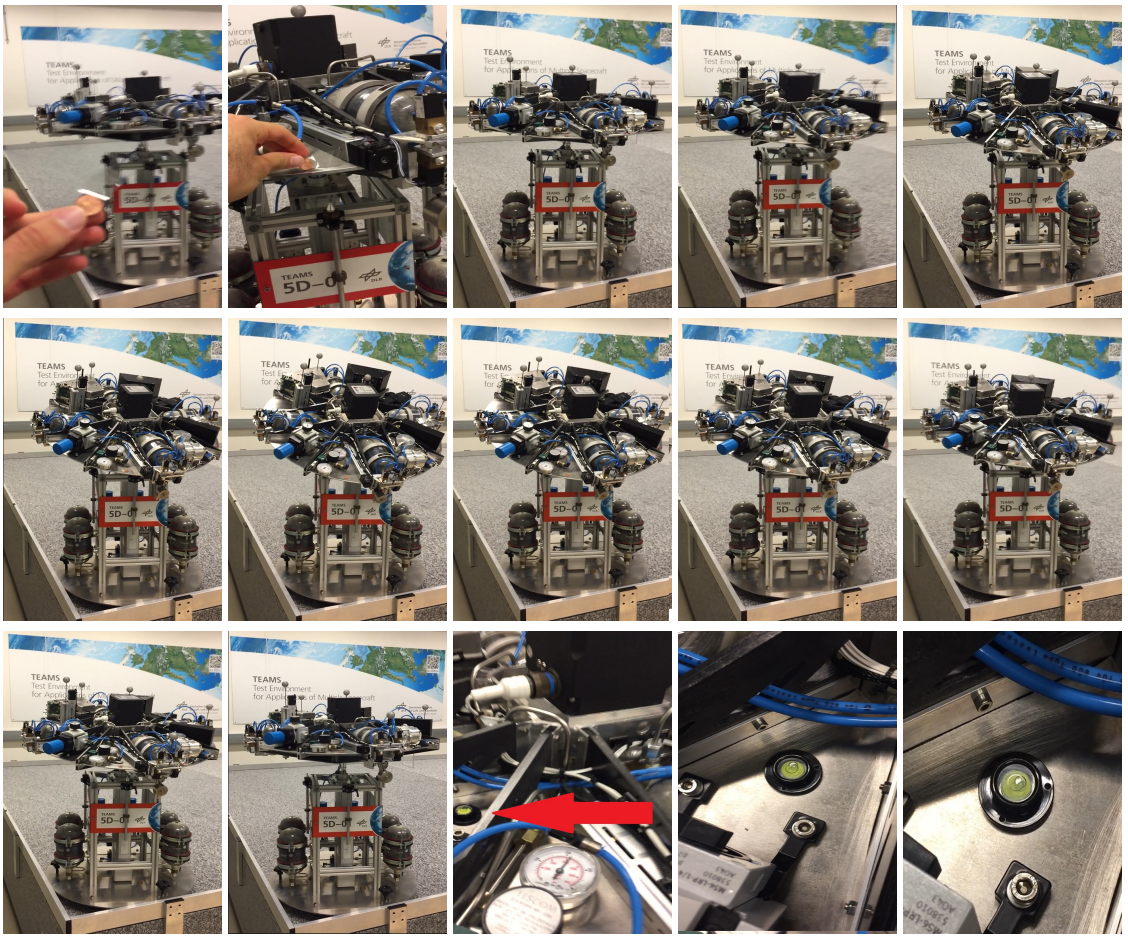

FIGURE 6.8: Exp 3: 15 Scenes from the Experiment

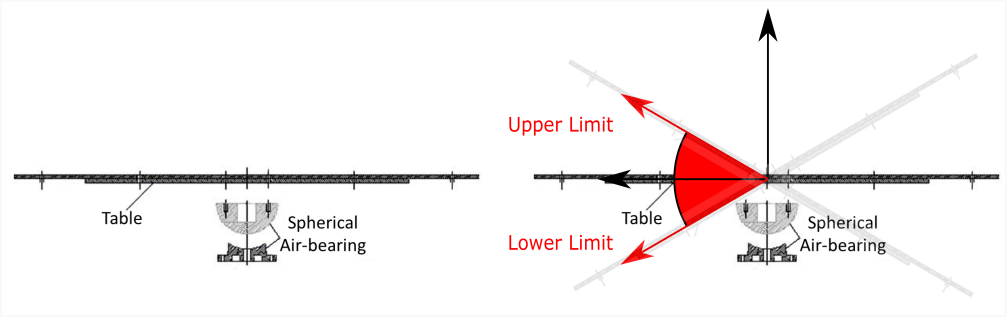

FIGURE 6.9: Illustration of the Attitude Stage & It's Limitations on the Right

Remark 23. In, **experiment #4**, control of nonlinear attitude dynamics in the presence of dynamic uncertainties of the spacecraft, i.e. fuel sloshing, flexible modes, or modeling errors, are studied. Furthermore, an input disturbance is added to the simulated scenario in order to simulate, i.e. thruster mismatch, during the spacecraft maneuvers.

In the experiment #3, it was shown that in the ideal situation where the attitude platform is perfectly balanced, both PD and MPC controllers show satisfactory results. However, later on, only MPC with integral action was successful to show robustness to output disturbance. In order to further elaborate the performance of the MPC, the air inside the tanks at the upper stage is slightly depleted. First, the balancing system was turned off and sufficient air is used to create an imbalance in the system. Fig. 6.10-d) illustrates torque history. The green arrows show the imbalance and its trend over time. In other words, not only there exists an initial imbalance, but also, it's changing over time. The change over time is due to the depletion of the fuel, air, in the tanks. Second, at time t=200s, an external disturbance torque is applied as can be seen in Fig. 6.10-a)-f). It can be seen from Fig. 6.10-d) that MPC inherently estimates the torque required to compensate the imbalance for offset-free attitude control. What is more, when the external disturbance is applied, MPC acts quickly and also addresses it. In Fig. 6.10-b), a peak can be seen at t=200 as the input disturbance is applied. However, the torque command rapidly goes down to negative values as depicted with the yellow line in Fig. 6.10-d) while the absolute torque command integral booms at the end of time interval 5 from roughly 40Nmm to 160Nmm as depicted in Fig. 6.10-f).
One must note that the fluctuations are due to thruster characteristics. In the literature, one of the reasons known as *minimum impulse bit* which occurs between the thruster being fully off and generating its minimum thrust which is slightly above zero. This area has limits and also referred to *dead-zone* and illustrated in Fig. 6.11 with two options: rounding to zero and differential thrust [42].

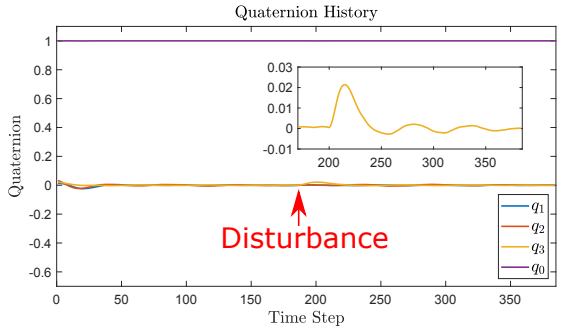

a) Quaternion History

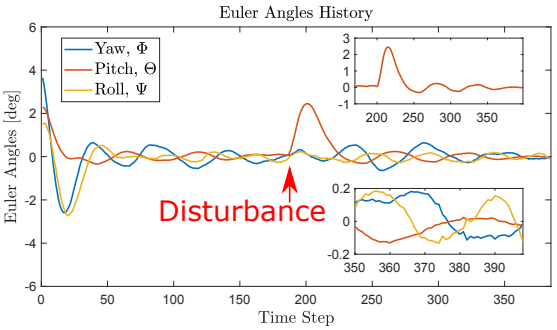

b) Euler Angles History

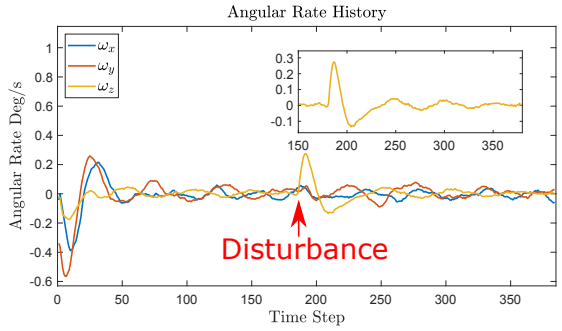

d) Angular Rate History

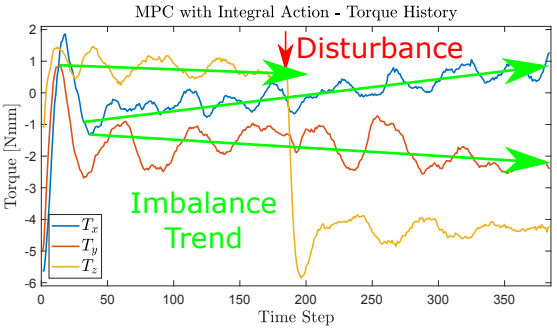

d) Torque History

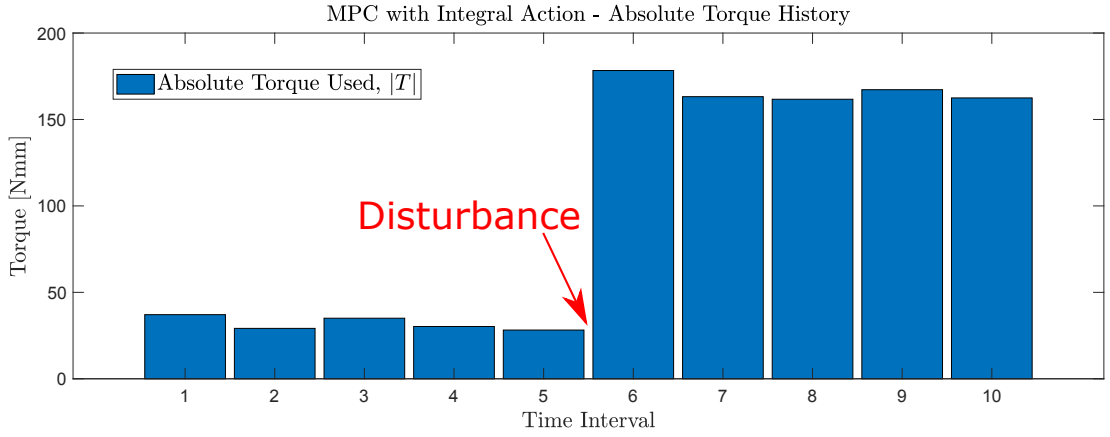

f) Absolute Torque History

FIGURE 6.10: Exp 4 - Input Disturbance & Uncertainty: MPC with Integral Action

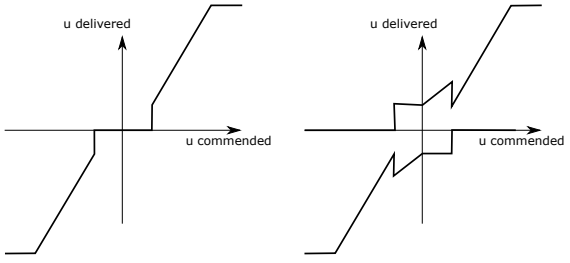

FIGURE 6.11: Illustration of Minimum Impulse Bit

6.2.4 Dual Quaternions for Translational Motion

In this section, we employed the PD controller to control the attitude and MPC with no integral action for translational motion control. Running simulation is always practical and definitely gives hints about how experiments or real flight would result in. However, they are as good as how accurate modeling is done. The critical parameters of the model employed for the prediction of the states are the Moment of Inertia (MoI), mass and the sampling time for the double integrator case. What is more, our simulation model does not include the residual drag, thruster mismatch, minimum impulse bit, etc. Hence, in the following simulation results from the perfect conditions, i.e., no disturbance, perfect thruster, perfect knowledge of MoI, and artificially deteriorated condition, e.g. uncertainty on the mass, residual thrust, are presented and compared with the experimental results.

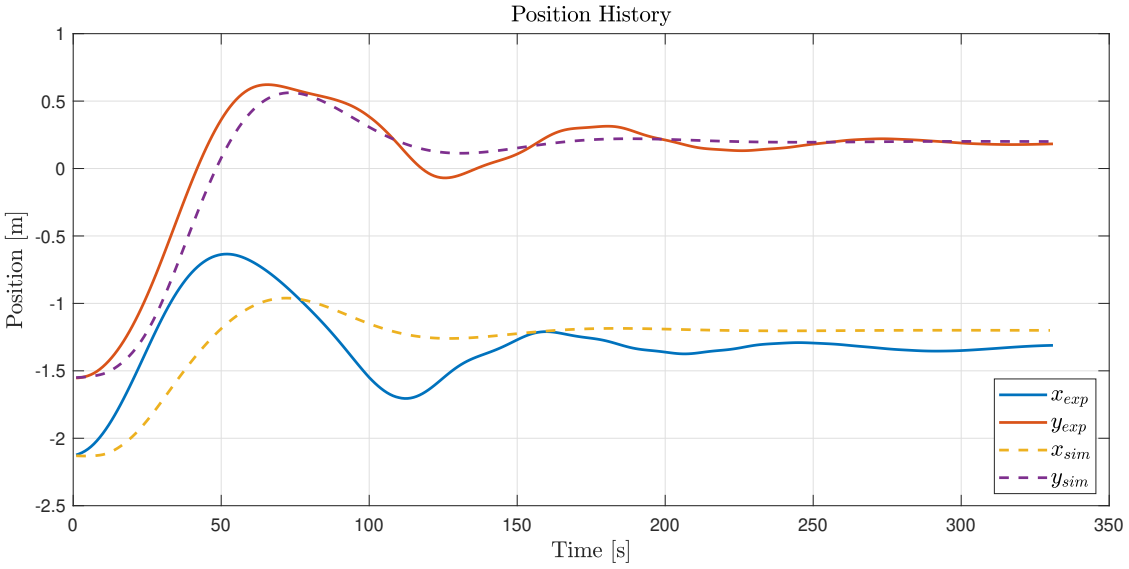

FIGURE 6.12: Exp 5: Position History in Inertial Frame

The experimentation result and simulation results show a remarkable similarity. In Fig. 6.12, position history is given. It is seen that the $y-axis$ experimental result is slightly more aggressive than the simulation result; however, after roughly 240s, the oscillation is damped and the satellite arrives at the steady state for y-axis. Similarly, the $x-axis$ results are more aggressive but the main difference is the offset. More elaboration about this offset will be given next.

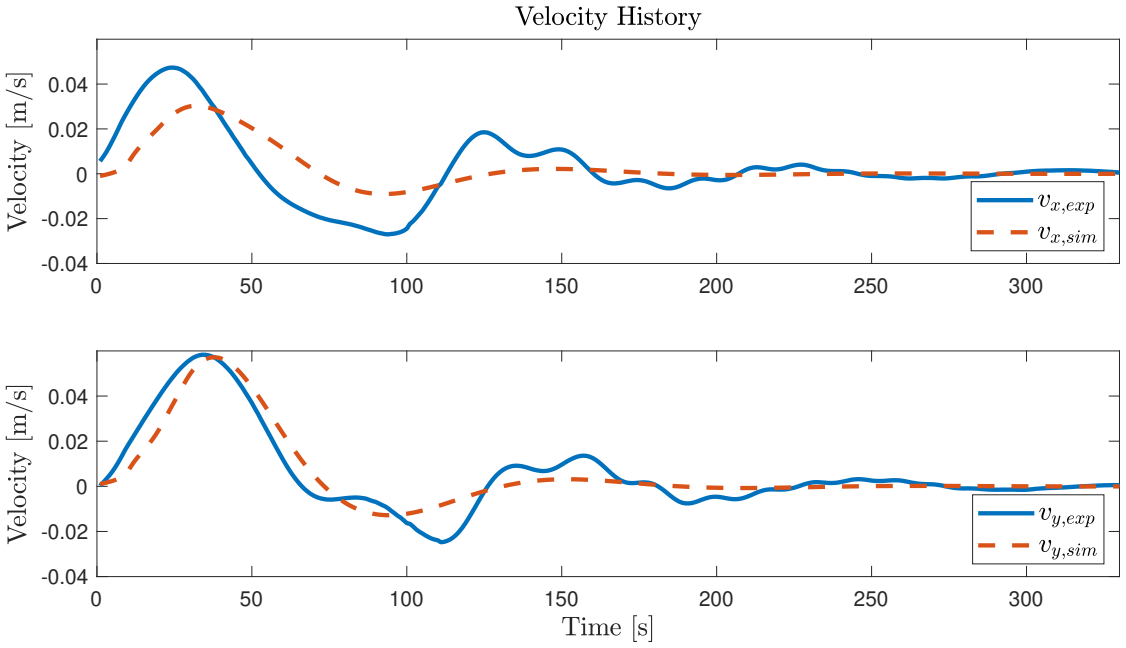

FIGURE 6.13: Exp 5: Velocity History in Inertial Frame

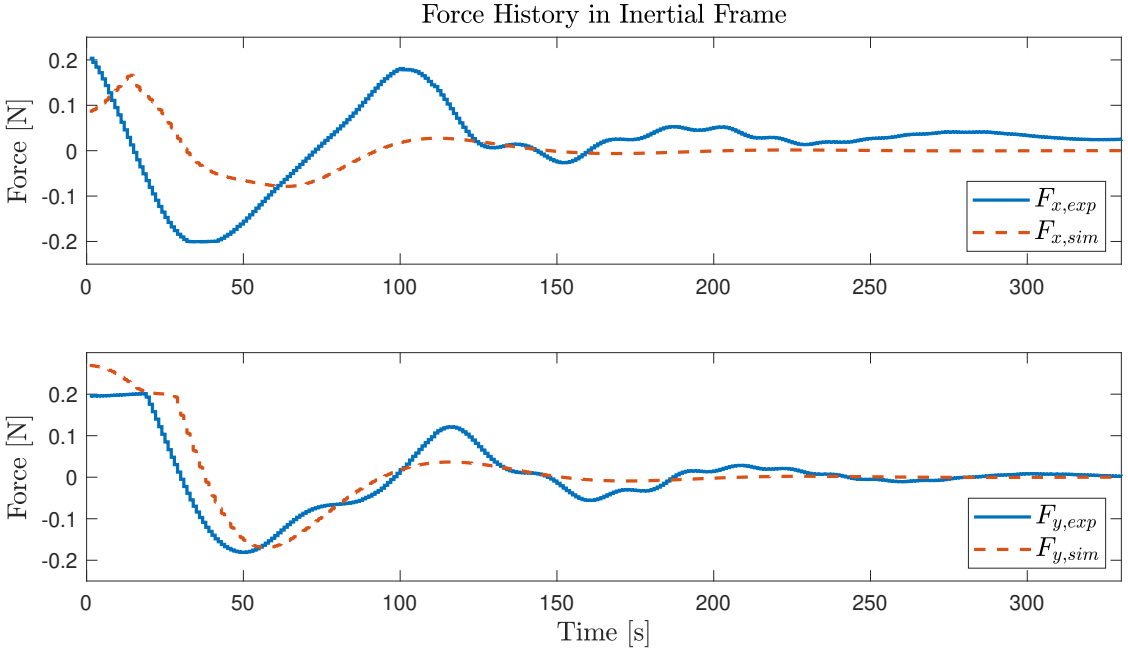

FIGURE 6.14: Exp 5: Force History in Inertial Frame

6.2.5 Dual Quaternions For 6-DOF Motion Control

6.2.5.1 Simultaneous Discretization

In this experiment, dual quaternion based MPC formulation is employed to address full 6-DOF motion control and applied into TEAMS5D vehicle that can validate the

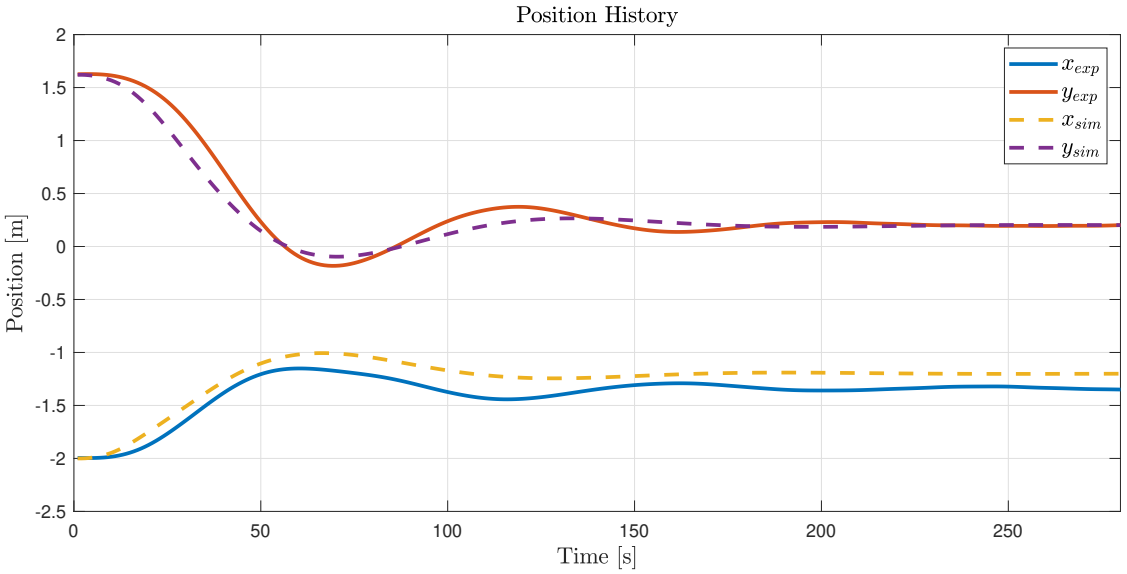

FIGURE 6.15: Exp 6: Position History in Inertial Frame (Simultaneous Discretization)

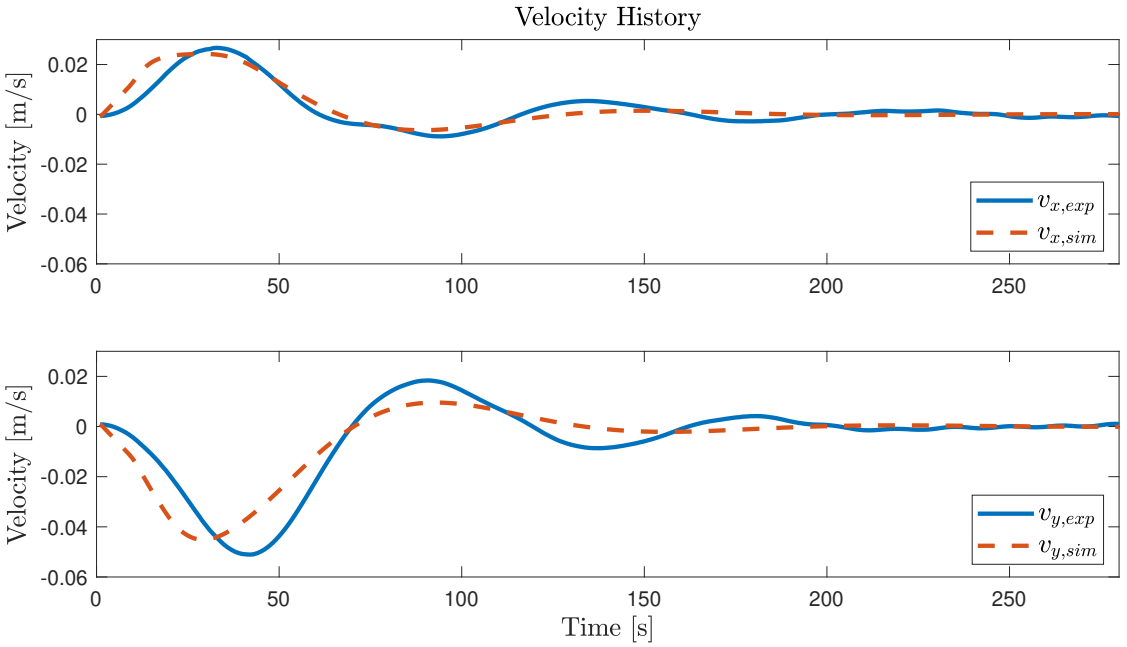

FIGURE 6.16: Exp 6: Velocity History in Inertial Frame (Simultaneous Discretization)

5-DOF motion. For the experiments, the same coupled double integrator model defined in the body frame of the controlled satellite is used. However, in the first one, the discretization is done sequentially as suggested in [49] and secondly, discretization is done simultaneously. Both forms are explained in Chapter 4.

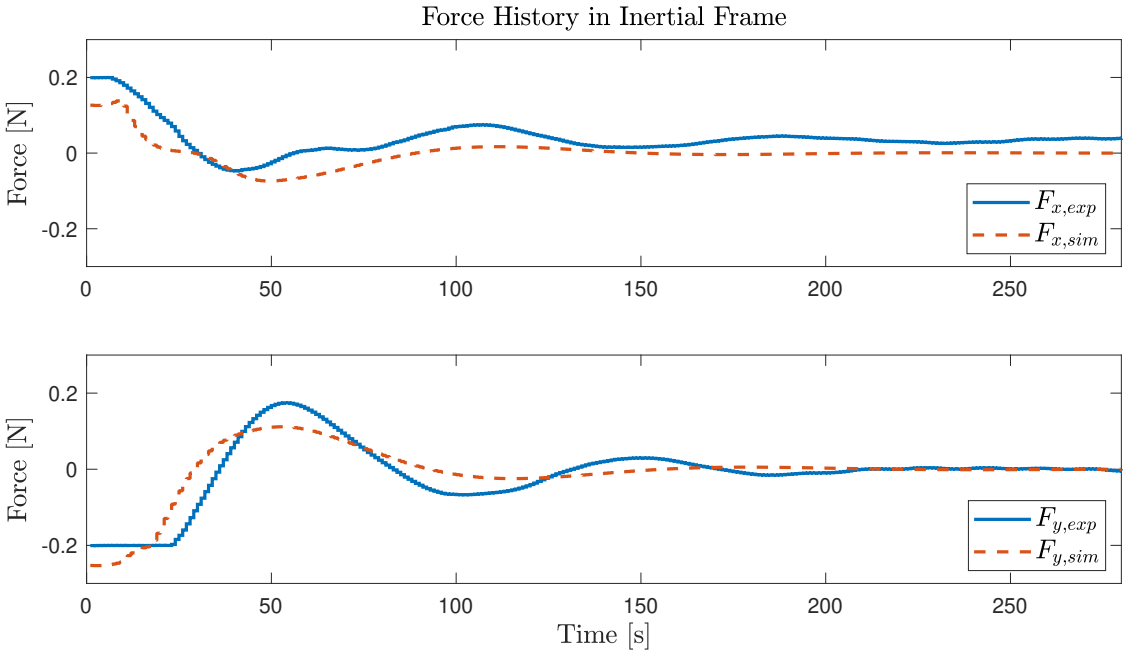

FIGURE 6.17: Exp 6: Force History in Inertial Frame (Simultaneous Discretization)

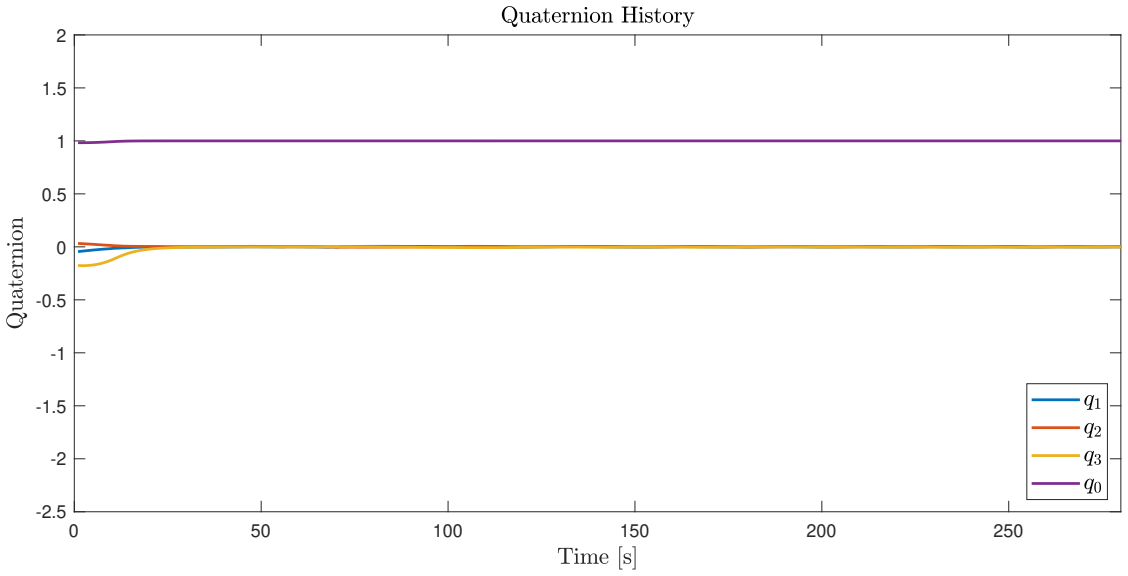

FIGURE 6.18: Exp 6: Quaternion History in Inertial Frame (Simultaneous Discretization)

6.2.5.2 Sequential Discretization

Comparing Fig. 6.15 and Fig. 6.21, it can seen that the results for the simultaneously discretized plant are less aggressive and show a similar trend to its simulation. Still, it can be seen from Fig. 6.15 and Fig. 6.21 both simultaneously and sequentially discretized plants can be controlled but experience offset in the x-axis in

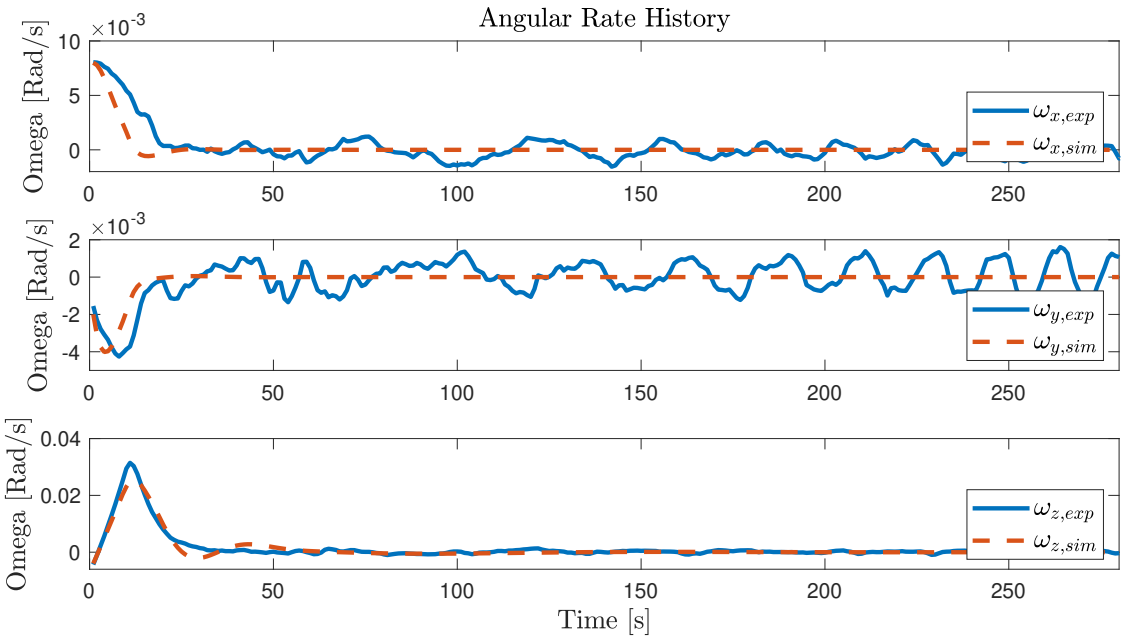

FIGURE 6.19: Exp 6: Angular Rate History (Simultaneous Discretization)

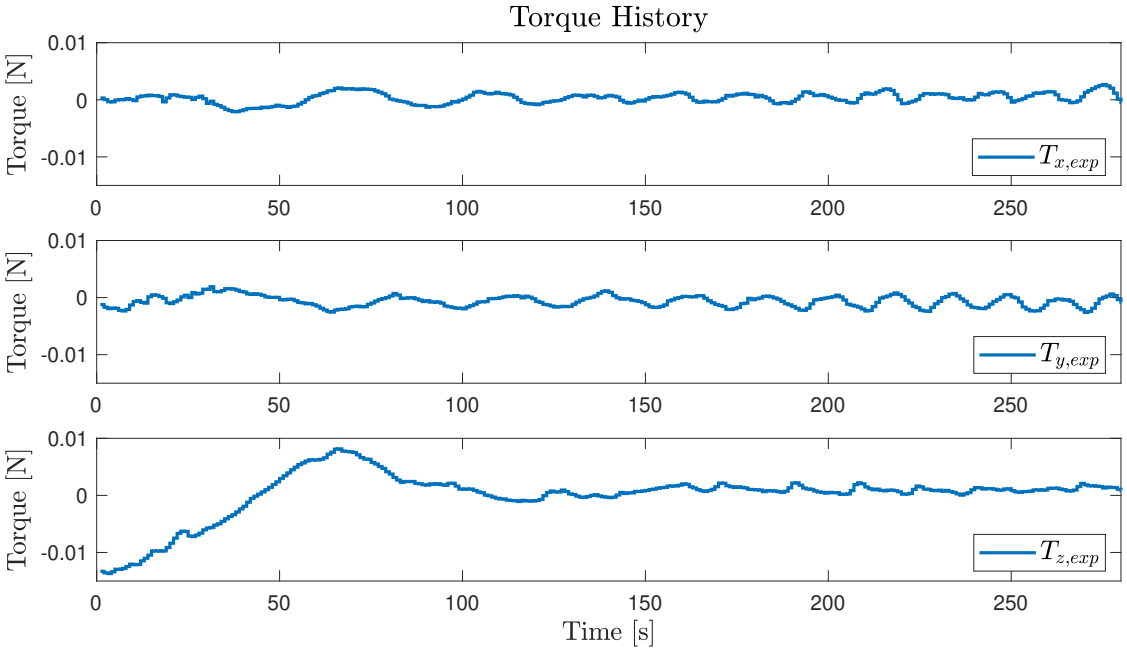

FIGURE 6.20: Exp 6: Torque History (Simultaneous Discretization)

every experiment.

It is seen in Fig. 6.23 that the commanded force & torque values overlap after slightly more than 100 seconds. Fig. 6.15 illustrates that the position reference in $x$direction, 0.2m, is reached but there is a remarkable offset in the y-axis. To better understand the cause, thruster activity history as well as the force implemented &

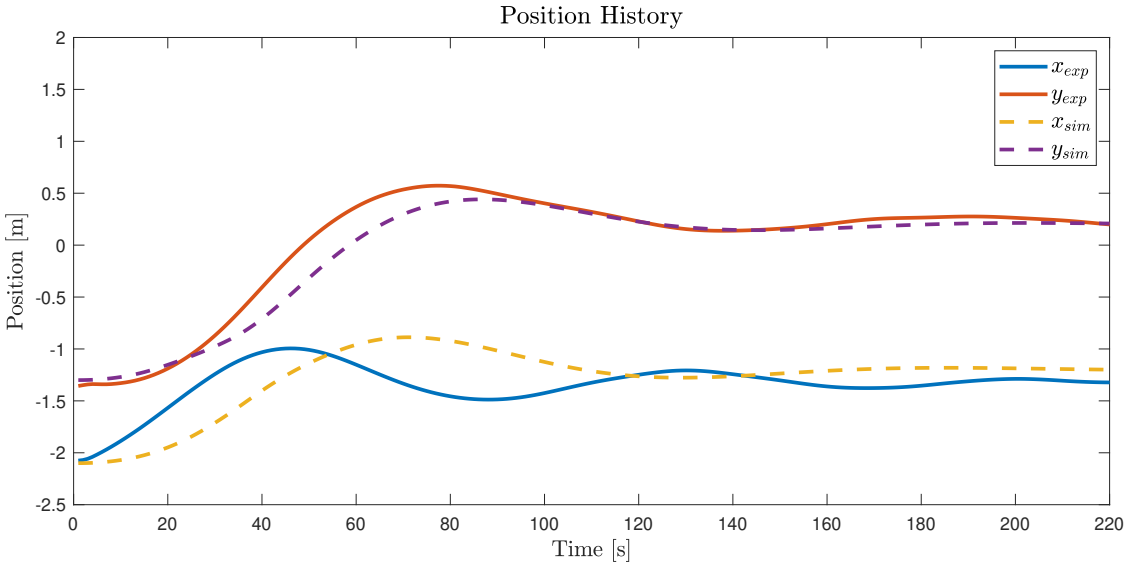

FIGURE 6.21: Exp 7: Position History in Inertial Frame (Sequential Discretization)

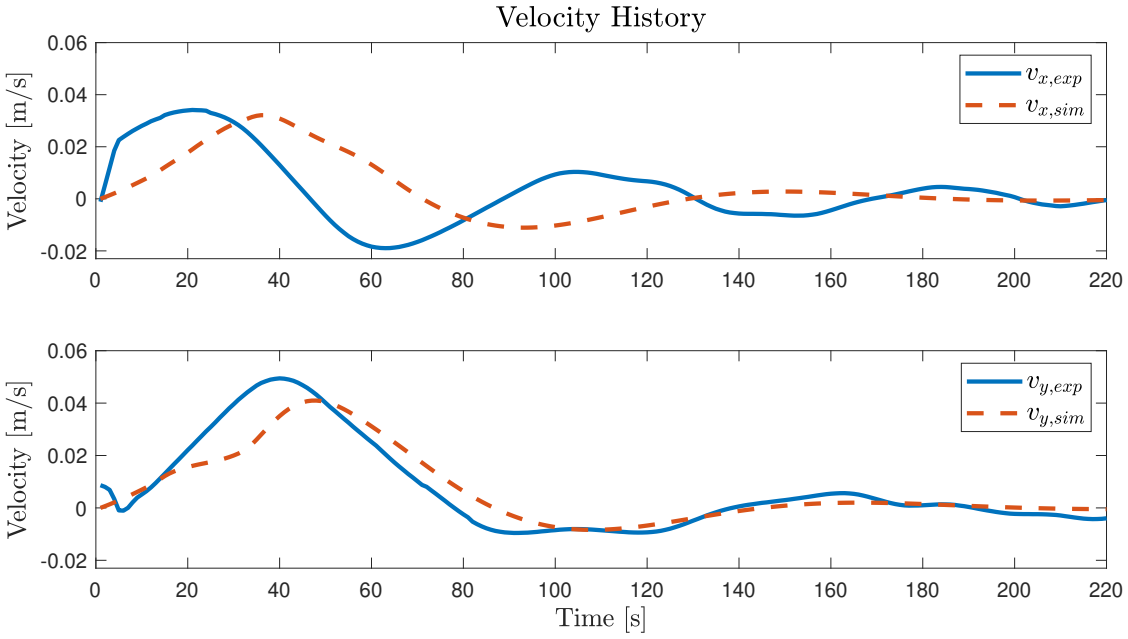

FIGURE 6.22: Exp 7: Velocity History in Inertial Frame (Sequential Discretization)

commanded can be investigated. Firstly, Fig. 6.23 illustrates the force history in the inertial frame. It is seen that after $t = 100s$, the commanded force oscillates around $0.05N$. However, if the velocity history in Fig. 6.22 is checked, there is no acceleration in the positive x direction despite the positive thrust. One might suspect that this is due to the dead zone of thrusters as shown in Fig. 6.11. However, the thrusters individually can generate at max, $65mN$ of thrust and

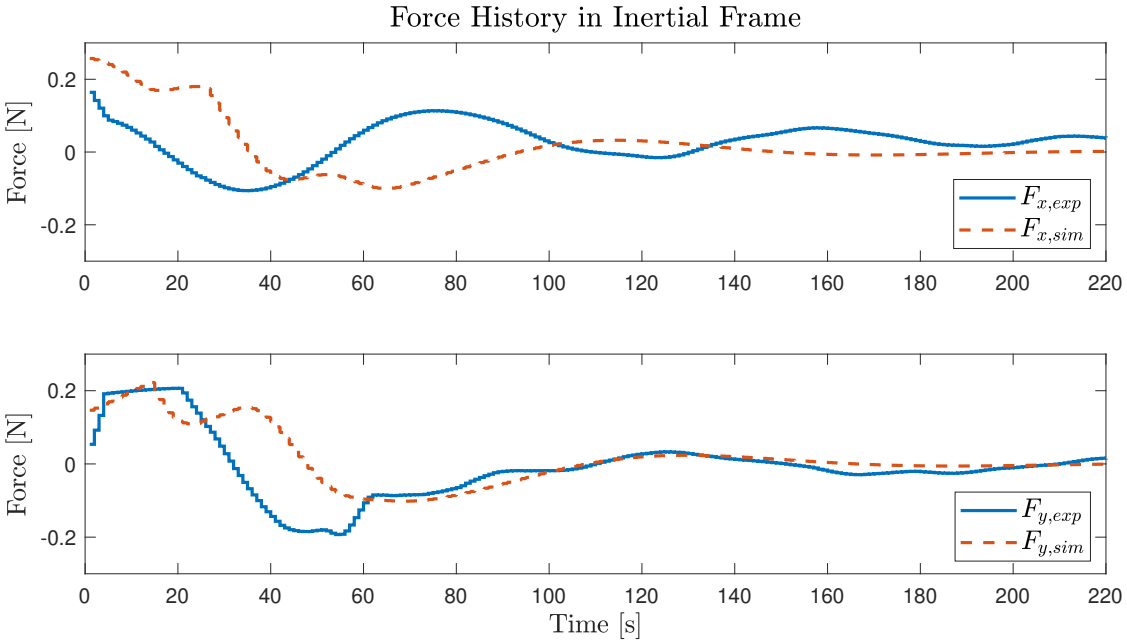

FIGURE 6.23: Exp 7: Force History in Inertial Frame (Sequential Discretization)

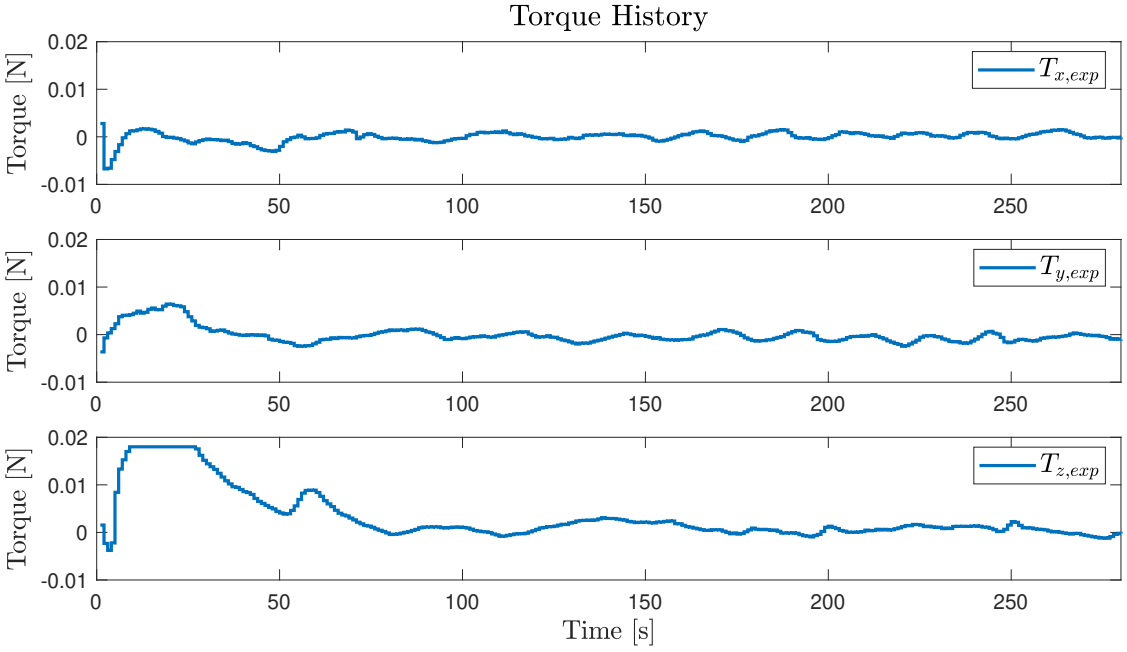

FIGURE 6.24: Exp 7: Torque History in Inertial Frame (Sequential Discretization)

commanded $50mN$ is just below its limit and far from the dead zone, i.e., $4mN$. It is concluded that during this experiments, one of the thrusters was not functional and state-space representation without integral action is not capable of addressing this failure, commands oscillatory $F_{com} \approx 0.04 \pm 0.02mN$ net force in the x-axis instead. An important contribution of this thesis is the validation that the proposed

controller can be implemented real-time on an experimental test bench in German Aerospace Center (DLR) [44, 45]. Therefore, this thesis bridges the gap between theory and real practice with hardware-in-the-loop tests. The work presented is a pioneering work which addresses the practical implementation of MPC using models that handles the coupling between translational and rotational dynamics via dual quaternions, multiple thruster allocation problem and constraints. The technical challenges of solving two separate optimization problem online & on-board and actuating the spacecraft with only thrusters are explained in Chapter 5. The work paves the way for future satellite servicing missions as it can save fuel & address safety concerns due to constrained optimization-based formulation. In addition, this work can enable agile maneuvers due to the thruster allocation strategy and full utilization capability thanks to the optimization theory behind.

6.3 Lessons Learned

6-DOF spacecraft motion control problem is highly nonlinear, strongly cross coupled, and constrained. An important contribution of this thesis is the validation that the proposed controller can be implemented real-time on an experimental test bench in German Aerospace Center (DLR) [44, 45]. Therefore, this thesis bridges the gap between theory and real practice with hardware-in-the-loop tests. The work presented is a pioneering work which addresses the practical implementation of MPC using models that handles the coupling between translational and rotational dynamics via dual quaternions, multiple thruster allocation problem, and constraints. The work paves the way for future satellite servicing missions as it can save fuel & address safety concerns due to constrained optimization-based formulation. In addition, this work can enable agile maneuvers due to the thruster allocation strategy and full utilization capability thanks to the optimization theory behind. The lessons learned from the experiments are summarized in the following.

i. As a warm-up, in **experiment #2**, it was observed that the sampling time of 0.5s and 1s shows satisfactory result but anything higher does not meet the GNC criteria as the response becomes too slow. Also, a slight improvement in the attitude point is observed when sampling time decreased from 1s to 0.5s.

ii. In **experiment #3**, control of nonlinear attitude dynamics in the presence of output disturbance, i.e. atmospheric drag (simulated by adding a coin on the upper platform), is considered and a comparison study with PD controller is demonstrated. In the nominal conditions, no external disturbance and well-balanced platform, proposed MPC approach attitude pointing accuracy is 5 times better than traditional controllers. Specifically, proposed accuracy is +/-0.1 deg whilst the traditional approach is +/- 0.5 deg as can be seen in Fig. 6.6 inside the zoomed box. Secondly, when an external disturbance is applied, the proposed approach is capable rejecting the disturbance. The proposed controller also has sufficient robustness to model uncertainties since only a simplified model was used in the MPC design.

iii. Next, **experiment #4** started without the balancing of the attitude stage in order to simulate uncertainties of the spacecraft dynamics, i.e. fuel sloshing,

flexible modes, or modeling errors, are studied. Furthermore, an input disturbance is added to the simulated scenario in order to simulate, i.e. thruster mismatch, during the spacecraft maneuvers. After **experiment #3** and #**4**, robustness to modeling uncertainty, input, and output disturbances are intended to be demonstrated with a simple comparison. Subsequently, in **experiment #5**, translational motion control is conducted as follows: given an initial condition within the 4m by 5m experiment table, the objective is just to steer the satellite to the reference. The experiment may appear to be simple; however, there are 2 interesting observations to make. First, as mentioned in Chapter 2, the current state of art 5-DOF spacecraft motion control is based on LQR type optimal control scheme proposed in [143] . In this thesis, we took into account the magnitude of thrust the thruster could provide, 65mN/each thruster for an approximately 80kg of experimental platform, thus ideally could only produce a maximum acceleration of roughly 5.5 mm/s^2. Hence, with constrained optimization, the low thrust allocation is fully utilized, agility is obtained. Constrained MPC also provides a direct mechanism to incorporate the thruster constraints in the controller design. Secondly, although the platform is 2-D, the formulation and the experiments are pioneering experiments to test constrained optimization for 3-D spacecraft position control. This will bring the safety level of the relative proximity operations into another level since the constraints are explicitly handled and the risk of collision with the target is removed. We believe our work could contribute to earlier work shown in Fig. 6.25. In Fig. 6.25, on the left, the MIT-NASA SPHERES project and astronaut Scott Kelly, on the right, experimental results when 40cm step input given is illustrated. Both traditional robust technique and unconstrained optimal control theory, namely H_∞ and LQR fail to meet with the mission objective which was no overshoot. With the proposed MPC approach, the no overshoot objective could be achieved.

iv. Next, in **experiment #6** and #**7**, two different discretization strategy, namely simultaneous and sequential discretization are demonstrated for 5-DOF spacecraft motion control towards rendezvous and docking with uncooperative targets. The sequential discretization is derived in [37] . In Chapter 4 of this thesis, the simultaneous discretization is derived (see Eqns. (4.55, 4.50)). Both discretization methods are experimental tested for the first time. These experiments are first-ever experiments that are designed

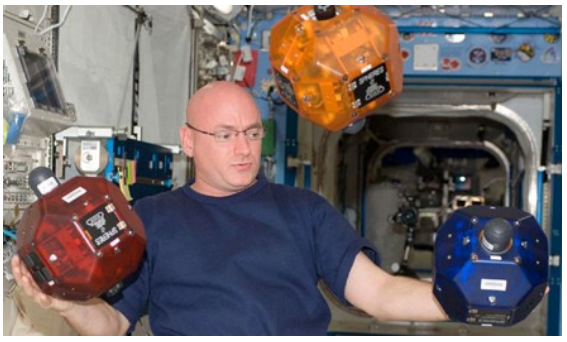

(A) Astronaut Scott Kelly poses for a photograph with three MIT Spheres [195]

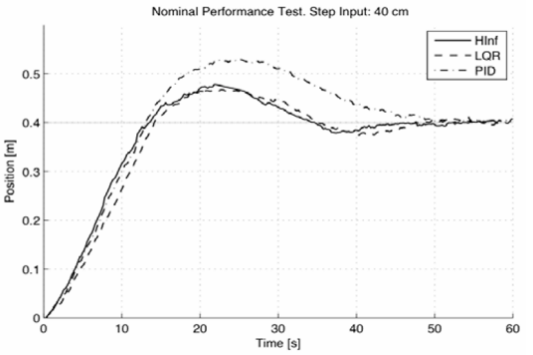

(B) Nominal Performance with a Step Input of 40 cm [133]

FIGURE 6.25: Demonstration of SPHERES project and their results

to address 6-DOF spacecraft motion control with embedded optimization running in real-time. Furthermore, both experiments are the pioneer experiments that employed dual quaternions to couple translational and rotational motion. As a result, we are now able to explicitly incorporate in the formulation, (1) the actuator constraints, (2) the knowledge of the docking features of both chaser satellite and target satellite, and (3) nonlinear couplings between the translational and rotational motion. Both of the discretization strategies show a similar trend and a clear difference cannot be spotted from the experimental results. Yet, one can note that position offset remains in both cases and hence, integral action should be implemented not only on the position states but also on rotational states, quaternions. Lastly, it was noticed that the implemented input is slightly different than commanded input when full translational and rotational motion is addressed. This is because the proposed algorithm is not aware of how the thrust and torque values are mapped on the thrusters. Therefore, conflict occurs when full torque and thrust are commanded. This can be avoided by introducing a new set of equality constraints that defines the thruster allocation stage which will be left as future work.

Remark 24. Prediction horizon and control horizon are important considerations in the MPC design because they affect stability, performance and computation requirement. For the prediction horizon, it is important to make sure that MPC is able to see the future sufficiently long and not 'short-sighted'. It is realized that the prediction and control horizons' effects did not differ from the fundamentals of MPC design where lower prediction and control horizon i.e. 1 to 5 results in

stability issues due to being shortsighted and very long predictions result in diminishing return in the performance but increases the computation burden critically. We were unable to run MPC prediction horizon Np greater than 20 due to the real-time requirement constraint. Just to recap, there are 6 inputs (3 torque and 3 force inputs) and if Np = 20, (assuming that Np = Nc), there will be 120 decision variables. Moreover, recall from the Chapter 4, the nonlinear model is linearized every time-step and thus, additional computations were needed which limited the choice of prediction horizon. Eventually, prediction horizon is kept at 20 for the experiments with sampling time Ts = 1s and at 10 for the experiments with sampling time Ts = 0.5s.

Chapter 7

Conclusions & Future Work

7.1 Conclusions

This dissertation addressed the gap between the matured Linear Model Predictive Control theory with the final phase of an automated Rendezvous and Docking scenario, with consideration for 6-DOF translational and rotational motion couplings, thruster configuration, constraints, real-time implementation issues and validation with experimental work. It was seen that the MPC framework can bring safe, propellant-efficient trajectories for impulsively-actuated spacecraft operating in close proximity to other objects. In addition, MPC shows robustness to the single thruster failures and can be formulated to account for thruster configuration in the RVD problem. The thesis's main contribution is its ability to obtain online solutions at the sub-second level while optimizing the cost function with respect to the constraints, translational and rotational motion couplings. Moreover, with LTV MPC formulation, RVD operations in elliptic orbit can be efficiently done as MPC has the capability to take into account the future prediction models at the time instant the optimization problem is formulated and solved. Furthermore, *Inscribed Polygon Approach* is developed to address the QCQP problem arising in single-axis thruster configuration. It has been validated via simulations in NHFEM that the proposed method provides quasi circle input constraint realization, in other words, the controller can well approximate to full utilization of the thruster. In summary, the proposed approach appears to have the potential for future automated

missions, enabling real-time computation of low-cost trajectories in-orbit without ground intervention.

7.2 Future Work

This work will be extended with the following items:

- **Plume Impingement:** The idea is to ensure that vehicles converge to the desired states without colliding & repelling each other and causing contamination, degradation of sensors or damaging surfaces such as solar arrays, due to the direction of thrusters. This is a non-convex problem and required convexification will be done, the constraint will be explicitly taken into account.

- **Field of View:** Although in the simulations it is assumed that the knowledge of the states of target is available and during the experiments, the localization is done by the motion capture lab, guidance and control strategy must ensure that on-board navigation sensors are faced within the Field-Of-View, i.e., stars or target docking port. Hence, FoV constraints will be formulated and explicitly taken into account.

- **Robustness study:** When the chaser spacecraft operates near constraints, i.e. Line-of-Sight constraint, with a small unmodeled disturbance, the system can be pushed out from the feasible region and no optimization result can be found. To address this challenge we will conduct a robustness study for measurement errors and unmodeled disturbances.

  Vibration is one of the challenges related to spacecraft maneuvering operations. Considering the fact that structural designs are based on zero-G conditions, it is even more troublesome when docking a tumbling spacecraft with flexible structures such as solar arrays. Hence, it is a problem to solve how to couple the flexible structure dynamics with the rigid body translational and rotational motion in an integrated control design. In the future, we will integrate the flexible modes of the target into our model with input from Thales Alenia Space (TAS).

- **Integrated Thruster Allocation** The distinctive feature of MPC paradigm is the ability to handle constraints. In this thesis, the thruster allocation

problem is an independent block from MPC. This results in infeasible solutions due to conflicts between Force and Torque commands. Firstly, the thruster geometry will be formulated as an inequality constraint such that every commanded force and torque inputs are feasible. Secondly, assuming that the fault of the thruster is detected, re-configurable equality constraint based on the current availability of the thrusters will be formulated. This will make the G&C block to aware of the thruster failures while optimizing the cost function with respect to the other constraints.

- **Experimentation Extensions:** The future task will finally aim at validating the kinematics on the robotic rendezvous test bench in TAS-France before the engineering prototype is developed. To this end, the algorithms will first be embedded in a **dSpace module** to demonstrate the real-time simulation of the MPC control loop. Then, the **robotic test bench** will be used to reproduce in real-time the spacecraft motion obtained in simulation. Finally, the real feedback provided by dedicated sensors (e.g., stereo and TOF cameras) will be used to close the loop and perform a Hardware-in-the-Loop (HIL) validation of the whole activity. The flow of experimental work is standard Thales Alenia Space study cycle.

Appendix A

Relative Motion Dynamics Equations

A.1 Clohessy-Wiltshere-Hill (CWH) Equations

A.1.1 Derivations

To begin, let us make a few assumptions:

- There is only a single gravitational attractor that yields a spherically-symmetric gravitational field (inverse-square law gravitation).
- There are no forces exerted between the chaser and target (that is, we neglect their mutual gravitation and assume the spacecraft do not influence one another).
- The target spacecraft moves in a perfect circle about the attractor (a constraint which requires that the target exert zero net translational thrust at all times).

The scenario can be visualized in Fig. A.1. In essence, we assume that each spacecraft moves according to Restricted Two-Body Problem (Keplerian) dynamics (in the Earth-Centered Inertial (ECI) X-Y-Z frame), with the target constrained to perfect circular orbit (to which we attach a moving Local-Vertical, Local-Horizontal

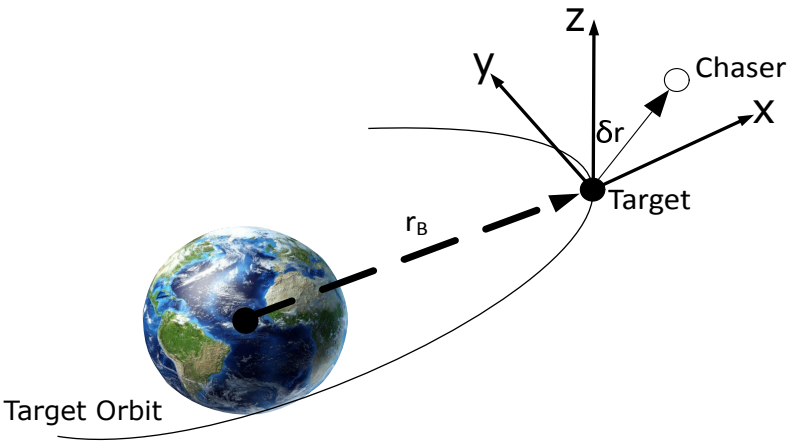

FIGURE A.1: LVLH Frame

(LVLH) $\delta x - \delta y - \delta z$ frame). The accuracy of these assumptions is limited by orbit insertion/determination errors and by orbital perturbations, including atmospheric drag, attractor oblateness, and third-body effects. For these reasons, the CWH equations are only useful for modeling short duration maneuvers, where "short" implies a sufficiently-small duration (typically a few target orbital periods, or less) such that these uncertainties and perturbations do not have time to drive predicted motions significantly far from the truth.
To describe this mathematically, we have for the chasing spacecraft that:

$$\dot{\mathbf{p}} = -\frac{GMm}{r^3}\mathbf{r} + \mathbf{F}$$

using Newton's Law of Gravitation (and neglecting relativistic effects), where G is the universal gravitational constant, M is the attractor mass, m is the chaser mass, $\mathbf{p}$ is its linear momentum, and $\mathbf{F}$ is its applied thrust. Writing $\dot{\mathbf{p}}$ as $(\dot{m}\mathbf{v}) = \dot{m}\mathbf{v} + m\dot{\mathbf{v}}$, let us assume that m is approximately constant (i.e., that propellant usage during proximity operations is small compared to the total spacecraft mass, such that the term $\dot{m}\mathbf{v} \ll m\dot{\mathbf{v}}$, where $\ll$is applied component-wise). Then we can re-express our dynamics as

$$\ddot{\mathbf{r}} = -\frac{\mu}{r^3}\mathbf{r} + \frac{\mathbf{F}}{m} \tag{A.1}$$

where $\mu = GM$ is the gravitational parameter associated with the gravitational attractor.

It follows analogously for the target (i.e., the LVLH frame origin, or reference

point) that

$$\ddot{\mathbf{r}}_{ref} = -\frac{\mu}{r_{ref}^3}\mathbf{r}_{ref} \tag{A.2}$$

Now, by our circular orbit assumption, r_{ref} is equal to a constant and the LVLH frame angular velocity satisfies $\omega_{ref} = \dot{\theta}\hat{Z} = \dot{\theta}\hat{\delta z}$. Combined with Fig. A.1, it follows that:

$$\mathbf{r}_{ref} = r_{ref}\hat{\mathbf{r}}_{ref} = r_{ref}\hat{\delta x}$$

$$\dot{\mathbf{r}}_{ref} = \left(r_{ref}\dot{\hat{\delta x}}\right) = \cancelto{0}{\dot{r}_{ref}}\hat{\delta x} + r_{ref}\dot{\hat{\delta x}} = r_{ref}\dot{\theta}\hat{\delta y}$$

$$\ddot{r}_{ref} = \left(r_{ref}\ddot{\hat{\delta x}}\right) = \cancelto{0}{\ddot{r}_{ref}}\hat{\delta x} + r_{ref}\ddot{\hat{\delta x}} = -r_{ref}\dot{\theta}^2\hat{\delta x}$$

where we used the facts that $\dot{\hat{\delta x}} = \omega_{ref} \times \hat{\delta x} = \dot{\theta}\hat{\delta z} \times \hat{\delta x} = \dot{\theta}\hat{\delta y}$ and that $\ddot{\hat{\delta x}} = \omega_{ref} \times \dot{\hat{\delta x}} = \dot{\theta}\hat{\delta z} \times \dot{\theta}\hat{\delta y} = -\dot{\theta}^2\hat{\delta x}$. Substituting into Eqn. (A.2),

$$-r_{ref}\dot{\theta}^2\hat{\delta x} = -\frac{\mu}{r_{ref}^3}\left(r_{ref}\hat{\delta x}\right)$$

we see immediately that $\dot{\theta}^2 = \frac{\mu}{r_{ref}^3}$, which yields (taking only the positive solution):

$$n_{ref} \triangleq \dot{\theta} = \sqrt{\frac{\mu}{r_{ref}^3}} \tag{A.3}$$

where n_{ref}, a constant, is the mean motion of the target spacecraft orbit. Integrating, we find that:

$$\theta(t) = \int_{t_0}^{t} n_{ref}dt = n_{ref}(t - t_0) \tag{A.4}$$

for the polar angle (true/eccentric/mean anomaly) of the target spacecraft.

Turning our attention to the chaser spacecraft, let us express the inertial dynamics of Eqn. (A.1) in the target LVLH frame. These relative dynamics will give us the equations necessary for linearization. From Fig. A.1, note that $\mathbf{r} = \mathbf{r}_{ref} + \delta\mathbf{r}$. It follows that $\ddot{\mathbf{r}} = \ddot{\mathbf{r}}_{ref} + \ddot{\delta\mathbf{r}}$, which means we now need only find an expression for

$\ddot{\delta\mathbf{r}}$. Let $\dot{(\cdot)}$ and $\mathring{(\cdot)}$ denote time derivatives to one another, that:

$$\dot{\delta r} = \mathring{\delta r} + \omega_{ref} \times \delta r$$

$$\begin{aligned}\ddot{\delta r} &= \left(\mathring{\delta r} + \dot{\omega_{ref}} \times \delta r\right) = \dot{\mathring{\delta r}} + (\omega_{ref}\dot{} \times \delta r) = \left(\mathring{\mathring{\delta r}} + \omega_{ref} \times \mathring{\delta r}\right) + \left(\cancelto{0}{\dot{\omega}_{ref}} \times \delta r + \omega_{ref} \times \dot{\delta r}\right) \\ &= \left(\mathring{\mathring{\delta r}} + \omega_{ref} \times \mathring{\delta r}\right) + \left(\omega_{ref} \times \mathring{\delta r} + \omega_{ref} \times (\omega_{ref} \times \delta r)\right) \\ &= \mathring{\mathring{\delta r}} + 2\omega_{ref} \times \mathring{\delta r} + \omega_{ref} \times (\omega_{ref} \times \delta r)\end{aligned}$$

where we used that $\dot{\omega}_{ref} = \left(n_{ref}\dot{\hat{\delta z}}\right) = \dot{n}_{ref}\hat{\delta z} + n_{ref}\dot{\hat{\delta z}} = 0$, since both n_{ref} and $\hat{\delta z}$ are constant.

Resolving into the LVLH coordinate frame,

$$\delta r = \begin{bmatrix}\delta x \\ \delta y \\ \delta z\end{bmatrix} \quad \delta v = \mathring{\delta r} = \begin{bmatrix}\dot{\delta x} \\ \dot{\delta y} \\ \dot{\delta z}\end{bmatrix} \quad \mathring{\mathring{\delta r}} = \begin{bmatrix}\ddot{\delta x} \\ \ddot{\delta y} \\ \ddot{\delta z}\end{bmatrix} \quad \omega_{ref} = \begin{bmatrix}0 \\ 0 \\ n_{ref}\end{bmatrix} \tag{A.5}$$

$$r = \begin{bmatrix}r_{ref} + \delta x \\ \delta y \\ \delta z\end{bmatrix} \quad F = \begin{bmatrix}F_{\delta x} \\ F_{\delta y} \\ F_{\delta z}\end{bmatrix} \tag{A.6}$$

we find that: =

$$\begin{aligned}\ddot{r} &= \ddot{r}_{ref} + \ddot{\delta r} \\ &= \begin{bmatrix}-r_{ref}n_{ref}^2 \\ 0 \\ 0\end{bmatrix} + \left(\begin{bmatrix}\ddot{\delta x} \\ \ddot{\delta y} \\ \ddot{\delta z}\end{bmatrix} + 2\left(\begin{bmatrix}0 \\ 0 \\ n_{ref}\end{bmatrix} \times \begin{bmatrix}\dot{\delta x} \\ \dot{\delta y} \\ \dot{\delta z}\end{bmatrix}\right) + \begin{bmatrix}0 \\ 0 \\ n_{ref}\end{bmatrix} \times \left(\begin{bmatrix}0 \\ 0 \\ n_{ref}\end{bmatrix} \times \begin{bmatrix}\delta x \\ \delta y \\ \delta z\end{bmatrix}\right)\right) \\ &= \begin{bmatrix}-r_{ref}n_{ref}^2 \\ 0 \\ 0\end{bmatrix} + \left(\begin{bmatrix}\ddot{\delta x} \\ \ddot{\delta y} \\ \ddot{\delta z}\end{bmatrix} + 2\begin{bmatrix}-n_{ref}\dot{\delta y} \\ n_{ref}\dot{\delta x} \\ 0\end{bmatrix} + \begin{bmatrix}0 \\ 0 \\ n_{ref}\end{bmatrix} \times \begin{bmatrix}-n_{ref}\delta y \\ n_{ref}\delta x \\ 0\end{bmatrix}\right) \\ &= \begin{bmatrix}\ddot{\delta x} - 2n_{ref}\dot{\delta y} - n_{ref}^2(r_{ref} + \delta x) \\ \ddot{\delta y} + 2n_{ref}\dot{\delta x} - n_{ref}^2\delta y \\ \ddot{\delta z}\end{bmatrix}\end{aligned}$$

Equating with Eqn. (A.1), and rearranging:

$$\begin{bmatrix} \ddot{\delta x} \\ \ddot{\delta y} \\ \ddot{\delta z} \end{bmatrix} = -\frac{\mu}{r^3} \begin{bmatrix} r_{ref} + \delta x \\ \delta y \\ \delta z \end{bmatrix} + \begin{bmatrix} 2n_{ref}\dot{\delta y} + n_{ref}^2(r_ref + \delta x) \\ -2n_{ref}\dot{\delta x} + n_{ref}^2 \delta y \\ 0 \end{bmatrix} + \frac{1}{m} \begin{bmatrix} F_{\delta x} \\ F_{\delta y} \\ F_{\delta z} \end{bmatrix} \tag{A.7}$$

we obtain the non-linear equations of motion for the chaser spacecraft in the LVLH frame, where $r = \sqrt{(r_{ref} + \delta x)^2 + \delta y^2 + \delta z^2}$.
To linearize these equations of motion, we must first put them into first-order form. Define our state $\mathbf{x}$ as the relative position and velocity vector, $\mathbf{x} \triangleq [\delta r^T, \delta v^t]^T$, and let our control $\mathbf{u}$ be the specific force (force per unit mass),$\mathbf{u} \triangleq \mathbf{F}/m$. Then:

$$\dot{x} = \begin{bmatrix} \delta \mathbf{v} \\ \mathbf{f(x,u)} \end{bmatrix} \tag{A.8}$$

where $\mathbf{f(x,u)}$ is the right-hand side of Eqn. (A.7). We aim to linearize Eqn. (A.8) about the equilibrium point at the LVLH origin ($x_{eq} = 0$ with $u_{eq} = 0$), corresponding to the unforced circular orbit of the target. Restricting our attention to only the velocity equations (as the position dynamics are already linear),

$$f(x,u) \cong f(x_{eq}, u_{eq}) + \left.\frac{\partial f}{\partial x}\right|_{x_{eq}, u_{eq}} (x - x_{eq}) + \left.\frac{\partial f}{\partial u}\right|_{x_{eq}, u_{eq}} (u - u_{eq}) \tag{A.9}$$

using Eqn. (A.7), it is straightforwards exercise to show that the Jacobian matrices $\frac{\partial f}{\partial x}$ and $\frac{\partial f}{\partial u}$ can be expressed in the LVLH frame as

$$\frac{\partial f}{\partial x} = \begin{bmatrix} -\frac{\mu}{r^3} + \frac{3\mu(r_{ref}+\delta x)^2}{r^5} + n_{ref}^2 & \frac{3\mu(r_{ref}+\delta x)\delta y}{r^5} & \frac{3\mu(r_{ref}+\delta x)\delta z}{r^5} & 0 & 2n_{ref} & 0 \\ \frac{3\mu\delta y(r_{ref}+\delta x)}{r^5} & \frac{-\mu}{r^3} + \frac{3\mu\delta y^2}{r^5} + n_{ref}^2 & \frac{3\mu\delta y\delta z}{r^5} & -2n_{ref} & 0 & 0 \\ \frac{3\mu\delta z(r_{ref}+\delta x)}{r^5} & \frac{3\mu\delta z\delta y}{r^5} & \frac{-\mu}{r^3} + \frac{3\mu\delta z^2}{r^5} & 0 & 0 & 0 \end{bmatrix}$$

$$\frac{\partial f}{\partial u} = \begin{bmatrix} 1 & 0 & 0 \\ 0 & 1 & 0 \\ 0 & 0 & 1 \end{bmatrix}$$

Substituting into Eqn. (A.9) and evaluating at $x_{eq} = u_{eq} = 0$, we find that $f(x_{eq}, u_{eq}) = 0$ and hence:

$$f(x,u) \cong \begin{bmatrix} 3n_{ref}^2 & 0 & 0 & 0 & 2n_{ref} & 0 \\ 0 & 0 & 0 & -2n_{ref} & 0 & 0 \\ 0 & 0 & -nref^2 & 0 & 0 & 0 \end{bmatrix} x + \begin{bmatrix} 1 & 0 & 0 \\ 0 & 1 & 0 \\ 0 & 0 & 1 \end{bmatrix} u$$

Substituting into Eqn. (A.8), we obtain, finally, the linear Clohessy-Wiltshire-Hill (CWH) equations:

$$\dot{x} = \underbrace{\begin{bmatrix} 0 & 0 & 0 & 1 & 0 & 0 \\ 0 & 0 & 0 & 0 & 1 & 0 \\ 0 & 0 & 0 & 0 & 0 & 1 \\ 3n_{ref}^2 & 0 & 0 & 0 & 2n_{ref} & 0 \\ 0 & 0 & 0 & -2n_{ref} & 0 & 0 \\ 0 & 0 & -n_{ref}^2 & 0 & 0 & 0 \end{bmatrix}}_{\triangleq \mathbf{A}} x + \underbrace{\begin{bmatrix} 0 & 0 & 0 \\ 0 & 0 & 0 \\ 0 & 0 & 0 \\ 1 & 0 & 0 \\ 0 & 1 & 0 \\ 0 & 0 & 1 \end{bmatrix}}_{\triangleq \mathbf{B}} u \tag{A.10}$$

where x=$[\delta x, \delta y, \delta z, \delta \dot{x}, \delta \dot{y}, \delta \dot{z}]^T$ are the position and velocity coordinates of the chaser as expressed in the LVLH frame, $\mathbf{u}=\frac{1}{m}[F_{\delta x}, F_{\delta y}, F_{\delta z}]^T$ is the specific thrust of the chaser resolved in the LVLH frame, and n_{ref} is the mean motion of the target spacecraft orbit, as given by Eqn. (A.3).

A.1.2 Analytical Solutions to the CWH Equations

The CWH equations represented by Eqn. (A.10) admit a closed-form solution. To derive it, we make use of the Laplace Transform $\mathcal{L}$ as well as its inverse $\mathcal{L}^{-1}$, defined for causal systems as

$$\mathcal{L}(f(t)) = F(s) = \int_{t_0}^{\infty} e^{-st} f(t) dt \tag{A.11a}$$

$$\mathcal{L}^{-1}(F(s)) = f(t) = \left[\frac{1}{2\pi j}\right] \lim_{T\to\infty} \int_{\gamma - jT}^{\gamma + jT} e^{st} F(s) \tag{A.11b}$$

where γ is a real number large enough to ensure that the vertical line of integration Re(s)=γ in the complex plane lies to the right of any singularities of F(s). As we will see, these two operations turn out to be very useful in simplifying ordinary differential equation (ODE) expressions.
We begin by applying the Laplace transform to both sides of Eqn. (A.10):

$$\begin{aligned}
\mathcal{L}(\dot{x}(t)) &= \mathcal{L}(\mathbf{A}x(t) + \mathbf{B}u(t)) \\
s\mathcal{L}(x(t)) - e^{-st_0}x(t_0) &= \mathbf{A}\mathcal{L}(x(t)) + \mathbf{B}\mathcal{L}(\mathbf{u}(t)) \\
(s\mathbf{I} - \mathbf{A})\mathbf{X}(s) &= e^{-st_0}x(t_0) + \mathbf{B}\mathbf{U}(s) \\
\mathbf{X}(s) &= (s\mathbf{I} - \mathbf{A})^{-1}e^{-st_0}x(t_0) + (s\mathbf{I} - \mathbf{A})^{-1}\mathbf{B}\mathbf{U}(s)
\end{aligned}$$

where on the second line we used integration-by-parts (for the left-hand-side) and the linearity of the Laplace Transform (for the right-hand-side). If we now apply the Inverse Laplace Transform, we find:

$$\mathbf{x}(t) = \mathcal{L}^{-1}(\mathbf{X}(s)) = \mathcal{L}^{-1}((s\mathbf{I} - \mathbf{A})^{-1}e^{-st_0})\mathbf{x}(t_0) + \mathcal{L}^{-1}(s\mathbf{I} - \mathbf{A})^{-1}\mathbf{B}\mathbf{U}(s))$$

where we again rely on linearity to simplify the right-hand-side. Now, let φ(s) represent the Laplace Transform of some time-domain function Φ(t). We make use of two well-known facts: (i) the Inverse Laplace Transform of the exponential e^{-st_0} times φ(s) creates a shift in the time-domain $\mathcal{L}^{-1}(\varphi(s)e^{-st_0}) = \Phi(t - t_0)$, and (ii) the Inverse Laplace Transform of the product of two s-domain functions φ(s) and $\mathbf{G}$(s) is given by $\mathcal{L}^{-1}(\varphi(s)\mathbf{G}(s)) = \Phi(t) * \mathbf{g}(t)$, a convolution integral in the time domain (verification of both properties is a straightforward exercise in calculus that we do not show here). Setting $\varphi(s) = (s\mathbf{I} - \mathbf{A})^{-1}$ and G(s)=BU(s)in this case, we obtain:

$$x(t) = \Phi(t - t_0)x(t_0) + \int_{t_0}^{t} \Phi(t - \tau)Bu(\tau)d\tau \tag{A.12}$$

Equation A.12 reveals that to find the solution x(t) to tour dynamic equations, we need only determine $\Phi(t) = \mathcal{L}^{-1}((sI - A)^{-1})$. Note that the argument, $(sI - A)^{-1}$, called the resolvent of $\mathbf{A}$, is defined at all s$\in \mathcal{C}$ except for the eigenvalues of $\mathbf{A}$. If we re-express the resolvent in terms of its power series,

$$(sI - A)^{-1} = \frac{1}{s}\left(\mathbf{I} - \frac{\mathbf{A}}{s}\right)^{-1} = \frac{1}{s}\left(\mathbf{I} + \frac{\mathbf{A}}{s} + \left(\frac{\mathbf{A}}{s}\right)^2 + \dots\right) = \frac{\mathbf{I}}{s} + \frac{\mathbf{A}}{s^2} + \frac{\mathbf{A}^2}{s^3} + \dots$$

(valid at all s values with $|s|$ sufficiently-large and far from the eigenvalues of $\mathbf{A}$), we obtain and expression that is easier to evaluate inside the Inverse Laplace Transform:

$$\Phi(t) = \mathcal{L}^{-1}((s\mathbf{I} - \mathbf{A})^{-1}) = \mathbf{I} + t\mathbf{A} + \frac{(t\mathbf{A})^2}{2!} + \dots = \sum_{k=0}^{\infty} \frac{(t\mathbf{A})^k}{k!} \triangleq e^{t\mathbf{A}} \tag{A.13}$$

where $e^{t\mathbf{A}}$ is called the matrix exponential of $\mathbf{A}$. Putting Eqn. (A.12) and Eqn. (A.13) together, the solution to our system dynamics (applicable, in fact, to any LTI system) is therefore given by:

$$x(t) = e^{\mathbf{A}(t-t_0)}x(t_0) + \int_{t_0}^{t} e^{\mathbf{A}(t-\tau)}\mathbf{B}\mathbf{u}(\tau)d\tau \tag{A.14}$$

Hence all that remains to compute a closed-form expression for the matrix $\Phi(t) = e^{\mathbf{A}t} = \mathcal{L}^{-1}((s\mathbf{I}\text{-}\mathbf{A})^{-1})$, called the state transition matrix of our system. Rather than evaluating the infinite sum in Eqn. (A.13) it actually turns out to be much simpler to use the Inverse Laplace Transform directly on the elements of the resolvent of $\mathbf{A}$. Substituting the CWH system matrix $\mathbf{A}$, shown in Eqn. (A.10),

$$(s - \mathbf{I\text{-}A}) = \begin{bmatrix} s & 0 & 0 & -1 & 0 & 0 \\ 0 & s & 0 & 0 & -1 & 0 \\ 0 & 0 & s & 0 & 0 & -1 \\ -3n_{ref}^2 & 0 & 0 & s & -2n_{ref} & 0 \\ 0 & 0 & 0 & 2n_{ref} & s & 0 \\ 0 & 0 & n_{ref}^2 & 0 & 0 & s \end{bmatrix}$$

$$(s - \mathbf{I\text{-}A})^{-1} = \begin{bmatrix} \frac{4n_{ref}^2+s^2}{s(n_{ref}^2+s^2)} & 0 & 0 & \frac{1}{n_{ref}^2+s^2} & \frac{2n_{ref}}{s(n_{ref}^2+s^2)} & 0 \\ \frac{-6n_{ref}^3}{s^2(n_{ref}^2+s^2)} & \frac{1}{s} & 0 & \frac{-2n_{ref}}{s(n_{ref}^2+s^2)} & \frac{-3n_{ref}^2+s^2}{s^2(n_{ref}^2+s^2)} & 0 \\ 0 & 0 & \frac{s}{n_{ref}^2+s^2} & 0 & 0 & \frac{1}{n_{ref}^2+s^2} \\ \frac{3n_{ref}^2}{n_{ref}^2+s^2} & 0 & 0 & \frac{s}{n_{ref}^2+s^2} & \frac{2n_{ref}}{n_{ref}^2+s^2} & 0 \\ \frac{-6n_{ref}^3}{s(n_{ref}^2+s^2)} & 0 & 0 & \frac{-2n_{ref}}{n_{ref}^2+s^2} & \frac{-3n_{ref}^2+s^2}{s(n_{ref}^2+s^2)} & 0 \\ 0 & 0 & \frac{-n_{ref}^2}{n_{ref}^2+s^2} & 0 & 0 & \frac{s}{n_{ref}^2+s^2} \end{bmatrix}$$

it now becomes a straightforward matter of applying the Inverse Laplace Transfrom to each element of $(s\mathbf{I} - \mathbf{A})^{-1}$ (easily achieved via a combination of partial fraction decompositions and a table of elementary Laplace Transforms). Introducing $\theta(t) = n_{ref}t$ as the polar angle (true anomaly) of the target spacecraft, the result (once all the dust settles) turns out to be:

$$\Phi(t) = \begin{bmatrix} 4 - 3cos\theta & 0 & 0 & \frac{1}{n_{ref}}sin\theta & \frac{2}{n_{ref}}(1 - cos\theta) & 0 \\ 6sin\theta - 6\theta & 1 & 0 & \frac{2}{n_{ref}}(cos\theta - 1) & \frac{1}{n_{ref}}(4sin\theta - 3\theta) & 0 \\ 0 & 0 & cos\theta & 0 & 0 & \frac{1}{n_{ref}}sin\theta \\ 3n_{ref}sin\theta & 0 & 0 & cos\theta & 2sin\theta & 0 \\ 6n_{ref}(cos\theta - 1) & 0 & 0 & -2sin\theta & 4cos\theta - 3 & 0 \\ 0 & 0 & -n_{ref}sin\theta & 0 & 0 & cos\theta \end{bmatrix} \tag{A.15}$$

To make our solution explicit for impulsive dynamics resolved in the CWH frame (the rotating Local-Vertical, Local-Horizontal frame of the target spacecraft), suppose that we apply the control trajectory $\mathbf{u}(t) = \sum_{i=1}^{N} \Delta v_i \delta(t - \tau_i)$ to our chaser spacecraft, comprising N impulses $\Delta v_i = [\Delta v_{\delta x,i}, \Delta v_{\delta y,i}, \Delta v_{\delta z,i}]^T$ at burn times τ_i for $i \in [1, \ldots, N]$. Define the chaser initial state as $x(t_0) = x_0 = [\delta x_0, \delta y_0, \delta z_0, \delta \dot{x}_0, \delta \dot{y}_0, \delta \dot{z}_0]^T$. Then the chaser state transition equations are given by:

$$\delta x(t) = (4 - 3cos\theta)\delta x_0 + \left(\frac{1}{n_{ref}} sin\theta\right) \delta \dot{x}_0 + \left(\frac{2}{n_{ref}}(1 - cos\theta)\right) \delta \dot{y}_0 \tag{A.16}$$

$$+ \sum_{i=1}^{N_t} \left[\left(\frac{1}{n_{ref}} sin\theta_i\right) \Delta v_{\delta x,i} + \left(\frac{2}{n_{ref}}(1 - cos\theta_i)\right) \Delta v_{\delta y,i} \right]$$

$$\delta y(t) = (6sin\theta - 6\theta)\delta x_0 + \delta y_0 + \left(\frac{2}{n_{ref}}(cos\theta - 1)\right) \delta \dot{x}_0 + \left(\frac{1}{n_{ref}}(4sin\theta - 3\theta)\right) \delta \dot{y}_0 \tag{A.17}$$

$$+ \sum_{i=1}^{N_t} \left[\left(\frac{2}{n_{ref}}(cos\theta_i - 1)\right) \Delta v_{\delta x,i} + \left(\frac{1}{n_{ref}}(4sin\theta_i - 3\theta_i)\right) \Delta v_{\delta y,i} \right]$$

$$\delta z(t) = (cos\theta)\delta z_0 + \left(\frac{1}{n_{ref}} sin\theta\right) \delta \dot{z}_0 + \sum_{i=1}^{N_t} \left(\frac{1}{n_{ref}} sin\theta_i\right) \Delta v_{\delta z,i} \tag{A.18}$$

$$\delta \dot{x}(t) = (3n_{ref} sin\theta)\delta x_0 + (cos\theta)\delta \dot{x}_0 + (2sin\theta)\delta \dot{y}_0 + \sum_{i=1}^{N_t} [(cos\theta_i)\Delta v_{\delta x,i} + (2sin\theta_i)\Delta v_{\delta y,i}] \tag{A.19}$$

$$\delta \dot{y}(t) = (6n_{ref}(cos\theta - 1))\delta x_0 + (-2sin\theta)\delta \dot{x}_0 + (4cos\theta - 3)\delta \dot{y}_0 \tag{A.20}$$

$$+ \sum_{i=1}^{N_t} [(-2sin\theta_i)\Delta v_{\delta x,i} + (4cos\theta_i - 3)\Delta v_{\delta y,i}]$$

$$\delta \dot{z}(t) = (-n_{ref} sin\theta)\delta z_0 + (cos\theta)\delta \dot{z}_0 + \sum_{i=1}^{N_t} (cos\theta_i)\Delta v_{\delta z,i} \tag{A.21}$$

where $\theta = n_{ref}(t - t_0), \theta_i = n_{ref}(t - \tau_i)$, and $N_t = \sum_{i=1}^{N} \mathbb{1}[\tau_i \leq t]$ is the number of burns occuring at or before time t.

List of Author's Publications

Journal Articles & Conference Proceedings

Published & Accepted

- **Iskender, O. B.,** Ling, KV., Dubanchet, V., "Constraints Tightening Approach Towards Model Predictive Control Based Rendezvous and Docking with Uncooperative Targets," in 2018 European Control Conference (ECC). IEEE, 2018, pp. 380-385.
- **Iskender, O. B.,** Ling, K. V., Dubanchet, V., Simonini, L., "Inscribed Polygon Method for Spacecraft Maneuvering Problem Arising in Single Axis Thruster Configuration." 2019 12th Asian Control Conference (ASCC). IEEE, 2019, pp. 1466–1471.
- **Iskender, O. B.,** Ling, K. V., Dubanchet, V., Simonini, L., Schlotterer, M., Seelbinder, D., Theil, S., "Attitude Control of Spacecrafts with Thrusters and Embedded Optimization." In 70th International Astronautical Congress (IAC). International Astronautical Federation, 2019.
- **Iskender, O. B.,**, Wee Meng, N.G., Ling, K. V., Dubanchet, V., "Detumbling and Attitude Control of Cubesats via Multi-Model Based Embedded Optimization." In 70th International Astronautical Congress (IAC). International Astronautical Federation, 2019.
- **Iskender, O. B.,** Ling, K. V., Dubanchet, V., Simonini, L., Schlotterer, M., Seelbinder, D., Theil, S., Maciejowski, J.M., "Dual Quaternion Based Autonomous Rendezvous and Docking Via Model Predictive Control." In 70th International Astronautical Congress (IAC). International Astronautical Federation, 2019.

- **Iskender, O. B.,** Ling, K. V., Dubanchet, V., Simonini, L., Dellandrea, B., Maciejowski, J.M., "A Tutorial on Model Predictive Control for Spacecraft Maneuvering Problem with Theory, Experimentation and Applications." Global Space Exploration Conference, 2020, (Accepted).

- **Iskender, O. B.,** Ling, K. V., Dubanchet, V., Simonini, L., Dellandrea, B., Maciejowski, J.M., "Hardware-In-the-Loop Experiments of Guidance & Control laws for Space Servicing Missions based on Model Predictive Control using Dual-Quaternions." Global Space Exploration Conference, 2020, (Accepted).

Bibliography

[1] "Dragon set to deliver supplies to international space station," https://blogs.nasa.gov/spacex/2018/03/26/dragon-set-to-deliver-supplies-to-international-space-station/, 2017, accessed: 2019-08-04.

[2] "Artist's view of esa's atv johannes kepler approaching the international space station," http://www.esa.int/ESA_Multimedia/Missions/Automated_Transfer_Vehicle_ATV/(offset)/140/(sortBy)/view_count/(result_type)/images, 2011, accessed: 2019-08-04.

[3] "Europe prepares for mars courier," https://www.esa.int/Science_Exploration/Human_and_Robotic_Exploration/Exploration/Europe_prepares_for_Mars_courier, accessed: 2020-03-03.

[4] "A try-out mission for space debris clean-up?" https://www.esa.int/Safety_Security/Clean_Space/A_try-out_mission_for_space_debris_clean-up, accessed: 2020-03-03.

[5] NASA, "On-orbit satellite servicing study," https://sspd.gsfc.nasa.gov/images/NASA_Satellite%20Servicing_Project_Report_0511.pdf, Apr. 2020, accessed: 2020-04-05.

[6] D. D. Mazanek, R. G. Merrill, S. P. Belbin, D. M. Reeves, B. J. Naasz, P. A. Abell, and K. Earle, "Asteroid redirect robotic mission: Robotic boulder capture option overview," in *AIAA SPACE 2014 Conference and Exposition*, 2014, p. 4432.

[7] "Esa's potential space garbage collector nets itself a drone," https://newatlas.com/esa-drone-net-capture/43777/#gallery, accessed: 2019-07-28.

[8] W. Fehse, *Automated rendezvous and docking of spacecraft*. Cambridge university press, 2003, vol. 16.

[9] "NASA to use giant 3d printing spider robots to construct huge spacecraft," http://ccar.colorado.edu/asen5050/projects/projects_2004/mccall/, 2004, accessed: 2019-07-02.

[10] H. Benninghoff, F. Rems, E.-A. Risse, and C. Mietner, "European proximity operations simulator 2.0 (epos)-a robotic-based rendezvous and docking simulator," *Journal of large-scale research facilities JLSRF*, 2017.

[11] M. Saponara, V. Barrena, A. Bemporad, E. Hartley, J. M. Maciejowski, A. Richards, A. Tramutola, and P. Trodden, "Model predictive control application to spacecraft rendezvous in mars sample return scenario," in *Progress in Flight Dynamics, Guidance, Navigation, Control, Fault Detection, and Avionics*, 2013, pp. 137–158.

[12] D. P. Scharf, F. Y. Hadaegh, and S. R. Ploen, "A survey of spacecraft formation flying guidance and control. part ii: control," in *Proceedings of the 2004 American control conference*, vol. 4. IEEE, 2004, pp. 2976–2985.

[13] T. E. Carter, "State transition matrices for terminal rendezvous studies: brief survey and new example," *Journal of Guidance, Control, and Dynamics*, vol. 21, no. 1, pp. 148–155, 1998.

[14] J. Sullivan, S. Grimberg, and S. D'Amico, "Comprehensive survey and assessment of spacecraft relative motion dynamics models," *Journal of Guidance, Control, and Dynamics*, vol. 40, no. 8, pp. 1837–1859, 2017.

[15] J. L. Goodman, "History of space shuttle rendezvous," The National Aeronautics and Space Administration, Tech. Rep., 2011.

[16] Y. Luo, J. Zhang, and G. Tang, "Survey of orbital dynamics and control of space rendezvous," *Chinese Journal of Aeronautics*, vol. 27, no. 1, pp. 1–11, 2014.

[17] J. L. Goodman, "History of space shuttle rendezvous and proximity operations," *Journal of Spacecraft and Rockets*, vol. 43, no. 5, pp. 944–959, 2006.

[18] Y. Ohkami and I. Kawano, "Autonomous rendezvous and docking by engineering test satellite vii: a challenge of japan in guidance, navigation and control—breakwell memorial lecture," *Acta Astronautica*, vol. 53, no. 1, pp. 1–8, 2003.

[19] P. Labourdette, E. Julien, F. Chemama, and D. Carbonne, "Atv jules verne mission maneuver plan," in *Proceedings of the International Symposium on space flight dynamics, Toulouse, France*, 2008.

[20] T. Davis, M. T. Baker, T. Belchak, and W. Larsen, "Xss-10 micro-satellite flight demonstration program," in *2003 17th Annual AIAA/USU Conference on Small Satellites*. AIAA/USU, 2003.

[21] T. M. Davis and D. Melanson, "Xss-10 microsatellite flight demonstration program results," in *Spacecraft platforms and infrastructure*, vol. 5419. International Society for Optics and Photonics, 2004, pp. 16–25.

[22] S. Croomes, "Overview of the dart mishap investigation results," *NASA Report*, pp. 1–10, 2006.

[23] A. Flores-Abad, O. Ma, K. Pham, and S. Ulrich, "A review of space robotics technologies for on-orbit servicing," *Progress in Aerospace Sciences*, vol. 68, pp. 1–26, 2014.

[24] R. B. Friend, "Orbital express program summary and mission overview," in *Sensors and Systems for space applications II*, vol. 6958. International Society for Optics and Photonics, 2008, p. 695803.

[25] W. Xu, B. Liang, and Y. Xu, "Survey of modeling, planning, and ground verification of space robotic systems," *Acta Astronautica*, vol. 68, no. 11-12, pp. 1629–1649, 2011.

[26] A. B. Bosse, W. J. Barnds, M. A. Brown, N. G. Creamer, A. Feerst, C. G. Henshaw, A. S. Hope, B. E. Kelm, P. A. Klein, F. Pipitone *et al.*, "Sumo: spacecraft for the universal modification of orbits," in *Spacecraft Platforms and Infrastructure*, vol. 5419. International Society for Optics and Photonics, 2004, pp. 36–46.

[27] H. Benninghoff, T. Boge, and T. Tzschichholz, "Hardware-in-the-loop rendezvous simulation involving an autonomous guidance, navigation and control system," in *IAA Conference on Dynamics and Control of Space Systems*. International Academy of Astronautics (IAA), 2012.

[28] D. Reintsema, J. Thaeter, A. Rathke, W. Naumann, P. Rank, and J. Sommer, "Deos–the german robotics approach to secure and de-orbit malfunctioned satellites from low earth orbits," in *Proceedings of the i-SAIRAS*. Japan Aerospace Exploration Agency (JAXA) Japan, 2010, pp. 244–251.

[29] K. Alfriend, S. R. Vadali, P. Gurfil, J. How, and L. Breger, *Spacecraft formation flying: Dynamics, control and navigation*. Butterworth-Heinemann, 2009, vol. 2.

[30] C. E. Garcia, D. M. Prett, and M. Morari, "Model predictive control: theory and practice—a survey," *Automatica*, vol. 25, no. 3, pp. 335–348, 1989.

[31] S. J. Qin and T. A. Badgwell, "A survey of industrial model predictive control technology," *Control engineering practice*, vol. 11, no. 7, pp. 733–764, 2003.

[32] J. M. Maciejowski, *Predictive control: with constraints*. Prentice Hall, 2002.

[33] T. J. Besselmann, S. Almér, P. Jörg, H. J. Ferreau *et al.*, "Model predictive control in the multi-megawatt range," *IEEE Transactions on Industrial Electronics*, vol. 63, no. 7, pp. 4641–4648, 2015.

[34] S. Bolognani, S. Bolognani, L. Peretti, and M. Zigliotto, "Design and implementation of model predictive control for electrical motor drives," *IEEE Transactions on industrial electronics*, vol. 56, no. 6, pp. 1925–1936, 2008.

[35] Y. Xie, R. Ghaemi, J. Sun, and J. S. Freudenberg, "Model predictive control for a full bridge dc/dc converter," *IEEE Transactions on Control Systems Technology*, vol. 20, no. 1, pp. 164–172, 2011.

[36] R. Verschueren, S. De Bruyne, M. Zanon, J. V. Frasch, and M. Diehl, "Towards time-optimal race car driving using nonlinear MPC in real-time," in *53rd IEEE conference on decision and control*. IEEE, 2014, pp. 2505–2510.

[37] K. Kunz, S. M. Huck, and T. H. Summers, "Fast model predictive control of miniature helicopters," in *2013 European Control Conference (ECC)*. IEEE, 2013, pp. 1377–1382.

[38] M. Kamel, M. Burri, and R. Siegwart, "Linear vs nonlinear MPC for trajectory tracking applied to rotary wing micro aerial vehicles," *IFAC-PapersOnLine*, vol. 50, no. 1, pp. 3463–3469, 2017.

[39] E. N. Hartley, "A tutorial on model predictive control for spacecraft rendezvous," in *European Control Conference (ECC)*. IEEE, 2015, pp. 1355–1361.

[40] P. Axelrad, "Autonomous rendezvous and docking," http://coe-cst.org/wp-content/uploads/2019/02/Axelrad-244-Autonomous-Rendezvous-and-Docking.pdf, accessed:2019-07-11.

[41] D. C. Woffinden and D. K. Geller, "Navigating the road to autonomous orbital rendezvous," *Journal of Spacecraft and Rockets*, vol. 44, no. 4, pp. 898–909, 2007.

[42] E. N. Hartley, M. Gallieri, and J. M. Maciejowski, "Terminal spacecraft rendezvous and capture with lasso model predictive control," *International Journal of Control*, vol. 86, no. 11, pp. 2104–2113, 2013.

[43] TAS, "Thales alenia space," https://www.thalesgroup.com/en/global/activities/space#key-figures, Apr. 2020, accessed: 2020-04-05.

[44] DLR, "Institute of space systems," https://www.dlr.de/irs, Aug. 2019, accessed: 2020-04-05.

[45] DLR "Teams," https://www.dlr.de/irs/en/desktopdefault.aspx/tabid-11360, Aug. 2019, accessed: 2020-04-05.

[46] B. Acikmese and S. R. Ploen, "Convex programming approach to powered descent guidance for mars landing," *Journal of Guidance, Control, and Dynamics*, vol. 30, no. 5, pp. 1353–1366, 2007.

[47] A. Weiss, I. Kolmanovsky, M. Baldwin, and R. S. Erwin, "Model predictive control of three dimensional spacecraft relative motion," in *2012 American Control Conference (ACC)*. IEEE, 2012, pp. 173–178.

[48] J. A. Starek, "Sampling based motion planning for safe and efficient spacecraft proximity operations," Ph.D. dissertation, Stanford University, 2016.

[49] U. Lee and M. Mesbahi, "Constrained autonomous precision landing via dual quaternions and model predictive control," *Journal of Guidance, Control, and Dynamics*, vol. 40, no. 2, pp. 292–308, 2017.

[50] "Two private satellites just docked in space in historic first for orbital servicing," https://www.space.com/private-satellites-docking-success-northrop-grumman-mev-1.html, accessed: 2020-06-10.

[51] M. J. Sonter, "The technical and economic feasibility of mining the near-earth asteroids," *Acta Astronautica*, vol. 41, no. 4, pp. 637–647, 1997.

[52] C. E. Hellweg and C. Baumstark-Khan, "Getting ready for the manned mission to mars: the astronauts' risk from space radiation," *Naturwissenschaften*, vol. 94, no. 7, pp. 517–526, 2007.

[53] E. W. Messerschmid and F. Renk, *Space stations*. Wiley Online Library, 1999.

[54] D. Zimpfer and P. Spehar, "STS-71 shuttle/MIR GNC mission overview," *Spaceflight mechanics 1996*, pp. 441–460, 1996.

[55] J. Fabrega, M. Frezet, and J.-L. Gonnaud, "ATV GNC During Rendezvous," in *Spacecraft Guidance, Navigation and Control Systems*, vol. 381, 1997, p. 85.

[56] O. Kawasaki, K. Yamanaka, T. Imada, and T. Tanaka, "The on-orbit demonstration and operations plan of the H-II transfer vehicle (HTV)," in *The 51th Int. Astronautical Congress, Rio de Janeiro, Brazil*, 2000.

[57] F. Zhang, Y. Fu, S. Zhu, H. Liu, B. Guo, and S. Wang, "Safe path planning for free-floating space robot to approach noncooperative spacecraft," *Proceedings of the Institution of Mechanical Engineers, Part G: Journal of Aerospace Engineering*, vol. 232, no. 7, pp. 1258–1271, 2018.

[58] A. Fejzić, "Development of control and autonomy algorithms for docking to complex tumbling satellites," Ph.D. dissertation, Massachusetts Institute of Technology, 2008.

[59] E. N. Hartley, P. A. Trodden, A. G. Richards, and J. M. Maciejowski, "Model predictive control system design and implementation for spacecraft rendezvous," *Control Engineering Practice*, vol. 20, no. 7, pp. 695–713, 2012.

[60] D. K. Geller, "Linear covariance techniques for orbital rendezvous analysis and autonomous onboard mission planning," *Journal of Guidance, Control, and Dynamics*, vol. 29, no. 6, pp. 1404–1414, 2006.

[61] D. Dana-Bashian, H. Hablani, and M. Tapper, "Guidance algorithms for autonomous rendezvous of spacecraft with a target vehicle in circular orbit," in *AIAA Guidance, Navigation, and Control Conference and Exhibit*, 2001, p. 4393.

[62] S. Nolet, E. Kong, and D. W. Miller, "Autonomous docking algorithm development and experimentation using the SPHERES testbed," in *Spacecraft Platforms and Infrastructure*. International Society for Optics and Photonics, 2004, pp. 1–15.

[63] S. Nolet, "Development of a guidance, navigation and control architecture and validation process enabling autonomous docking to a tumbling satellite," Ph.D. dissertation, Massachusetts Institute of Technology, 2007.

[64] H. B. Hablani, "Autonomous inertial relative navigation with sight-line-stabilized sensors for spacecraft rendezvous," *Journal of Guidance, Control, and Dynamics*, vol. 32, no. 1, pp. 172–183, 2009.

[65] J. Ruiz and J. Hart, "A comparison between orion automated and space shuttle rendezvous techniques," in *AIAA Guidance, Navigation, and Control Conference*, 2010.

[66] R. Zanetti, "Optimal glideslope guidance for spacecraft rendezvous," *Journal of Guidance, Control, and Dynamics*, vol. 34, no. 5, pp. 1593–1597, 2011.

[67] J. Zhang, G.-j. Tang, Y.-Z. Luo, and H.-y. Li, "Orbital rendezvous mission planning using mixed integer nonlinear programming," *Acta Astronautica*, vol. 68, no. 7-8, pp. 1070–1078, 2011.

[68] G. Arantes and L. S. Martins-Filho, "Guidance and control of position and attitude for rendezvous and dock/berthing with a noncooperative/target spacecraft," *Mathematical Problems in Engineering*, 2014.

[69] Y. Ariba, D. Arzelier, L. S. Urbina, and C. Louembet, "V-bar and r-bar glideslope guidance algorithms for fixed-time rendezvous: A linear programming approach," *IFAC-PapersOnLine*, vol. 49, no. 17, pp. 385–390, 2016.

[70] C. Tournes and Y. Shtessel, "Automatic docking using optimal control and second order sliding mode control," in *AIAA Guidance, Navigation and Control Conference and Exhibit*, 2007.

[71] W. Lu, Y. Geng, X. Chen, and F. Zhang, "Relative position and attitude coupled control for autonomous docking with a tumbling target,"," *International Journal of Control and Automation*, vol. 4, no. 4, pp. 1–22, 2011.

[72] C. Pukdeboon, "Finite-time second-order sliding mode controllers for spacecraft attitude tracking," *Mathematical Problems in Engineering*, 2013.

[73] B. Chen and Y. Geng, "Simulation of rendezvous and docking between service spacecraft and non-cooperative target with matlab-simulink and stk," in *Proceeding of the 11th World Congress on Intelligent Control and Automation*. IEEE, 2014, pp. 5727–5732.

[74] J. Yang and E. Stoll, "Adaptive sliding mode control for spacecraft proximity operations based on dual quaternions," *Journal of Guidance, Control, and Dynamics*, vol. 42, no. 11, pp. 2356–2368, 2019.

[75] E. Capello, E. Punta, F. Dabbene, G. Guglieri, and R. Tempo, "Sliding-mode control strategies for rendezvous and docking maneuvers," *Journal of Guidance, Control, and Dynamics*, vol. 40, no. 6, pp. 1481–1487, 2017.

[76] B. Keller, S. Tadikonda, and J. Mapar, "Autonomous acquisition, rendezvous, & docking using a video guidance sensor: Experimental testbed results," in *AIAA Guidance, Navigation, and Control Conference and Exhibit*, 2002, p. 4846.

[77] Q. Wang and G.-R. Duan, "Robust global stabilization of spacecraft rendezvous system via gain scheduling," *International Journal of Automation and Computing*, vol. 11, no. 4, pp. 426–433, 2014.

[78] H. Dong, Q. Hu, and M. R. Akella, "Safety control for spacecraft autonomous rendezvous and docking under motion constraints," *Journal of Guidance, Control, and Dynamics*, vol. 40, no. 7, pp. 1680–1692, 2017.

[79] ——, "Dual-quaternion-based spacecraft autonomous rendezvous and docking under six-degree-of-freedom motion constraints," *Journal of Guidance, Control, and Dynamics*, vol. 41, no. 5, pp. 1150–1162, 2018.

[80] I. Lopez and C. R. McInnes, "Autonomous rendezvous using artificial potential function guidance," *Journal of Guidance, Control, and Dynamics*, vol. 18, no. 2, pp. 237–241, 1995.

[81] A. B. Roger and C. R. McInnes, "Safety constrained free-flyer path planning at the international space station," *Journal of Guidance, Control, and Dynamics*, vol. 23, no. 6, pp. 971–979, 2000.

[82] S. B. McCamish, M. Romano, S. Nolet, C. M. Edwards, and D. W. Miller, "Flight testing of multiple-spacecraft control on SPHERES during close-proximity operations," *Journal of Spacecraft and Rockets*, vol. 46, no. 6, pp. 1202–1213, 2009.

[83] D. Zhang, S. Song, and R. Pei, "Safe guidance for autonomous rendezvous and docking with a non-cooperative target," in *AIAA guidance, navigation, and control conference*, 2010, p. 7592.

[84] J. D. M. NOZ, "Rapid path-planning algorithms for autonomous proximity operations of satellites," Ph.D. dissertation, University of Florida, 2011.

[85] R. I. Zappulla, H. Park, J. Virgili-Llop, and M. Romano, "Experiments on autonomous spacecraft rendezvous and docking using an adaptive artificial potential field approach," in *AAS/AIAA Space Flight Mechanics meeting*, 2016.

[86] S. Li, R. Mehra, R. Smith, and R. Beard, "Multi-spacecraft trajectory optimization and control using genetic algorithm techniques," in *2000 IEEE Aerospace Conference. Proceedings*, vol. 7. IEEE, 2000, pp. 99–108.

[87] Y. H. Kim and D. B. Spencer, "Optimal spacecraft rendezvous using genetic algorithms," *Journal of Spacecraft and Rockets*, vol. 39, no. 6, pp. 859–865, 2002.

[88] Y.-Z. Luo, Y.-J. Lei, and G.-J. Tang, "Optimal multi-objective nonlinear impulsive rendezvous," *Journal of guidance, control, and dynamics*, vol. 30, no. 4, pp. 994–1002, 2007.

[89] Y.-Z. Luo, H.-Y. Li, and G.-J. Tang, "Hybrid approach to optimize a rendezvous phasing strategy," *Journal of guidance, control, and dynamics*, vol. 30, no. 1, pp. 185–191, 2007.

[90] Y. Crispin and D. Seo, "Rendezvous between two active spacecraft with continuous low thrust," in *Advances in Spacecraft Technologies*. IntechOpen, 2011, pp. 585–596.

[91] M. Paluszek and S. Thomas, "Generalized 3d spacecraft proximity path planning using a," in *Infotech@ Aerospace*, 2005, p. 7043.

[92] P. Bodin, R. Larsson, F. Nilsson, C. Chasset, R. Noteborn, and M. Nylund, "Prisma: an in-orbit test bed for guidance, navigation, and control experiments," *Journal of Spacecraft and Rockets*, vol. 46, no. 3, pp. 615–623, 2009.

[93] G. Francis, E. Collins, O. Chuy, and A. Sharma, "Sampling-based trajectory generation for autonomous spacecraft rendezvous and docking," in *AIAA Guidance, Navigation, and Control (GNC) Conference*, 2013, p. 4549.

[94] J. Phillips, L. Kavraki, and N. Bedrossian, "Spacecraft rendezvous and docking with real-time, randomized optimization," in *AIAA Guidance, Navigation, and Control Conference and Exhibit*, 2003, p. 5511.

[95] J. A. Starek, E. Schmerling, G. D. Maher, B. W. Barbe, and M. Pavone, "Real-time, propellant-optimized spacecraft motion planning under clohessy-wiltshire-hill dynamics," in *2016 IEEE Aerospace Conference*. IEEE, 2016, pp. 1–16.

[96] J. A. Starek, E. Schmerling, G. D. Maher, B. W. Barbee, and M. Pavone, "Fast, safe, propellant-efficient spacecraft motion planning under clohessy–wiltshire–hill dynamics," *Journal of Guidance, Control, and Dynamics*, vol. 40, no. 2, pp. 418–438, 2016.

[97] R. Bevilacqua and M. Romano, "Quasi-optimal control for path constrained relative spacecraft maneuvers based on dynamic programming," *Nonlinear Dynamics and Systems Theory*, vol. 8, no. 2, pp. 137–150, 2008.

[98] H. Choset and D. Kortenkamp, "Path planning and control for free-flying inspection robot in space," *Journal of Aerospace Engineering*, vol. 12, no. 2, pp. 74–81, 1999.

[99] J. Virgili-Llop, C. Zagaris, R. Zappulla, A. Bradstreet, and M. Romano, "A convex-programming-based guidance algorithm to capture a tumbling object on orbit using a spacecraft equipped with a robotic manipulator,"

The International Journal of Robotics Research, vol. 38, no. 1, pp. 40–72, 2019.

[100] L. Breger, J. How, and A. Richards, "Model predictive control of spacecraft formations with sensing noise," in *Proceedings of the 2005, American Control Conference, 2005.* IEEE, 2005, pp. 2385–2390.

[101] A. Richards and J. P. How, "Model predictive control of vehicle maneuvers with guaranteed completion time and robust feasibility," in *Proceedings of the 2003 American Control Conference, 2003.*, vol. 5. IEEE, 2003, pp. 4034–4040.

[102] H. Park, S. DiCairano, and I. Kolmanovsky, "Model predictive control of spacecraft docking with a non-rotating platform," *IFAC Proceedings Volumes*, vol. 44, no. 1, pp. 8485–8490, 2011.

[103] H. Park, S. Di Cairano, and I. Kolmanovsky, "Model predictive control for spacecraft rendezvous and docking with a rotating/tumbling platform and for debris avoidance," in *Proceedings of the 2011 American Control Conference*. IEEE, 2011, pp. 1922–1927.

[104] R. Vazquez, F. Gavilan, and E. F. Camacho, "Trajectory planning for spacecraft rendezvous with on/off thrusters," *IFAC Proceedings Volumes*, vol. 44, no. 1, pp. 8473–8478, 2011.

[105] S. Di Cairano, H. Park, and I. Kolmanovsky, "Model predictive control approach for guidance of spacecraft rendezvous and proximity maneuvering," *International Journal of Robust and Nonlinear Control*, vol. 22, no. 12, pp. 1398–1427, 2012.

[106] F. Gavilan, R. Vazquez, and E. F. Camacho, "Chance-constrained model predictive control for spacecraft rendezvous with disturbance estimation," *Control Engineering Practice*, vol. 20, no. 2, pp. 111–122, 2012.

[107] P. Li, X. Yue, H. Dai, and X. Chi, "6dof terminal guidance for autonomous spacecraft capture free floating objects using state dependent model predictive," in *5th Int. Conf. Spacecr. Form. Fly. Mission. Technol*, no. 1, 2013.

[108] G. Deaconu, C. Louembet, and A. Théron, "Minimizing the effects of navigation uncertainties on the spacecraft rendezvous precision," *Journal of Guidance, Control, and Dynamics*, vol. 37, no. 2, pp. 695–700, 2014.

[109] P. A. Felisiak, K. Sibilski, W. Wroblewski, and J. Z. Sasiadek, "Spacecraft rendezvous in elliptical orbit using nonlinear model predictive control," in *AIAA Guidance, Navigation, and Control Conference*, 2014, p. 0090.

[110] M. Leomanni, E. Rogers, and S. B. Gabriel, "Explicit model predictive control approach for low-thrust spacecraft proximity operations," *Journal of Guidance, Control, and Dynamics*, vol. 37, no. 6, pp. 1780–1790, 2014.

[111] C. Petersen, A. Jaunzemis, M. Baldwin, M. Holzinger, and I. Kolmanovsky, "Model predictive control and extended command governor for improving robustness of relative motion guidance and control," in *Proc. AAS/AIAA space flight mechanics meeting*, 2014.

[112] A. Weiss, M. Baldwin, R. S. Erwin, and I. Kolmanovsky, "Model predictive control for spacecraft rendezvous and docking: Strategies for handling constraints and case studies," *IEEE Transactions on Control Systems Technology*, vol. 23, no. 4, pp. 1638–1647, 2015.

[113] C. Zagaris, M. Baldwin, C. Jewison, and C. Petersen, "Survey of spacecraft rendezvous and proximity guidance algorithms for on-board implementation," *Advances in the Astronautical Sciences (AAS/AIAA Spaceflight Mechanics 2015)*, vol. 155, pp. 131–150, 2015.

[114] C. Zagaris, H. Park, J. Virgili-Llop, R. Zappulla, M. Romano, and I. Kolmanovsky, "Model predictive control of spacecraft relative motion with convexified keep-out-zone constraints," *Journal of Guidance, Control, and Dynamics*, vol. 41, no. 9, pp. 2054–2062, 2018.

[115] J. B. Rawlings, "Tutorial overview of model predictive control," *IEEE Control Systems*, vol. 20, no. 3, pp. 38–52, 2000.

[116] F. Allgöwer, T. A. Badgwell, J. S. Qin, J. B. Rawlings, and S. J. Wright, "Nonlinear predictive control and moving horizon estimation—an introductory overview," in *Advances in Control*. Springer, London, 1999, pp. 391–449.

[117] D. Q. Mayne, J. B. Rawlings, C. V. Rao, and P. O. Scokaert, "Constrained model predictive control: Stability and optimality," *Automatica*, vol. 36, no. 6, pp. 789–814, 2000.

[118] A. Richards and J. P. How, "Model predictive control of vehicle maneuvers with guaranteed completion time and robust feasibility," in *American Control Conference, 2003. Proceedings of the 2003*, vol. 5. IEEE, 2003, pp. 4034–4040.

[119] V. Manikonda, P. Arambel, M. Gopinathan, R. Mehra, and F. Hadaegh, "A model predictive control-based approach for spacecraft formation keeping and attitude control," in *American Control Conference, 1999. Proceedings of the 1999*, vol. 6. IEEE, 1999, pp. 4258–4262.

[120] E. C. Kerrigan and J. M. Maciejowski, "Robust feasibility in model predictive control: Necessary and sufficient conditions," in *Decision and Control, 2001. Proceedings of the 40th IEEE Conference on*, vol. 1. IEEE, 2001, pp. 728–733.

[121] P. Scokaert and D. Mayne, "Min-max feedback model predictive control for constrained linear systems," *IEEE Transactions on Automatic control*, vol. 43, no. 8, pp. 1136–1142, 1998.

[122] S. Di Cairano, H. Park, and I. Kolmanovsky, "Model predictive control approach for guidance of spacecraft rendezvous and proximity maneuvering," *International Journal of Robust and Nonlinear Control*, vol. 22, no. 12, pp. 1398–1427, 2012.

[123] L. S. Breger and J. P. How, "Safe trajectories for autonomous rendezvous of spacecraft," *Journal of Guidance, Control, and Dynamics*, vol. 31, no. 5, pp. 1478–1489, 2008.

[124] R. Krenn, A. Gibbesch, G. Binet, and A. Bemporad, "Model predictive traction and steering control of planetary rovers," 2^{nd} *Symposium on Advanced Space Technologies in Robotics and Automation, ASTRA*, 2013.

[125] A. Vachon, A. Desbiens, E. Gagnon, and C. Bérard, "Launch ascent guidance by discrete multi-model predictive control," *Acta Astronautica*, vol. 95, pp. 101–110, 2014.

[126] C. A. Pascucci, S. Bennani, and A. Bemporad, "Model predictive control for powered descent guidance and control," in *Control Conference (ECC), 2015 European.* IEEE, 2015, pp. 1388–1393.

[127] Y. Xing, K. Low, and M. Pham, "Distributed model predictive control of satellite attitude using hybrid reaction wheels and magnetic actuators," in *Industrial Electronics and Applications (ISIEA), 2012 IEEE Symposium on*. IEEE, 2012, pp. 230–235.

[128] A. Walsh, S. Di Cairano, and A. Weiss, "MPC for coupled station keeping, attitude control, and momentum management of low-thrust geostationary satellites," in *American Control Conference (ACC), 2016*. IEEE, 2016, pp. 7408–7413.

[129] D. Y. Lee, R. Gupta, U. V. Kalabić, S. Di Cairano, A. M. Bloch, J. W. Cutler, and I. V. Kolmanovsky, "Geometric mechanics based nonlinear model predictive spacecraft attitude control with reaction wheels," *Journal of Guidance, Control, and Dynamics*, pp. 1–11, 2016.

[130] C. D. Petersen, F. Leve, and I. Kolmanovsky, "Model predictive control of an underactuated spacecraft with two reaction wheels," *Journal of Guidance, Control, and Dynamics*, pp. 1–13, 2016.

[131] "Guidance, navigation, and control technology assessment for future planetary science missions," https://solarsystem.nasa.gov/docs/GNC20Tech20Assess_Part20III_Surface20GNC_20130402_soo.pdf, accessed: 2019-08-04.

[132] "Advanced gn&c for assembly of large and flexible structures and vehicles - expro plus," http://www.rosa.ro/index.php/en/communication/itt/1140-1b090-nano-satellites-for-commercial-telecommunications-services.html, accessed: 2019-08-04.

[133] C. Andrade, R. Ramirez-Mendoza, M. Giacoman-Zarzar, R. Morales, A. Fejzic, A. Saenz-Otero, and D. Miller, "Robust control applied towards rendezvous and docking," in *2009 European Control Conference (ECC)*. IEEE, 2009, pp. 1854–1859.

[134] C. M. Pong, A. Saenz-Otero, and D. W. Miller, "Autonomous thruster failure recovery on underactuated spacecraft using model predictive control," *Advances in the Astronautical Sciences*, 2011.

[135] S. Vromen, F. de Bruijn, and E. Mooij, "Guidance for autonomous rendezvous and docking with envisat using hardware-in-the-loop simulations," in *IWSCFF*, 2015.

[136] H. Park, C. Zagaris, J. Virgili Llop, R. Zappulla, I. Kolmanovsky, and M. Romano, "Analysis and experimentation of model predictive control for spacecraft rendezvous and proximity operations with multiple obstacle avoidance," in *AIAA/AAS Astrodynamics Specialist Conference*, 2016, p. 5273.

[137] H. Daitx, M. Schlotterer, J. Whidborne, and M. Sagliano, "Development of a combined attitude and position controller for a satellite simulator," in *67th International Astronautical Congress (IAC). International Astronautical Federation*, 2016.

[138] D.-M. Cho, D. Jung, and P. Tsiotras, "A 5-dof experimental platform for spacecraft rendezvous and docking," in *AIAA Infotech@ Aerospace Conference and AIAA Unmanned... Unlimited Conference*, 2009, p. 1869.

[139] M. Sabatini, G. B. Palmerini, and P. Gasbarri, "A testbed for visual based navigation and control during space rendezvous operations," *Acta Astronautica*, vol. 117, pp. 184–196, 2015.

[140] Y. Eun, G.-N. Kim, J. Hyun, and S.-Y. Park, "Experimental results on the vision-based navigation system for spacecraft operation in proximity using ground test facility," in *2018 Space Flight Mechanics Meeting*, 2018, p. 2222.

[141] D. C. Sternberg, C. Pong, N. Filipe, S. Mohan, S. Johnson, and L. Jones-Wilson, "Jet propulsion laboratory small satellite dynamics testbed simulation: on-orbit performance model validation," *Journal of Spacecraft and Rockets*, vol. 55, no. 2, pp. 322–334, 2017.

[142] T. Rybus and K. Seweryn, "Planar air-bearing microgravity simulators: review of applications, existing solutions and design parameters," *Acta Astronautica*, vol. 120, pp. 239–259, 2016.

[143] L. Guarnaccia, R. Bevilacqua, and S. P. Pastorelli, "Suboptimal lqr-based spacecraft full motion control: Theory and experimentation," *Acta Astronautica*, vol. 122, pp. 114–136, 2016.

[144] U. Lee and M. Mesbahi, "Optimal power descent guidance with 6-dof line of sight constraints via unit dual quaternions," in *AIAA Guidance, Navigation, and Control Conference*, 2015, p. 0319.

[145] W. Xu, B. Liang, Y. Xu, C. Li, and W. Qiang, "A ground experiment system of free-floating robot for capturing space target," *Journal of Intelligent & Robotic Systems*, vol. 48, no. 2, pp. 187–208, 2007.

[146] B. P. McCarthy, "Flight hardware development for a space-based robotic assembly and servicing testbed," Ph.D. dissertation, Massachusetts Institute of Technology, 2014.

[147] F. Aghili, "Pre-and post-grasping robot motion planning to capture and stabilize a tumbling/drifting free-floater with uncertain dynamics," in *Robotics and Automation (ICRA), 2013 IEEE International Conference on.* IEEE, 2013, pp. 5461–5468.

[148] J. A. Starek, B. Açıkmeşe, I. A. Nesnas, and M. Pavone, "Spacecraft autonomy challenges for next-generation space missions," in *Advances in Control System Technology for Aerospace Applications.* Springer, 2016, pp. 1–48.

[149] G. W. Hill, "Researches in the lunar theory," *American journal of Mathematics*, vol. 1, no. 1, pp. 5–26, 1878.

[150] W. Clohessy and R. Wiltshire, "Terminal guidance system for satellite rendezvous," *Journal of the Aerospace Sciences*, vol. 27, no. 9, pp. 653–658, 1960.

[151] G. Inalhan, M. Tillerson, and J. P. How, "Relative dynamics and control of spacecraft formations in eccentric orbits," *Journal of guidance, control, and dynamics*, vol. 25, no. 1, pp. 48–59, 2002.

[152] H. Schaub and K. T. Alfriend, "J 2 invariant relative orbits for spacecraft formations," *Celestial Mechanics and Dynamical Astronomy*, vol. 79, no. 2, pp. 77–95, 2001.

[153] S. A. Schweighart and R. J. Sedwick, "Cross-track motion of satellite formations in the presence of j2 disturbances," *Journal of Guidance, Control, and Dynamics*, vol. 28, no. 4, pp. 824–826, 2005.

[154] G. Xu and D. Wang, "Nonlinear dynamic equations of satellite relative motion around an oblate earth," *Journal of Guidance, Control, and Dynamics*, vol. 31, no. 5, pp. 1521–1524, 2008.

[155] J. Tschauner and P. Hempel, "Rendezvous zu einem in elliptischer bahn umlaufenden ziel," *Astronautica Acta*, vol. 11, no. 2, pp. 104–+, 1965.

[156] D.-W. Gim and K. T. Alfriend, "State transition matrix of relative motion for the perturbed noncircular reference orbit," *Journal of Guidance, Control, and Dynamics*, vol. 26, no. 6, pp. 956–971, 2003.

[157] D.-W. Gim and K. T. Alfriend "Satellite relative motion using differential equinoctial elements," *Celestial Mechanics and Dynamical Astronomy*, vol. 92, no. 4, pp. 295–336, 2005.

[158] D. Wang, B. Wu, and E. K. Poh, "Dynamic models of satellite relative motion around an oblate earth," in *Satellite Formation Flying*. Springer, 2017, pp. 9–41.

[159] I. Newton, *Mathematical principles of natural philosophy*. A. Strahan, 1802.

[160] H. Schaub and J. L. Junkins, *Analytical mechanics of space systems*. American Institute of Aeronautics and Astronautics, 2005.

[161] J. R. Wertz, *Spacecraft attitude determination and control*. Springer Science & Business Media, 2012, vol. 73.

[162] W. Clifford, "Preliminary sketch of biquaters," *Mathematical Papers*, 1873.

[163] H.-L. Pham, V. Perdereau, B. V. Adorno, and P. Fraisse, "Position and orientation control of robot manipulators using dual quaternion feedback," in *2010 IEEE/RSJ International Conference on Intelligent Robots and Systems*. IEEE, 2010, pp. 658–663.

[164] A. Perez and J. M. McCarthy, "Dual quaternion synthesis of constrained robotic systems," *ASME Journal of Mechanical Design*, vol. 126, pp. 425–435, 2004.

[165] J. Mattingley and S. Boyd, "Cvxgen: A code generator for embedded convex optimization," *Optimization and Engineering*, vol. 13, no. 1, pp. 1–27, 2012.

[166] H. J. Ferreau, C. Kirches, A. Potschka, H. G. Bock, and M. Diehl, "qpoases: A parametric active-set algorithm for quadratic programming," *Mathematical Programming Computation*, vol. 6, no. 4, pp. 327–363, 2014.

[167] K. Yamanaka and F. Ankersen, "New state transition matrix for relative motion on an arbitrary elliptical orbit," *Journal of guidance, control, and dynamics*, vol. 25, no. 1, pp. 60–66, 2002.

[168] O. B. Iskender, K. V. Ling, and V. Dubanchet, "Constraints tightening approach towards model predictive control based rendezvous and docking with uncooperative targets," in *2018 European Control Conference (ECC)*. IEEE, 2018, pp. 380–385.

[169] R. Vazquez, F. Gavilan, and E. F. Camacho, "Pulse-width predictive control for ltv systems with application to spacecraft rendezvous," *Control Engineering Practice*, vol. 60, pp. 199–210, 2017.

[170] O. B. Iskender, K. V. Ling, V. Dubanchet, and L. Simonini, "Inscribed polygon method for spacecraft maneuvering problem arising in single axis thruster configuration," in *2019 12th Asian Control Conference (ASCC)*. IEEE, 2019, pp. 1466–1471.

[171] L. Gurobi Optimization, "Gurobi optimizer reference manual," http://www.gurobi.com, 2018, accessed: 2020-04-05.

[172] E. D. Andersen, "On formulating quadratic functions in optimization models: Technical report," https://docs.mosek.com/whitepapers/qmodel.pdf, 2018, accessed: 2020-04-05.

[173] M. Grant and S. Boyd, "Cvx: Matlab software for disciplined convex programming, version 2.1," http://cvxr.com/cvx/, 2014, accessed: 2020-04-05.

[174] J. T. Betts, "Survey of numerical methods for trajectory optimization," *Journal of guidance, control, and dynamics*, vol. 21, no. 2, pp. 193–207, 1998.

[175] F. Fahroo and I. M. Ross, "Direct trajectory optimization by a chebyshev pseudospectral method," *Journal of Guidance, Control, and Dynamics*, vol. 25, no. 1, pp. 160–166, 2002.

[176] D. G. Hull, "Conversion of optimal control problems into parameter optimization problems," *Journal of Guidance, Control, and Dynamics*, vol. 20, no. 1, pp. 57–60, 1997.

[177] J. Vlassenbroeck and R. Van Dooren, "A chebyshev technique for solving nonlinear optimal control problems," *IEEE transactions on automatic control*, vol. 33, no. 4, pp. 333–340, 1988.

[178] S. Boyd and L. Vandenberghe, *Convex optimization*. Cambridge university press, 2004.

[179] F. Curti, M. Romano, and R. Bevilacqua, "Lyapunov-based thrusters' selection for spacecraft control: analysis and experimentation," *Journal of guidance, control, and dynamics*, vol. 33, no. 4, pp. 1143–1160, 2010.

[180] J. Garus, "Optimization of thrust allocation in the propulsion system of an underwater vehicle," *International Journal of Applied Mathematics and Computer Science*, vol. 14, pp. 461–467, 2004.

[181] H. Benninghoff, F. Rems, E.-A. Risse, P. Irmisch, I. Ernst, B. Brunner, M. Stelzer, R. Lampariello, R. Krenn, M. Reiner, C. Stangl, R. Faller, and O. Peinado, "Ricados - rendezvous, inspection, capturing and detumbling by orbital servicing," in *7th International Conference on Astrodynamics Tools and Techniques (ICATT)*, 2018.

[182] R. Bellman, "The theory of dynamic programming," Rand corp santa monica ca, Tech. Rep., 1954.

[183] E. B. Lee and L. Markus, "Foundations of optimal control theory," Minnesota Univ Minneapolis Center For Control Sciences, Tech. Rep., 1967.

[184] D. Q. Mayne, J. B. Rawlings, C. V. Rao, and P. O. Scokaert, "Constrained model predictive control: Stability and optimality," *Automatica*, vol. 36, no. 6, pp. 789–814, 2000.

[185] A. N. Venkat, J. B. Rawlings, and S. J. Wright, "Stability and optimality of distributed model predictive control," in *Proceedings of the 44th IEEE Conference on Decision and Control*. IEEE, 2005, pp. 6680–6685.

[186] F. Borrelli, A. Bemporad, and M. Morari, *Predictive control for linear and hybrid systems*. Cambridge University Press, 2017.

[187] H. K. Khalil and J. W. Grizzle, *Nonlinear systems*. Prentice hall Upper Saddle River, NJ, 2002, vol. 3.

[188] C. Petersen, "Advances in underactuated spacecraft control," Ph.D. dissertation, University of Michigan, 2016.

[189] M. Kvasnica, P. Grieder, M. Baotić, and M. Morari, "Multi-parametric toolbox (mpt)," in *International Workshop on Hybrid Systems: Computation and Control*. Springer, 2004, pp. 448–462.

[190] Y. Abbasi, H. Momeni, and A. Ramezani, "Robust tube–based model predictive control of piecewise affine systems with enlarging the region of attraction," *Journal of Vibration and Control*, p. 1077546320932024, 2020.

[191] U. Eren, A. Prach, B. B. Koçer, S. V. Raković, E. Kayacan, and B. Açıkmeşe, "Model predictive control in aerospace systems: Current state and opportunities," *Journal of Guidance, Control, and Dynamics*, vol. 40, no. 7, pp. 1541–1566, 2017.

[192] H. D. Curtis, *Orbital mechanics for engineering students*. Butterworth-Heinemann, 2013.

[193] S. Wehrmann and M. Schlotterer, "Coordinated orbit and attitude control of a satellite formation in a satellite simulator testbed," in *ESA Conference on Guidance, Navigation & Control Systems*, 2017.

[194] K. J. Åström and T. Hägglund, *PID controllers: theory, design, and tuning*. Instrument society of America Research Triangle Park, NC, 1995, vol. 2.

[195] "Astronaut scott kelly poses for a photograph with three mit spheres," https://www.researchgate.net/figure/5-SPHERES-on-the-ISS-Astronaut-Scott-Kelly-poses-for-a-photograph-with-three-MIT_fig5_297620855, accessed: 2020-03-03.